Modelling moisture ingress and impact on PV module degradation

Development of a FEM model to predict the moisture ingress and module degradation under different conditions

Daniel Jimenez Pelarda - 5643597

TU Delft

Modelling moisture ingress and impact on PV module degradation

Development of a FEM model to predict the moisture ingress and module degradation under different conditions

Thesis report

by

Daniel Jimenez Pelarda - 5643597

to obtain the degree of Master of Science
at the Delft University of Technology
to be defended publicly on August 28, 2023 at 10:00

Thesis committee:

Chair:	Dr. René van Swaaij
Supervisors:	Dr. Malte Vogt
	Youri Blom
External examiner:	Dr. Jianning Dong
Place:	EEMCS, Delft
Project Duration:	November, 2022 - August, 2023
Student number:	5643597

Faculty of Electrical Engineering, Mathematics and Computer Science · Delft University of Technology

Preface

Since I can remember I have had a fascination with technology. That is what motivated me to start my education at TU Eindhoven, where this passion for technical subjects grew even further. More importantly, my interest in sustainable energy technologies emerged. That motivated my decision to join TU Delft to study the Sustainable Energy Technology Master where in the last two years I have continued to grow as an engineer and as a person and to focus my interests in PV energy in particular. This project is the end product of everything I have been lucky to learn in this program.

I would like to thank my supervisor Dr. Malte Vogt for his support and invaluable feedback. I would also like to thank my daily supervisor Youri Blom for the continued guidance through the entirety of the project. I have thoroughly enjoyed carrying out this project under your supervision. I would also like to take the time to thank Dr. Ismail Kaaya and Dr. Nikoleta Kyranaki from the IMEC research center in Belgium for discussing the development of my project in numerous occasions.

Finally, I would like to acknowledge the people in my personal life that have provided my with unending support in this journey starting with my parents and siblings, who have been there for me through the entirety of my education. Last but not least, I would like to thank the friends that I have been lucky to make along the way who have made the journey a bit more fun and enjoyable.

Delft, 21^{st} August 2023
Daniel Jimenez Pelarda

Abstract

Solar energy is expected to be one of the main energy sources behind the transition to a sustainably powered society. One of the main reasons for this is the falling costs of PV modules. With falling capital costs other factors become key in determining the profitability of solar energy projects. One of these factors is the degradation of performance through the lifetime of the module. Therefore, it becomes increasingly important to understand the degradation behaviour of solar modules. One of the main causes of degradation is moisture. In this work the moisture ingress into PV modules and the degradation it causes are studied.

A moisture ingress model is developed using the FEM software COMSOL. The model uses Fick's second law of diffusion to model the diffusion of moisture in the module. The model also reflects the temperature dependent nature of parameters affecting moisture ingress by using an Arrhenius equation. The model is validated with experimental and simulated data from literature showing a good agreement. A brief comparison with alternative models such as analytical models and a simplified numerical model is also made. The model allows to simulate the moisture ingress into different PV modules in different conditions. The moisture ingress in 11 different locations with different climatic conditions is simulated. The moisture ingress is also simulated using 4 different encapsulants and 4 different backsheets. Finally, the model is adapted to simulate the moisture ingress into impermeable backsheet modules.

These results are used to find a relation between ambient conditions and the results delivered by the COMSOL model. A simplified relationship is found that holds for the different climates and encapsulants. It is found that the effective relative humidity in the environment is the key parameter in determining the amount of water that will be in the module once it reaches equilibrium. The time that it takes for a module to reach its moisture equilibrium content is determined by the temperature. The presence of these simplified relations can help in estimating the moisture ingress behaviour of a model without the need of carrying out a full FEM simulation. However, the dynamics of the system when using different backsheets does not follow the same simplified relations.

The degradation caused by water in the module is also studied. An analytical model is used to predict the degradation observed during damp heat tests. Due to the properties of the analytical model a different approach has to be followed for real life conditions. The degradation model is used to compare the expected degradation under different conditions. This shows that the expected degradation is larger in hot and humid climates while it is minimized in colder climates. The general degradation trend observed for the different climates is: Tropical > Arid > Temperate > Continental > Polar.

Contents

Nomenclature

List of Abbreviations

μc-Si	Micro-crystalline silicon
a-Si	Amorphous silicon
ARIMA	Autoregressive integrated moving average
BET	Brunauer–Emmett–Teller
c-Si	Crystalline silicon
CdTe	Cadmium Telluride
CIGS	Copper Indium Gallium Selenide
CSD	Classical seasonal decomposition
DH	Damp-Heat
EVA	Ethylene-vinyl acetate
FEM	Finite element method
Ga-As	Gallium-Arsenide
GHI	Global horizontal irradiance
ION	Ionomer
LCOE	Levelized cost of electricity
LID	Light induced degradation
mc-Si	multi-crystalline silicon
mono-Si	Monocrystalline silicon
PA	Polyamide
PDMS	Polydimethylsiloxane
PET	Polyethylene teraphtalate
POE	Polyolefin elastomer
PV	Photovoltaic
PVB	Polyisobutylene
PVB	Polyvinyl butyral
PVF	Polyvinyl fluoride
RMC	Relative moisture content
SLR	Simple linear regression
STL	seasonal trend decomposition
TPO	Thermoplastic polyolefin
TPSiOx	Tedlar-PET-SiO_x Backsheet
TPT	Tedlar-PET-Tedlar Backsheet
UV	Ultraviolet
WVTR	Water vapour transmission rate
PID	Potential induced degradation

Constants

k_B	Boltzmann's constant
R	Gas constant

List of Symbols

ΔT	Temperature variation [K]
E_a	Activation energy [kJ/mol] or [kJ]
I_{SC}	Short-circuit current [mA/cm^2]
P_{MPP}	Relative power at Maximum power point [-]
t_{eq}	time to reach equilibrium [h]
V_{OC}	Open circuit voltage [V]
X_0	Pre-exponential factor
X_{amb}	Ambient
X_{BS}	Backsheet
X_E	Enacapsulant
X_{mod}	Module
B	Power susceptibility factor
C	Concentration [kg/m^3]
C_N	Cycling rate
D	Diffusion coefficient [m^2/s]
K	Henry's constant

k	Rate constant [$1/time$]	RH	Relative humidity [-]
L	Degradation limiting factor	S	Solubility [kg/m^3]
l	length of diffusion path [m]	T	Temperature [K]
N	Number of cycles	U	Voltage [V]
n	Exponential constant [-]	u	Shape factor for power degradation

List of Figures

List of Tables

1

Introduction and literature review

This section will serve as an introduction into the topic of PV modules degradation. A summary of the information available in literature is presented. In section 1.1 some basic concepts necessary to discuss PV modules are explained. In section 1.2 the most important stress factors to which the modules are exposed to will be discussed. In section 1.3 the degradation modes that result from these stress factors and affect the performance of the PV modules are presented. The modelling approaches found in literature are discussed in section 1.4. Finally, the knowledge gap and research question and scope of the thesis are defined in section 1.5.

1.1. Introduction to PV technology

Renewable energy generation capacity is expected to increase by close to 2400 GW between 2022 and 2027 [1]. This represents a 75% increase on the current installed capacity. Wind and solar energy are projected to be the main drivers of the increase in renewable energy capacity representing 90% of the newly installed capacity [1]. Solar energy alone will jump from 1100 to 2350 GW installed capacity. The installation of renewable energy has been accelerating for many years. This is attributed to the negative effects of using traditional energy sources which rely mainly on fossil fuels [2]. Fossil fuels have finite resources and emit greenhouse gases meaning that a sustainable alternative is needed. More recently, the installation of renewable energy has been further incentivized by the rise in fossil fuel prices and the threat to energy security posed by the Russian invasion of Ukraine [1].

Over the years the cost of electricity produced using PV has fallen dramatically. The cost of producing electricity in a PV plant has fallen by 77% from 2005 to 2018 [3], mostly driven by a decrease in the cost of manufacturing solar PV modules. This lower capital cost for PV energy means that the degradation in performance is becoming more important in determining the LCOE of PV produced electricity [4]. The degradation rates reported in literature range from 0.5 to 2 % depending on the technology type and climatic conditions it is exposed to [4, 5, 6]. In extreme cases, the yearly degradation rate can reach 4 % [6]. After 20 years of operating lifetime, this large range of yearly degradation rates can result in a degradation ranging from 10 to 40% and up to 80% in extremely cases. This leads to huge differences in performance over the lifetime of the module. This makes it important to understand the mechanisms behind the degradation in performance of PV modules and the different parameters that affect the degradation.

1.1.1. Solar module structure and components

The degradation modes affect all parts of the module. However some are more likely to degrade over time or to cause failure. In this subsection the general structure of PV modules and the most important components will be presented. A visual representation of a PV module with the most important components labeled is shown in figure 1.1.

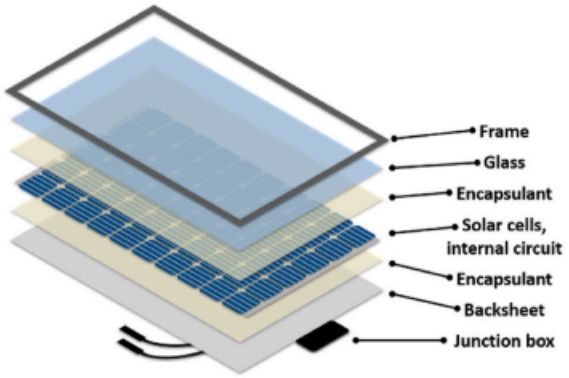

Figure 1.1: Most common configuration of a crystalline Silicon PV module [4]

Module packaging
In general, the module packaging consists of the glass front cover, the encapsulant, the backsheet, the edge seals and the module frame. Depending on the module design and technology, some of these components can change. For example, if lightweight and flexible PV is required the front glass cover will be swapped by a front-side polymeric sheet [4]. In contrast, in bifacial modules the backsheet is replaced by a glass sheet [7]. These are also called impermeable backsheets.

Low-iron soda-lime float glass is generally used as a front cover in PV modules due to its high transparency, mechanical robustness, low cost and its good properties as an electrical insulator [4]. Encapsulants are placed directly in contact with the solar cells to protect them from the environment [8]. Encapsulants must have high transparency, resistance to UV degradation and good adhesion characteristics [7]. The most common encapsulant material is Ethylene-vinyl acetate(EVA) [9]. Other materials that can be used as encapsulants are ionomers (ION), polyvinyl butyral (PVB), polyethylene teraphtalate (PET) and polyvinyl fluoride (PVF)[7]. Polymeric backsheets are used to provide electrical insulation and environmental protection. They are generally composed of three main layers: an outer layer that is designed to resist weathering, a core layer that should act as an electrical insulator and an inner layer to adhere to the encapsulant [7]. The most commonly used materials for each layer are Fluoropolymers, Polyethylene teraphtalate and EVA [4].

Solar cells
The semiconductor device is the main component of the PV module as it is the component that converts the incident light into electricity. There is a vast array of different technologies. Crystalline silicon (c-Si) technologies which include mono and multi-crystalline (mono-Si and mc-Si) which represent 95% of the installed capacity of PV technologies [10], thin film technologies represent the rest of the installed capacity. Thin film technologies include micromorph solar cells which include amorphous silicon (a-Si), micro crystalline ($\mu c - Si$) technologies, Copper Indium Gallium Selenide (CIGS), Gallium-Arsenide technologies (Ga-As), Cadmium Telluride (CdTe) cells and perovskite technologies [11].

The degradation mechanisms behind the decrease in performance for each solar cell are unique [4]. Furthermore, the dominant degradation mode can be determined by the manufacturing mode, for example, c-Si solar cells manufactured using the Czochralski method suffer from light-induced degradation caused by boron-oxygen defects in the Czorchalski wafer [12].

Other components
The solar cell internal circuitry is composed by solar cell metallization elements and interconnect wiring which have the purpose connecting the solar cells and strings of cells [4]. Solder interconnections are generally made from silver contacts bonded to a copper ribbon [13]. The junction is placed at the back of the module for the electrical connection of the module and protects the connections of the strings, external wiring, and often the bypass diodes [4, 9].By-pass diodes are used to protect solar cells from overheating in the event of the presence of current mismatch.

1.2. Stress factors

Stress factors are elements to which the PV module is exposed to throughout its lifetime and which will cause degradation modes and eventually lead to failure [4]. These are climatic stresses that are weather and location dependent. Understanding the effect of each of the climatic stresses is necessary to predict hoe the modules will degrade under different conditions.

Ambient Temperature

Ambient temperature is an important parameter when assessing the performance of PV modules. It is one of the most important factors that determines the operating temperature of the PV module, this influences the instantaneous efficiency of the module at any given time [14]. The temperatures at which a module will operate are also dependent on other ambient conditions (e.g. wind speed and solar irradiance), material dependent parameters (e.g. transmittance and absorptance), efficiency of the module and on how the module is mounted [10, 15].

Temperature plays a central role in accelerating many degradation modes [4, 16]. High temperature accelerates degradation mechanisms that involve chemical reaction and diffusion of chemical species, these processes are generally modelled to have an Arrhenius dependence on temperature [4]. The Arrhenius equation is used to describe the temperature dependence of the rate of a given process, the general form of this equation is given by equation 1.1. Degradation of encapsulants and backsheets also exhibits an Arrhenius dependence on temperature [4, 16] as they are caused by chemical reactions and diffusion of harmful chemical species. The dependence on temperature is characterized by a mechanism specific activation energy, E_a [17]. The activation energy is not only mechanism specific but is also dependent on the type of PV module technology since they use different materials for different layers [18]. In the equation below, k_B is the Boltzmann constant, T is the temperature and k_o is the rate constant.

$$k = k_o \cdot exp(\frac{-E_a}{k_B \cdot T}) \tag{1.1}$$

Temperature is also responsible for stress in PV modules due to mismatch of thermal expansion coefficients [13]. This mismatch in thermal expansion coefficients causes a difference in expansion volume of the different module components. This results in creep in the material due to thermal cycling which over time leads to fatigue [19]. This will eventually lead to cracks which will eventually cause the solder joint to be electrically open [13, 19]. The stress caused by temperature has a cyclic nature due to the diurnal and seasonal temperature cycles.

Relative Humidity

Humidity plays an important role in determining the lifetime performance of PV modules. The amount of humidity a PV module is exposed to is dependant on the climate in which it is installed [10]. Arid climates will expose PV modules to the lowest amount of humidity while tropical climates experience high humidities depending on the season [10]. Continued exposure of PV modules can cause moisture ingress into the module [14]. Water ingress into PV modules can be described by Fick's diffusion equation shown below [5, 7]. The parameters in this equation are the diffusion coefficient (D) which is a material dependent quantity and the curvature of the gradient in concentration which is the driving force behind the diffusion process.

$$\frac{\delta C(x,y,z,t)}{\delta t} = D \cdot \nabla^2 C(x,y,z,t) \tag{1.2}$$

The rate of ingress of moisture into the module is also dependent on the temperature as both the diffusion coefficient and the saturation concentration depend on temperature [17, 20]. In some special cases where the transport mechanism is influenced by the channels within the polymer rather than being determined by bulk properties other models such as dual transport are a better choice [7, 20]. The physical quantity used to describe humidity in literature is relative humidity (RH) which is defined as the ratio of the partial pressure of the water vapour and the water vapour saturation pressure in the ambient atmosphere [21]. After some time, the water concentration inside the module will reach equilibrium, the time needed to reach equilibrium and what the equilibrium value is depends on the ambient conditions and module design [4]. For breathable

modules (glass/backsheet) a few days to a week are enough to reach equilibrium values while for impermeable constructions a few years are needed [22].

This moisture contributes to a wide variety of degradation processes of the PV module [4, 7]:

- Causes delamination of the encapsulant material and other layers in the PV module by deteriorating adhesive bonds at interfaces between different layers
- Degradation of polymeric materials
- Accelerates the corrosion of metallization elements
- Causes mechanical stress through freeze-thaw cycles
- Plays an important role in PID

Additionally to its contribution to degradation of PV modules trapped humidity can worsen the performance of PV modules by decreasing the optical performance as a consequence of a rise in absorption [7].

UV irradiation
Another important parameter in PV module degradation is the amount of incident UV light [4, 8]. Extended exposure to UV light can trigger chemical reactions and lead to degradation of polymeric materials in PV modules [9]. Like temperature and humidity, the amount of UV irradiation received is also location dependant. Areas with high solar irradiance will receive higher UV irradiance. Altitude is another factor in determining the amount of UV radiation received by a module [23]. This is because at higher altitudes a smaller fraction of the UV light has been absorbed by the atmosphere when reaching the module. This is due to the fact that the light has had to travel through a smaller air mass. For this same reason, locations at low latitudes will also receive a larger amount of UV irradiation compared to higher latitude regions.

Degradation reactions occur because the photons in the ultraviolet region have enough energy to overcome the dissociation energy of covalent bonds of polymers [9]. The degradation of polymers can lead to the formation of water and acetic acid, which can in turn accelerate other degradation mechanisms such as delamination or corrosion of metallic components and can promote PID [7, 9]. There are three distinct regions in the UV spectrum : UVA (315-400 nm), UVB (280-315 nm) and UVC (100-280 nm). UVB is the most damaging region [9]. This is because UVA contributes a higher fraction of the power but its photons have lower energies. The reverse is true for UVC where the photons have higher energies but the fraction of incident power is lower than for UVB [4, 9]. The mechanism behind polymer degradation inside PV modules is not yet fully understood [24]. In the presence of oxygen, photo-oxidation takes place [9]. However, not all mechanisms reported in literature take into account the role played by oxygen [19].

Other stress factors
Mechanical loads are another environmental factor that plays a role in the degradation of PV modules [9, 14]. They can have a wide variety of origins [4, 25]. They can be caused previous to installation during the manufacturing process. They can arise in transportation or installation processes. Finally, the PV module is also exposed to mechanical loads during its lifetime. These can come from wind, hail, snow, etc. Due to the rigidity of the front glass and brittle nature of solar cells and metallization elements mechanical loads can result in the formation of cracks or in fractures [25].

Soiling is the accumulation of unwanted material on the surface of the PV modules. Soiling can be caused by dirt, dust, bird dropping and other elements that can accumulate on the PV surface [11]. Contrary to other stress factors it does not affect the long term reliability of the PV modules but it can affect the power production at a given point in time [4]. The effect of soiling on the power module can have a large variation, it can range from 0.03% after rainfall to 10-30% in dry periods (weeks without rain or cleaning) [10]. One way in which soiling can contribute to the long term degradation of PV modules is by causing partial shading which can lead to hotspot formation [4]. Another one is by the degradation of the anti-reflection coating, this is a result of the dirt and dust settling on the solar panel [11]. This results in a lower optical performance of the module.

High Voltage, PV modules are usually connected in series to increase the system voltage [18]. The module frames are grounded for safety reasons, this gives rise to a voltage difference between the solar cells and the module frame [7, 18]. This voltage difference is the main driving force behind PID which will be explained in the next section.

Internal stress factors, PV modules not only suffer from stress caused by external factors. Internal factors can also be a source of stress, these can originate from the manufacturing processes, material choices and design choices [4]. Poor processing can lead to defects in the module which can increase the rate of degradation [4, 11]. Design choices also have an effect on degradation rates. For example, the choice of encapsulant and choice of backsheet have an important effect on the permeation rate of moisture [7]. One could argue that these should not be classified as stresses due to the fact that they are always present throughout the life of the module. However, they are an important factor to consider when discussing the effect of stress factors on the degradation of the PV module.

1.3. Degradation modes

The stress factors presented above degrade the performance of the PV modules over their lifetime of 20-30 years [11, 16]. The stress factors will cause degradation modes which are physical/chemical processes which are responsible for the decrease in module performance. One of the complications when studying the degradation of PV modules throughout their lifetime is that each stress factor contributes to a variety of degradation modes [23]. Additionally, some degradation modes have an accelerating effect on other degradation modes. In this section, the most common degradation modes will be presented. The main relationships between stress factors and degradation modes are summarized in the figure below.

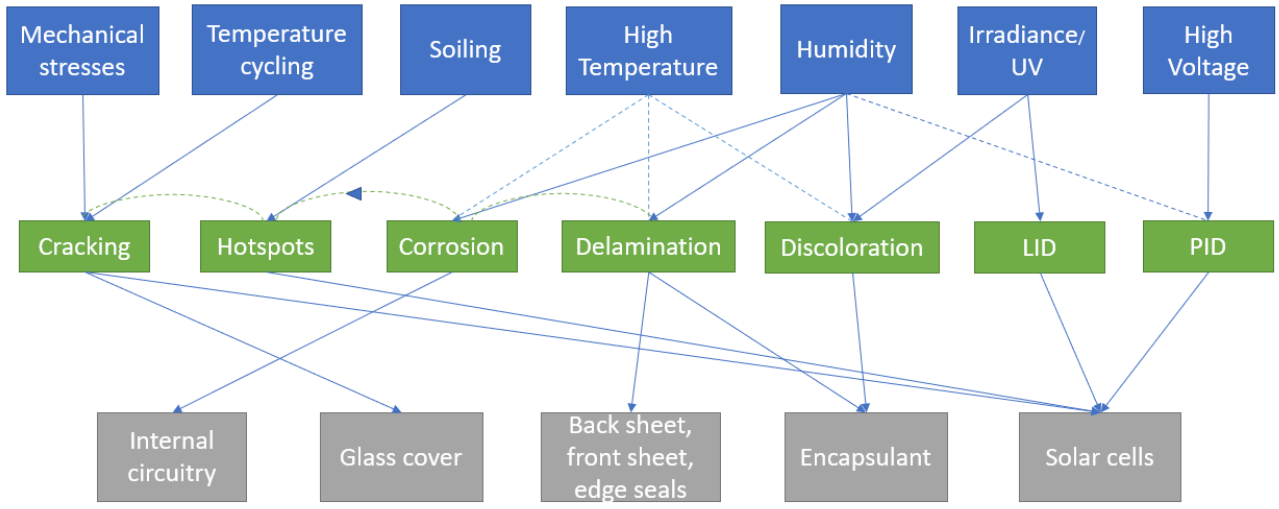

Figure 1.2: Diagram showing the relationship between the stress factors, degradation modes and module components. Only the most important relationships are shown for clarity. Solid lines represent the most important influences. The dashed lines represent secondary influences. Dashed lines between degradation modes represent the accelerating effects that can exist between degradation modes

Discoloration

Discoloration is the change of color of a material of the PV module throughout its lifetime that results in a lower transmittance and therefore decreases the output power [16]. From field studies, it is estimated that between 20 and 40% of PV modules of modules suffer from a form of discoloration at the end of their lifetime [26, 27]. There are two ways in which PV modules can suffer from discoloration, degradation of the encapsulant and discoloration of the grid fingers [11].

Discoloration of the encapsulant is the gradual change of colour of the encapsulant material which turns

light yellow at the beginning of the discolouration process and progresses until the encapsulant material is brown. The origin of the encapsulant discoloration is due to the appearance of chromophores (part of a molecule responsible for the observed colour) that result from EVA degradation [9, 24]. These chromophores have been identified as unsaturated bonds and carbonyl groups [9, 24]. The discolouration process is a result of accelerated by exposure to UV radiation, high temperatures and high relative humidity [11, 16]. Discoloration of the encapsulant decreases the light transmission of the encapsulant layer [16]. This results in a lower short circuit current, I_{sc}. A decrease of 6% to 8% is observed for initial discoloration while for complete discoloration, it can range from 10% to 13% [27]. Additionally, degradation of the EVA produces acetic acid which plays a role in the corrosion of metallization connections, promotes PID and can accelerate delamination [4].

The source of the discoloration of the grid fingers are four different Silver salts: Ag phosphate, Ag-sulphide, Ag-acetate, Ag-carbonate [11, 14]. The discoloration of contact fingers is also related to a different degradation mode called snail trails [11, 14]. These are irregular dark stripes and local discoloration of Silver contact fingers. They appear close to micro-cracks on the solar cells or close to the solar cell edge, however the reason behind their formation is still under investigation [14]. A picture of a module suffering from discoloration can be seen in the left part of Figure 1.3.

Corrosion
Corrosion is the deterioration of materials through chemical reactions with the environment [7, 14]. High temperatures and humidity are the main factors that accelerate corrosion [14]. These reactions can take place with a number of reactants: water, oxygen or other compounds such as acetic acid [4]. The moisture diffuses from the exterior into the PV module while the acetic acid is a degradation product of the EVA encapsulant. This means that the degradation of the encapsulant and delamination of interfaces will have an accelerating effect on corrosion due to the formation of acetic acid and the increase of moisture inside the module [27]. At the same time, corrosion can degrade the adhesion between different layers [16], which can make delamination worse. This is a perfect example of the reciprocal cause-effect relationship that some of these degradation modes have [27]. Corrosion can also cause contact failure which reduces the electrical performance of the module [8]. Metallization elements are susceptible to corrosion and cracking which can be accelerated by high temperature, moisture and the presence of acetic acid [7].

Delamination
Delamination refers to the loss of adhesion at the interface between two layers of the PV module [16]. The interfaces that can suffer from adhesion loss are the encapsulant-front glass, encapsulant-backsheet and encapsulant-solar cells [11, 14]. It occurs more commonly at the edges of the PV module [9]. Delamination is observed when the encapsulant loses its adhesive properties due to prolonged exposure of the PV module to high humidity and temperature conditions [27]. Exposure of the PV modules to salinity is also thought to play a role [9, 16]. Delamination affects the PV module in different ways. It increases the penetration of water into the module by compromising the physical insulation and reduces the optical performance of the module by increasing the reflection of light [11, 16]. Additionally, severe delamination can pose an electrical hazard [9]. To reduce the risk of delamination additives such as hindered amine light stabilizers can be used [9]. However these additives can worsen the discoloration of the encapsulant [9, 7].

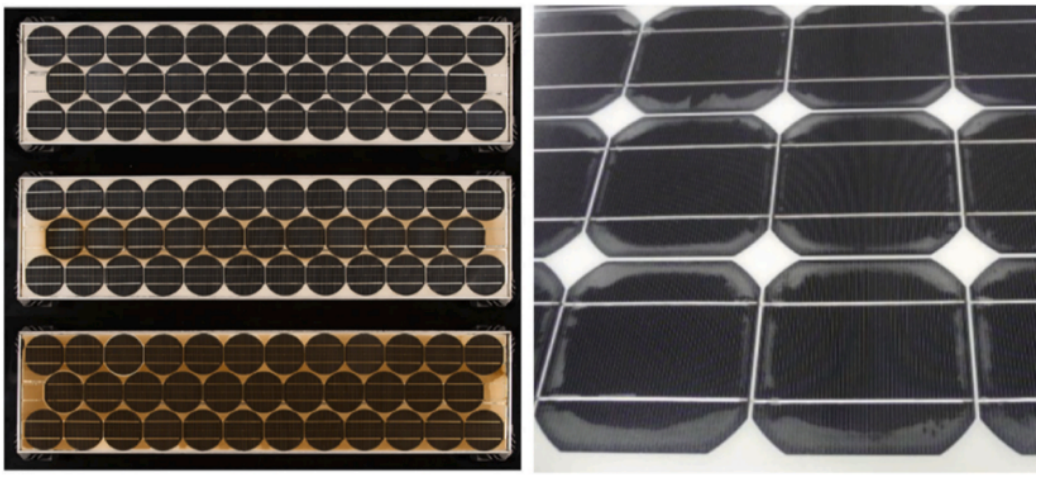

Figure 1.3: Visual representation of module discoloration. From no discoloration to yellowing and then to browning of the encapsulant (left) and module delamination occurring at the edges of the solar cells (right) [4]

Breakages/cracks
Breaks and cracks can appear on the PV module during installation, maintenance and especially the transport of the module to the installation site [11, 27]. They occur due to mechanical stress on the PV modules throughout its lifetime [14]. Micro-cracks can also appear during the fabrication process which are not initially detectable by visual inspection but can grow during the lifetime of the module [11, 14]. Rigid components of the module are more likely to experience breakage/cracks [25]. Cracks in the glass and backsheet can compromise the physical insulation of the module which can result in moisture ingress and electric shock [27]. Solar cells are brittle and rigid which means that they can suffer from cracks [4]. This can result in parts of the cells being disconnected from busbars [25].

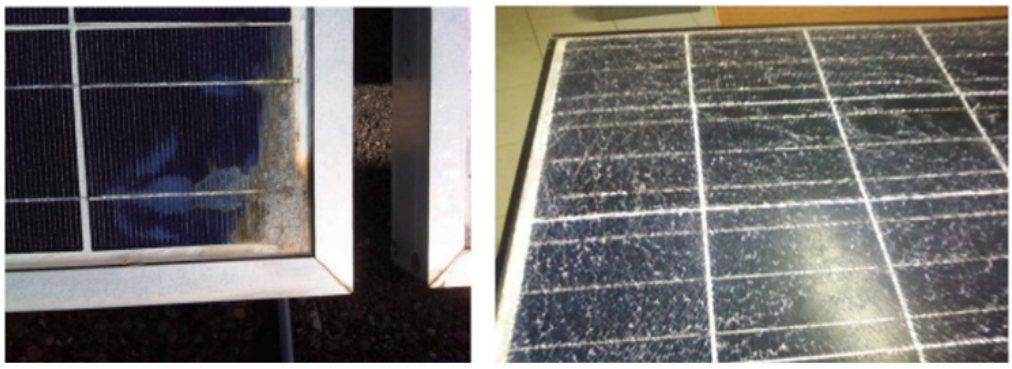

Figure 1.4: Picture of a module where the metallization components have been corroded (Note that in this picture delamination is also observed)[7] (left). Picture of a module with a cracked front glass [11](right).

The front glass cover can suffer from Breakage and cracks. These occur due to mechanical stress, hail, thermal stress and stress suffered during transportation and installation [14]. Micro-cracks formed during manufacturing are difficult to notice by visual inspection, they can result in the appearance of larger cracks. Backsheets and frontsheets can also suffer from cracking caused by exposure to high relative humidity and mechanical stresses [10]. Degradation of the backsheet will compromise the physical insulation of the module [4]. In the case of the frontsheet, its degradation will affect also the optical performance of the module.

Hotspots
Hotspots are areas of the photovoltaic module that have high temperatures which may result in degradation of the solar cells or other module components [11, 27]. Current mismatch between one or more solar cells and the string current makes the cell that is producing less current operate under reverse bias giving rise to the temperature rise [11, 14]. The most common cause of mismatch in current can is partial shading from soiling or other elements blocking one area of the module [14]. Broken cell interconnections can also result in the formation of hotspots [16]. The high temperatures caused by the hotspots can lead to damaged solar cells and broken interconnections [16]. Hotsposts are some of the most commonly observed degradation mechanism, affecting roughly a third of the installed modules [26, 27]. Notably it is the most common degradation mode in the first 10 years of the module's lifetime [26].

PID
PID, which stands for potential induced degradation is a result of the high electrical potential difference between the module frame and the solar cells [4, 16]. The solar modules are generally connected in series to increase the voltage output of the system and the module frames are grounded to protect people from electrical shocks, this gives rise to the electrical potential difference [27]. PID is an umbrella term for all degradation mechanisms caused by the potential difference between the cells and ground [28]. PID-shunting (PID-s) and surface polarization effect (PID-p) are the mechanisms identified for c-si technologies [18, 29]. PID-s occurs when the Na cations contained in the soda lime glass migrate into the solar cell causing a decrease in shunt resistance and a subsequent decrease in power output [18, 30]. Surface polarization occurs when n-type c-Si back-contact cells are subjected to a high positive potential which results in charges accumulating at the anti-reflective coating increasing surface recombination [30].

Light Induced degradation (LID)
Unlike other degradation mechanisms, LID affects the performance of the solar cells directly [31]. This means that the magnitude of the effect and the mechanism behind it will be different for each technology. a-Si technologies suffer from what is known as the Staebler-Wronski effect which can lower the efficiency of the cell by as much as 30% after 100 hours of light exposure [31, 10]. Czochralsky-grown monocrystalline silicon (Cz-Si) are also affected by LID [31]. This effect is linked to boron-oxygen defects in the wafer which results in a decrease in the minority carrier lifetime [12]. Annealing can help recover the lost performance for a-Si and Cz-Si [31]. Multicrystalline silicon wafers do not suffer from LID due to the lower oxygen impurity concentration [12, 31]. CdTe and CIGS technologies show a similar behaviour when exposed to light, they experience an initial increase followed by a long-term decrease in performance [31]. Differences in module architecture and fabrication process are also factors determining the extent of LID suffered by these technologies [31].

1.4. Modelling of degradation
There are a number of ways in which degradation is modeled through the lifetime of PV modules. The two main categories of models that are present in literature are statistical models or analytical models [29, 32]. The goal of the models is to calculate the degradation in performance suffered by a PV module depending on the environmental conditions it is exposed to.

1.4.1. Statistical models
Statistical models or data driven models are models that use statistical analysis of measured performance data to establish the degradation trend of the PV module [32]. The output of these models is generally the percentage by which a performance metric of the PV module has decreased for a given period of time (year, month, day or hour) [32]. Most models return the power degradation over time, other models look at the current or voltage specifically. Statistical models therefore do not the reflect the degradation modes affecting the module [29]. Another drawback affecting all of these methods is that it does not account for different material properties and in order to use it for different PV modules degradation data for the specific module technology is needed [29].

The most commonly used methods are [32, 29]:

- Simple linear regression (SLR) is the simplest method and it consists of fitting the performance data to a linear trend

- Classical seasonal decomposition (CSD) separates the seasonality and irregular components from the data to obtain a clear trend over time
- Seasonal trend decomposition using local regression (STL), similar to CSD but is more robust and can include trends for the first and last 6 months which is a limitation of CSD.
- Autoregressive integrated moving average (ARIMA) is a model which integrates autoregression, differencing and moving average as well as the three previously mentioned methods applied to seasonal trends. ARIMA is specifically developed for economic analysis.

These methods have different advantages and disadvantages in terms of simplicity, robustness and accuracy. STL is considered to be the most effective to predict the degradation rate of PV modules as it results in the lowest uncertainty levels [32]. However, other methods such as ARIMA produce similar results [29].

1.4.2. Analytical models

Analytical models are based on physical/chemical processes that are responsible for degradation of the PV modules and reflect the effect of the different environmental conditions [29]. However, they still do not include the effect of different module materials [29]. Analytical models is the use meteorological data to calculate a degradation rate. Some models focus on one specific degradation mode, they establish the relationship between the degradation mode and one or more environmental factors [29].

Peck model

The Peck model is the most commonly used model to obtain the degradation of a PV module due to the effect of relative humidity [33, 34]. The expression used to obtain the yearly degradation is given by equation 1.3:

$$k_{RH} = k_{0,RH} \cdot exp(\frac{-E_a}{k_B \cdot T}) \cdot RH^{n_{RH}} \tag{1.3}$$

The effect of temperature is also included in this expression as it is an important parameter in determining the rate of diffusion of moisture into the module [17]. The pre-exponential factor, k_0, and the exponential constant, n_{RH}, are empirical constants based on module characteristics [34]. Other examples of models used to determine the degradation rate due to the effect of relative humidity are the Eyring and the exponential model [29], given in equations 1.4 and 1.5 respectively.

$$k_{RH} = k_{0,RH} \cdot exp(\frac{-E_a}{k_B \cdot T} - \frac{b}{RH}) \tag{1.4}$$

$$R_{RH} = k_{0,RH} \cdot exp(\frac{-E_a}{k_B \cdot T}) \cdot e^{(n_{RH} \cdot RH)} \tag{1.5}$$

These degradation rates are meant to reflect the degradation in power output due to the degradation modes that are mainly driven by the effect of relative humidity. These are delamination, corrosion, discoloration and weaken solder bonds [33, 29]. These models use as input the relative humidity of the environment. However, the cause of degradation in reality is the presence of moisture in the module. This amount of moisture in the module is not equivalent to the RH in the environment as the modules are designed to be insulated form the environment. This causes a discrepancy between the climatic stress and the actual effect of the module. By using the ambient condition the difference between insulating capacities between different types of modules is ignored. This difference can be huge for example, if breathable backsheet and glass-glass modules are compared [22]. In order to assess the amount of moisture that enters the module a physical model that takes the relevant physics and material properties into account is needed.

The models also take temperature dependence into account. However, unlike for moisture, there are a number of models that are used to calculate the actual temperature of the module based on ambient temperature and other factors that will affect it such as wind speed and irradiance. These models can be based on a heat balance across the module which are normally referred to as fluid dynamic model [22]. Alternatively, simpler correlations can be used such as the Sandia model [20].

Modelling of UV induced degradation

Exposure to UV radiation is the stress factor that is mainly associated with degradation of polymeric components [9, 33]. Since both temperature and relative humidity and temperature also play a role in determining the

degradation rate of polymeric components an adapted form of Peck's model to include the effect of UV irradiation [33, 35] as can be seen in equation 1.6.

$$k_{UV} = k_{0,UV} \cdot exp(\frac{-E_a}{k_B \cdot T}) \cdot (1 + RH^{n_{RH}}) \cdot UV^{n_{UV}} \tag{1.6}$$

Since the degradation of the polymer encapsulant affects the current generated by the module, k_{UV} is the degradation rate of the I_{sc} [35]. This expression assumes that the degradation is proportional to the UV intensity at a given moment. This is the term UV $[\frac{W}{m^2}]$ in the above equation. To simplify the process or if the spectral data of the incident irradiance is missing, the UV intensity can be assumed to be 5 to 5.5% of the incident irradiance [29, 34].

Modelling Thermomechanical degradation
One way to model the effect of thermal cycles that the PV module is exposed to is to use the Coffin-Manson equation [29, 34]. This expression gives the number of cycles, N, that the module will undergo before failing. This is different from the other expressions shown before since it does not return a degradation rate but a number of cycles to failure instead.

$$N = \frac{1}{\Delta T^{n_T}} \tag{1.7}$$

To model the degradation rate Kaaya et al [33] proposed the following exponential model:

$$k_{TM} = k_{0,TM} \cdot \Delta T^{n_T} \cdot C_N \cdot exp(\frac{-E_a}{k_B \cdot T}) \tag{1.8}$$

As it can be seen from equation 1.8, the degradation rate does not only depend on the temperature variation, ΔT, but also on the cycling rate, C_N. The temperature variation can be calculated using either the flui dynamic model or a simpler correlation [20, 36].

Models for PID
Annigoni et al [37] proposed an adaptation of Hacke's model to include the effect of Voltage, U, in the degradation rate due to PID:

$$\frac{P_{max}}{P_{max(0)}} = 1 - k_0 \cdot exp(\frac{-E_a}{k_B \cdot T}) \cdot RH^n \cdot t^2 \cdot U \tag{1.9}$$

$$R_{PID} = k_{0,PID} \cdot exp(\frac{-E_a}{k_B \cdot T}) \cdot RH^{m_{RH}} \cdot t \cdot U \tag{1.10}$$

The above model gives the evolution of the maximal power output. Other models are based on the increase of leakage currents over time due to PID [29]. These leakage currents are the main way in which PID affects the performance of module by decreasing the output current [30].

Combined stress models
As already discussed, during its lifetime the PV module will degrade as a result of many mechanisms. These degradation modes occur at the same time. Therefore, to obtain a complete degradation model the models of individual stresses/degradation modes have to be combined.

Kaaya et al [33], proposed a unified model in which the effects of Relative humidity, Thermo-mechanical and UV induced degradation are included. The approach proposed consists of calculating the different degradation rates (k_i) using expressions 1.3,1.6 and1.8 and combining them to obtain a final rate k_{tot} in the following way, where β $[year^{-2}]$ is a normalization constant :

$$k_{tot} = \beta \cdot \prod_{i=1}^{3}(1 + k_i) - 1 \tag{1.11}$$

Subramaniyan et al [34], propose a different approach which consists of combining the expressions (1.3,1.8 and 1.6) to obtain an expression that encompasses all the effects. Combining these expressions yields the following expression:

$$k_{tot} = k_0 \cdot exp(\frac{-E_a}{k_B \cdot T}) \cdot (\Delta T)^{n_1} \cdot (UV)^{n_2} \cdot (RH)^{n_3} \tag{1.12}$$

1.5. Research goals and knowledge gap

In the current literature there is a great deal of information about the different degradation modes. The effect that stress factors have on the degradation modes is covered qualitatively. There is not much information about the quantitative effect of stresses on degradation. The most common approach is using analytical models which reflect the physics of the underlying process without modelling it in detail. These models rely on experimental data to be calibrated. This is a problem, as it makes it difficult to evaluate the lifetime of the PV modules if no previous data for a specific module is available. These models have to be calibrated for each module type specifically. However, they can still be used to assess the degradation performance of a given module under different conditions. In order to do so, the stresses caused on the module by climatic factors have to be modeled accurately.

Modelling of module temperature as a function of climatic conditions is an already well understood phenomenon. As already presented, it can be modeled by performing a heat balance over the PV module or using one of the simplified correlations. The UV irradiance that reaches the module can be approximated using the incident irradiance. The analytical models are currently using the RH of the environment rather than the actual moisture concentration inside the PV module. This is can lead to wrong results as the ambient RH does not reflect accurately the actual quantity of moisture inside the module. Therefore, the goal of this thesis is to **study the moisture ingress into PV modules and its effect on the degradation of PV modules.**

In order to answer the research question and achieve the goal of the project the following research goals have been established:

- Create a detailed model to calculate the moisture ingress into the PV module using COMSOL. This model will be based on the relevant physical processes that determine the ingress of moisture into the module. The model will also take into account the effect of material properties on the penetration of moisture into the module. This model will be validated using the available data in literature.
- The moisture ingress model will be used to model the moisture ingress into different modules under different conditions. The different conditions will be taken into account by simulating various locations with different climatic conditions. The effect of different materials will be studied by looking at different encapsulant and backsheet materials. Finally, moisture ingress into glass-glass modules will be studied.
- Use the moisture ingress COMSOL model to relate the moisture ingress to the degradation of the PV module. The goal is to find the best way to adapt the existing analytical degradation models to use the time dependant quantity of moisture in the module instead of using the average ambient relative humidity of a given location.

1.6. Structure of report

In order to answer the above research question the report is divided in the following chapters. Chapter 2 presents the development of the moisture ingress model based on the relevant physical processes. In this chapter, the developed model will also be validated using the available data in literature. Following, in chapter 3, the results of the moisture ingress model for different conditions is presented. The results for different climates and different materials for the encapsulant and backsheet will be analyzed. These results are analyzed in an attempt to try and find a correlation between the results for the moisture ingress model and material parameters and/or climatic conditions. Chapter 4 studies the most suitable approach to use the obtained results from the moisture ingress model to predict the degradation suffered by the module. Finally, in chapter 5, the conclusions of the report are summarized and suggestions for possible future work are outlined.

2

Modelling of moisture ingress into a PV module

In this chapter the relevant theory to understand the moisture ingress into PV modules will be discussed. Based on this theory, a model will be developed. This model is used in the next chapter to study the dependence of moisture ingress on ambient parameters and material properties. Section 2.1 discusses the theory necessary to understand how water enters a module. Section 2.2 presents the different material properties which determine the moisture ingress experienced by a module. Section 2.3 discusses the difference in approach between a breathable and an impermeable backsheet. In section 2.4 the equations that the model uses are presented and in section 2.5 the results obtained from the model are compared with results found in literature. In section 2.6, analytical models and simplified numerical models are discussed as alternatives to the developed model. In section 2.7, some limitations and possible improvements for the model are discussed. Finally in section 2.8 a small conclusion is presented.

2.1. Moisture transport mechanism

Transport of moisture through polymeric materials is a complex process which is not fully understood [38]. The overall process can be described by three steps[38, 39, 40]:

1. Sorption: Uptake of water by material at interface with air
2. Diffusion: Movement of water through the bulk of the polymeric material
3. Desorption: Release of water from the material back into the environment

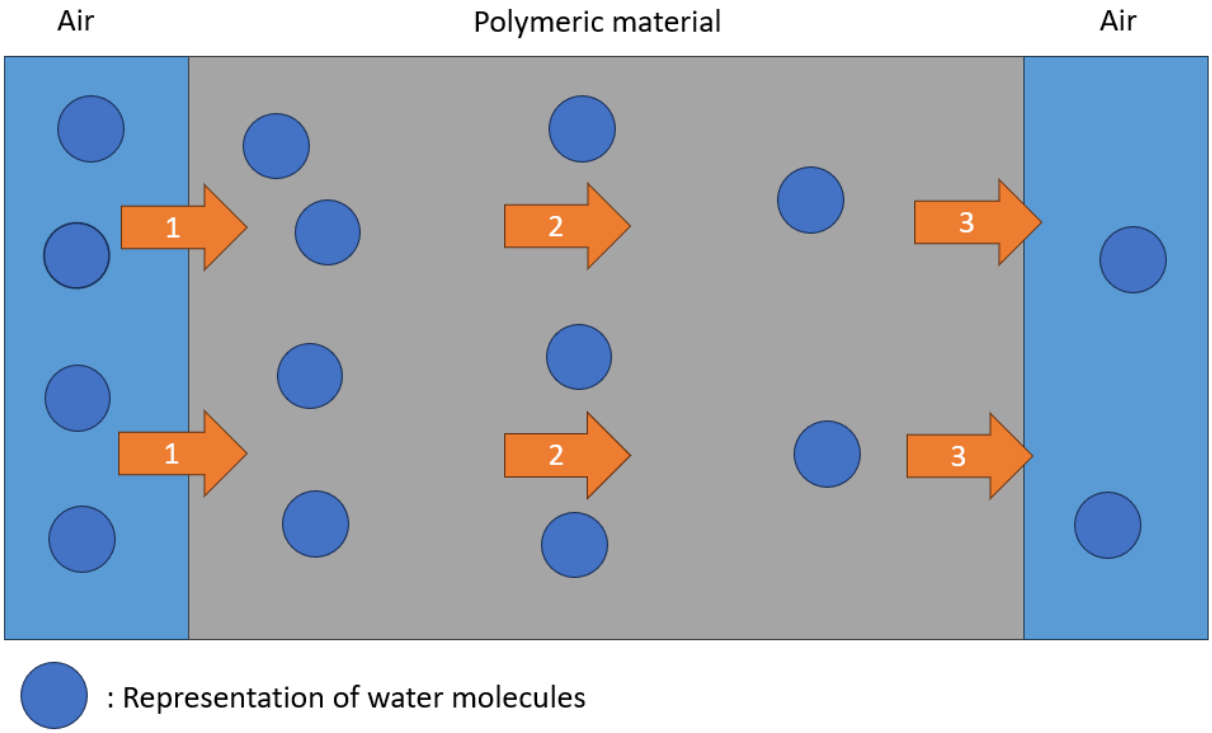

Figure 2.1: Graphical representation of the moisture permeation process through polymeric materials. The number in the arrows correspond to the numbers in the list above. Figure adapted from [40].

In figure 2.1 a graphical representation of the permeation process through a polymeric material is given. When discussing the time scale it takes for moisture ingress into polymeric materials used in PV modules to take place only the diffusion time is important [39]. This is because the time it takes for moisture to diffuse is much larger than the one it takes for sorption/desorption to take place. It is also important to note that in PV modules sorption and desorption do not happen at the same time. This is due to the fact that the module is in contact only with one environment. It is either gaining or releasing moisture back into the environment, not both at the same time. Sorption will happen in times where water is entering the module. Desorption will take place when the module is drying and moisture is exiting the module. However, the diffusion process alone is not enough to describe the quantity of water that enters the module. The equilibrium concentration at the interface needs to be defined. This is done using Henry's equilibrium law [5, 41].

Moisture diffusion in the different layers of PV modules is commonly described using Fick's second law of Diffusion [20, 22]. Fick's laws assume that the transport of moisture in a given material can be described by a single diffusion coefficient, meaning that the materials are treated as one homogeneous phase [42]. Additionally, Fickian theory assumes that the diffusion coefficient is independent of concentration [5, 22].

The motion of small molecules is driven by random molecular motion of individual molecules [43]. This will result in an effective motion of molecules from higher to lower concentration areas. As previously discussed in section 1.2, Fickian diffusion can be described by equation 2.1 (Fick's second law). This equation shows that the curvature of the concentration gradient (the second derivative with respect to position) within a material is the driving force behind the diffusion process. In the equation, D is the diffusion coefficient which relates the rate at which the concentration changes to the driving force for diffusion. C stands for concentration of a species in a given medium, water in the module in this case.

$$\frac{\partial C}{\partial t} = D \cdot \nabla^2 C \tag{2.1}$$

Not all materials exhibit strictly Fickian behaviour [20, 22]. Non-Fickian models can also be used to describe the transport of moisture within a material [7]. For example, Dual transport models have been proposed as

an alternative to Fickian models [42]. These models take into account two main mechanisms to model the diffusion process. There is a number of theories behind the nature of the two mechanisms. They can be based on considering the polymer as two heterogeneous phases with different diffusion coefficients or they can be based on different interactions of the polymer with the water molecules [42]. Dual transport models are a promising method that provides a better fit to moisture ingress measurements. However, there is not a dual transport model that can accurately reflect the physical properties of different materials used in PV modules under different conditions [42]. Therefore, in this work Fick's laws are used to predict the moisture ingress into PV modules. This is the approach followed in literature to model the moisture ingress [17, 20, 22].

2.2. Material parameters

One of the objectives of this project is to include the effect of material properties on the degradation of PV modules. In order to do so, material properties have to be present in the developed model. In this section the material properties that have an effect on moisture ingress will be discussed and relevant values found in literature will be presented as they will be used as model input. EVA was chosen as the material for the encapsulant as it is the most common material for this layer [9]. Choosing a reference material for the backsheet is not as straightforward. This is because they are composed of different layers with different properties and there is not one standard composition [7]. The chosen backsheets are PET (Polyethylene terephthalate) based as it is the most common core layer [7, 44]. Additionally, the role of PET is to prevent moisture ingress [44]. Therefore, it is reasonable to assume that the moisture ingress through the backsheet is limited by the mass transport through the PET layer.

2.2.1. Diffusion coefficient

Many physical characteristics of materials influence the diffusion coefficient (polarity, free volume, cristallinity, cross-linking degree...) of water through a polymer network [42, 43]. However, there is not one model that can describe the dependence on the relevant parameters of the diffusion coefficient [40]. Therefore, it remains an experimentally determined quantity [5, 40].

Diffusion coefficients are dependent on temperature, and this dependence can be modeled by an Arrhenius relationship [5, 45]. The general form of this expression is given by equation 2.2. D_0 is a pre-exponential factor and E_a is the activation energy that will describe the dependence on temperature. Both are experimentally obtained.

$$D = D_0 \cdot exp(\frac{-E_a}{R \cdot T}) \tag{2.2}$$

The glass transition temperature is an important parameter in determining the temperature dependence of the diffusion coefficient [43]. In PV module applications the polymers should always find themselves below their glass transition temperature for a material used in the backsheet and above the glass transition temperature in encapsulants [46, 47]. PET and EVA have a glass transition temperature of 77 and -15 $^{\circ}C$ respectively. Polymers below their glass transition temperature are harder and brittle and have lower chain mobility. In comparison, above their glass transition temperature polymers have a higher degree of chain mobility, unsaturation and free volume [5]. This results in polymers above their glass transition temperature having higher diffusion coefficients [5, 43].

As previously stated, the analysis of encapsulant and backsheet materials will be limited to EVA and PET based materials respectively. In order to carry out the simulations the diffusion coefficient of both materials is needed. An example of the diffusion coefficients for these materials can be seen in figure 2.2. The values for the parameters is given in table 2.1. The encapsulant has a diffusion coefficient orders of magnitude larger than the backsheet.

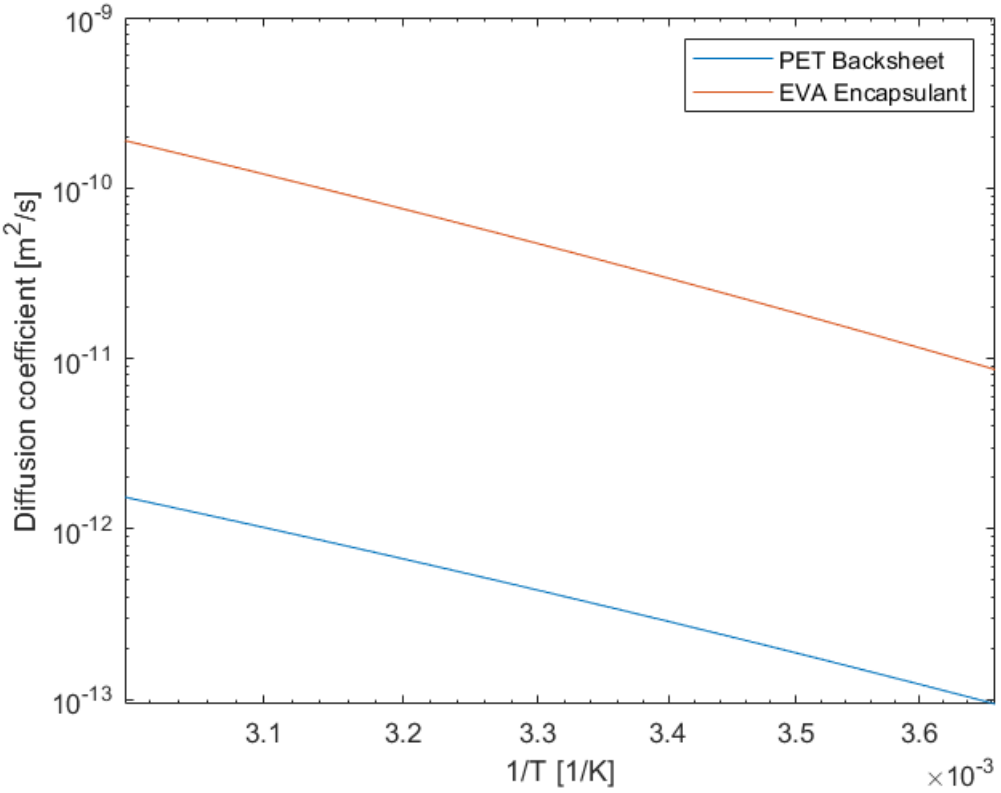

Figure 2.2: Diffusion coefficients of a PET based backsheet and an EVA encapsulant. Based on data from [40]

	$D_0\,[m^2/s]$	$E_a\,[kJ/mol]$
Encapsulant (EVA)	2.46×10^{-4}	38.97
Backsheet (PET)	5.1×10^{-7}	35.2

Table 2.1: Arrhenius expression parameters from different sources for Diffusion coefficient of EVA and PET based backsheets [40].

Additionally, the diffusion coefficient from different sources has been collected to use it as an input parameter in the model and to assess the degree of variability that different values from different sources can present. The parameters given in different sources can be found in table A.1. The values presented in different sources is analyzed in the appendix A.1. The takeaway is that the properties from different sources give results which generally agree with each other. However, in the case of backsheets which can be more varied in nature the results can be quite different.

2.2.2. Solubility

The diffusion coefficient alone is not enough to model how much water enters the PV modules, another quantity is needed to describe the absolute amount of water that is transported [40]. That quantity is the solubility of water in the different components of the PV module. It is important to note that, the term saturation concentration is used sometimes in literature to describe the same concept [22]. The solubility represents the maximum amount of water that can be absorbed in a material [5]. This is described by the solubility coefficient S [45]. This quantity can be given normalized to pressure or not. Depending on this the units of the solubility coefficient will be $\frac{g}{m^3 Pa}$ or $\frac{g}{m^3}$. This coefficient is also temperature dependent. The Arrhenius relation gives its dependence on temperature [5, 44].

$$S = S_0 \cdot exp(\frac{-E_a}{R \cdot T}) \tag{2.3}$$

Solubility for water in polymers is determined by a number of physical characteristics of polymers. Polarity of the polymer is an important parameter, polar polymers (hydrophilic) will have cohesive interactions with the water molecules resulting in a larger solubility [48]. Degree of crosslinking and degree of unsaturation are other parameters that can influence the water solubility of a polymer.

S_0 and and E_a are determined by fitting the above expression to experimental data. One of the drawbacks of the measurements of solubility is that it is not determined directly, it has to be calculated from the permeation coefficient and the diffusion coefficient [44]. The permeation coefficient is the product of the solubility and the diffusion coefficient and is a measure of the absolute quantity of water that is transported through a material [5]. An example of the values for the solubility parameter found in literature can be found in table 2.2. As can be seen in figure 2.3, the reported values indicate that the PET backsheet has a higher water solubility than the encapsulant. When expressed in g/m^3, solubility increases with temperature. This is caused by the increase in the saturation pressure with temperature. When normalizing to pressure, solubility decreases with increasing temperature [5]. This can be explained as at higher temperatures water molecules will move more freely resulting in a larger occupied volume leading to a lower solubility [5].

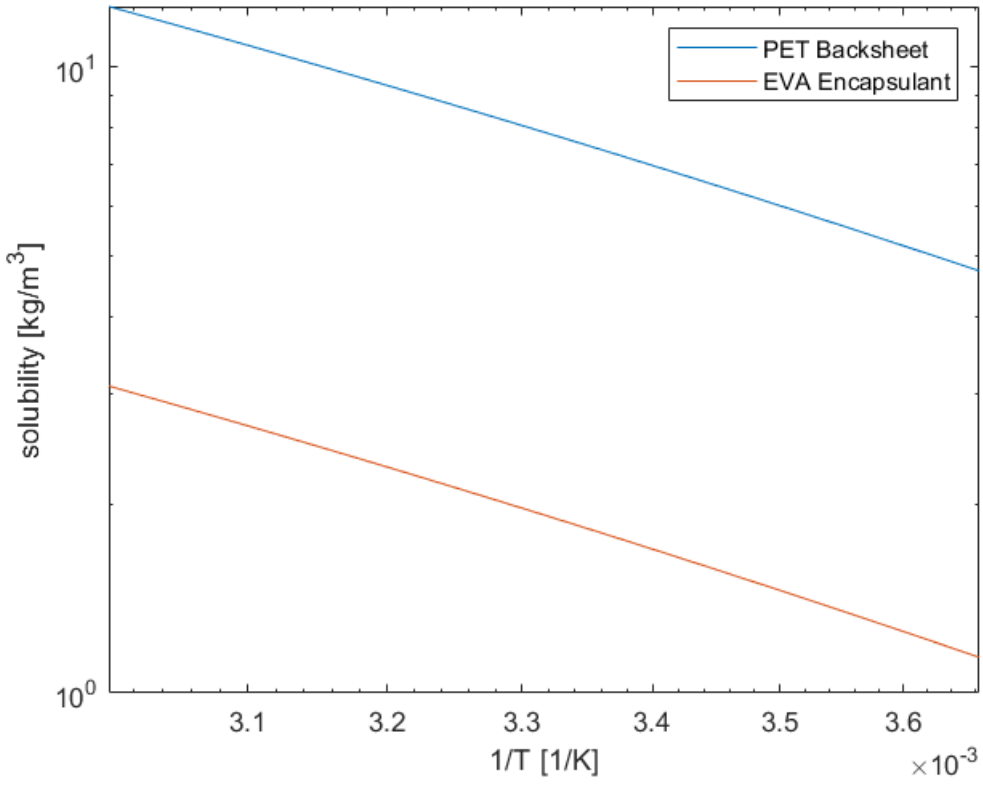

Figure 2.3: Solubility of a PET based backsheet and an EVA encapsulant. Based on data from [40]

	$S_0\ [g/m^3]$	$E_a\ [kJ/mol]$
Encapsulant (EVA)	2.91×10^5	12.58
Backsheet (PET)	1.048×10^6	12.26

Table 2.2: Arrhenius expression parameters for an EVA encapsulant and a PET backsheet [40]

As was done for the diffusion coefficient, values form different sources are also collected for the solubility. The results are analyzed in appendix A.2. Again, the results for the EVA encapsulant show a relatively good agreement while the solubility of PET backsheets varies more.

2.3. Module configuration

Modules can have different configurations depending on the design requirements for a given application [4, 7]. With respect to moisture ingress, one can distinguish between two different design approaches: Glass-Breathable backsheets or Glass-Glass modules [7]. Glass-Breathable backsheets can also be made impermeable by including a moisture barrier in the backsheet. Modules with polymeric transparent front sheets could also be considered as a different design approach. However, the moisture ingress into PV modules of this sort can be understood in a similar way to breathable backsheet modules by including moisture flow through the front sheet as well.

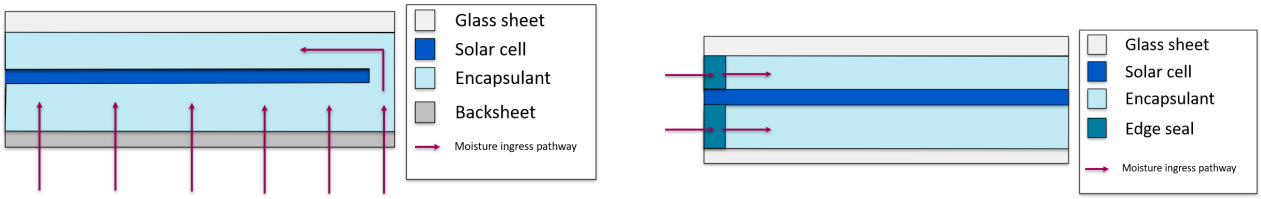

Figure 2.4: left:Schematic drawing of Breathable backsheet configuration; right:Schematic drawing of Breathable backsheet configuration

The module configuration determines the pathways that are available for moisture ingress into the module. In both cases, glass and solar cells can be treated as an impermeable barrier [21, 22]. For the breathable backsheet configuration the dominant moisture ingress pathway is through the backsheet. The only pathway available for moisture to reach the part of the encapsulant between the solar cell and the glass frontsheet is through the gaps in solar cells [21]. For glass-glass modules the moisture ingress pathway available is through the sides of the module. Here, edge seals become an important layer as they are placed in between the encapsulant and the outside environment. In literature, models that do not take into account edge seals can be found [45]. However, this can result in over-estimation of the moisture content in the module as the edge seals serve as protection against moisture ingress. The pathway through the side of the module is also present for breathable backsheet modules. However, the large difference in available area (sides of module compared to back surface) for the ingress of moisture makes this flow negligible [22].

2.4. Moisture ingress model

In this subsection the relevant equations that are needed to model moisture ingress into a PV module will be presented as well as the most important assumptions that were made in order to develop the model. The implementation of the model within COMSOL is also presented.

2.4.1. List of assumptions

- Ambient pressure is 1 atm and remains constant
- No reaction of water is considered with regards to the moisture ingress
- Interfaces are in equilibrium. Henry's law is used to describe the equilibrium. Henry's law states that there is a linear relationship between the concentration of two phases
- Solar cells and Glass frontsheet are taken to be impermeable layers
- The Diffusion of water in the module is assumed to be Fickian
- Material properties are assumed to remain the same through the module's life
- Temperature of module is calculated using Faiman model
- Temperature of module is homogeneous and determines the properties related to moisture ingress
- Backsheet is treated as one homogeneous layer

2.4.2. Model development

Ambient conditions are needed to simulate the moisture ingress into the module in real world conditions. For our model, these conditions are ambient temperature, wind speed, irradiance and relative humidity. The module temperature is calculated taking the ambient temperature, wind speed and irradiance as input parameter for the Faiman model. This model has been used in other papers modelling similar processes and is considered to describe the temperature of PV modules accurately [20]. The equation used is given in equation 2.4 where u_0 and u_1 are experimentally determined parameters equal to 32.6 $[\frac{W}{m^2C}]$ and 3.8 $[\frac{Ws}{m^3C}]$ respectively [20]. If data is available for module temperature this can also be used directly as input for the model.

$$T_{mod} = T_{amb} + \frac{G}{u_0 + u_1 \cdot v_{wind}} \tag{2.4}$$

The driving force behind the moisture diffusion transport between the module and the environment is the difference in concentration. This means that it is necessary to calculate the concentration of water at the interface of the module with the air. This concentration is a function of environmental factors and module material properties. The relevant environmental parameters are relative humidity (RH) and temperature. Relative humidity is defined as the ratio between the actual pressure of water in the air to the saturation at a given temperature [5]. It follows, that the pressure of water in air can the be calculated by multiplying the saturation pressure and the relative humidity. The saturation pressure is temperature dependant and there are a number of expressions that can be used to model the saturation pressure like the Antoine equation, Goff-Gratch equation or the Arden Buck equation [5, 20, 24]. All the previously mentioned formulas give similar results, in this report the Antoine equation is used [24]:

$$log_{10}(P_{sat,H_2O}) = a - \frac{b}{T + c} = 101325 \cdot (4.654 - \frac{1435.264}{T - 68.848}) \tag{2.5}$$

Ambient pressure also plays a role in determining the water pressure in the air. However, in the model a constant ambient pressure of 1 atm is assumed. The material depending parameter that affects the water concentration at the interface is the solubility parameter S. If the solubility of the material is known, Henry's law can be used to calculate the concentration at the interface [22, 49].

$$C_{Amb-BS} = S_{BS}(T) \cdot p_{act}(T) \cdot \frac{1}{M_{H_2O}} = S_{BS}(T) \cdot p_{sat}(T) \cdot RH_{eff} \cdot \frac{1}{M_{H_2O}} \tag{2.6}$$

This expression is valid with the solubility that is normalized with pressure. If the saturation concentration is given without being normalized to pressure the saturation pressure term is removed. In the above equation the molar mass is used to convert the concentration to molar concentration as that is the unit used by COMSOL. The above equation is valid for the interface of the backsheet with the environment, to model a glass-glass module the solubility of the edge seal is taken into account.

RH_{eff} is the effective relative humidity at the interface of the module. This is different than the RH in air because the module and air are not always in equilibrium due to the temperature fluctuations during the day [50]. This can be calculated by using the Magnus equation [17, 50].

$$RH_{eff} = RH \cdot \frac{p_{sat(T_{amb})}}{p_{sat(T_{mod})}} \tag{2.7}$$

The interface between the environment and the outer layer of the module is not the only interface that has to be dealt with. In both module configurations, there is a layer (Backsheet/Edge seal) between the encapsulant and the outside environment. The different layers have different solubilities. By assuming that Henry's law applies at this interface as well [49], one can write a relationship for the concentration of the two interfaces

(Equation 2.8) [22, 49]. The same can be done for the encapsulant and edge seal interface.

$$C_E = K \cdot C_{BS} = \frac{S_E}{S_{BS}} \cdot C_{BS} \tag{2.8}$$

To avoid repetition, the formulas above are given for a breathable backsheet module. When dealing with a glass-glass module the approach remains the same but the properties of the backsheet are interchanged with the properties of the edge seal.

2.4.3. COMSOL model

The model has been implemented using COMSOL Multiphysics 5.6 . In particular, the ”Transport of Diluted Species” physics node is used to model the transport of moisture into the module. The needed ambient parameters are all available in the ASHRAE 2017 database which is easily accessible through COMSOL. The relevant equations (2.2 2.3, 2.4,2.5) are setup as analytical functions. The concentration at the interface of the backsheet and air is given by equation 2.6. The glass frontsheet and solar cells are considered to be impermeable which is implemented using the No Flux condition. The difference in solubility between the backsheet and encapsulant is taken into account by using a partition condition at the interface between the two materials as is defined in equation 2.8.

The moisture ingress in breathable backsheet modules is modeled in 2D as can be seen from figure 2.4. Thanks to symmetry, the moisture ingress is simulated only until half the cell width. The moisture reaches the section between the glass and the cell through the space in between cells. This width of this channel is given half of the spacing between cells due to symmetry. The geometry is further reduced by removing the sections of encapsulant and backsheet where the gradient perpendicular to the moisture ingress direction disappears [20]. A representation of the COMSOL model can be seen in figure 2.5. This is done to decrease computation time. Please not that the Glass cover and the solar cell are added for clarity but are not actually there in the COMSOL model.

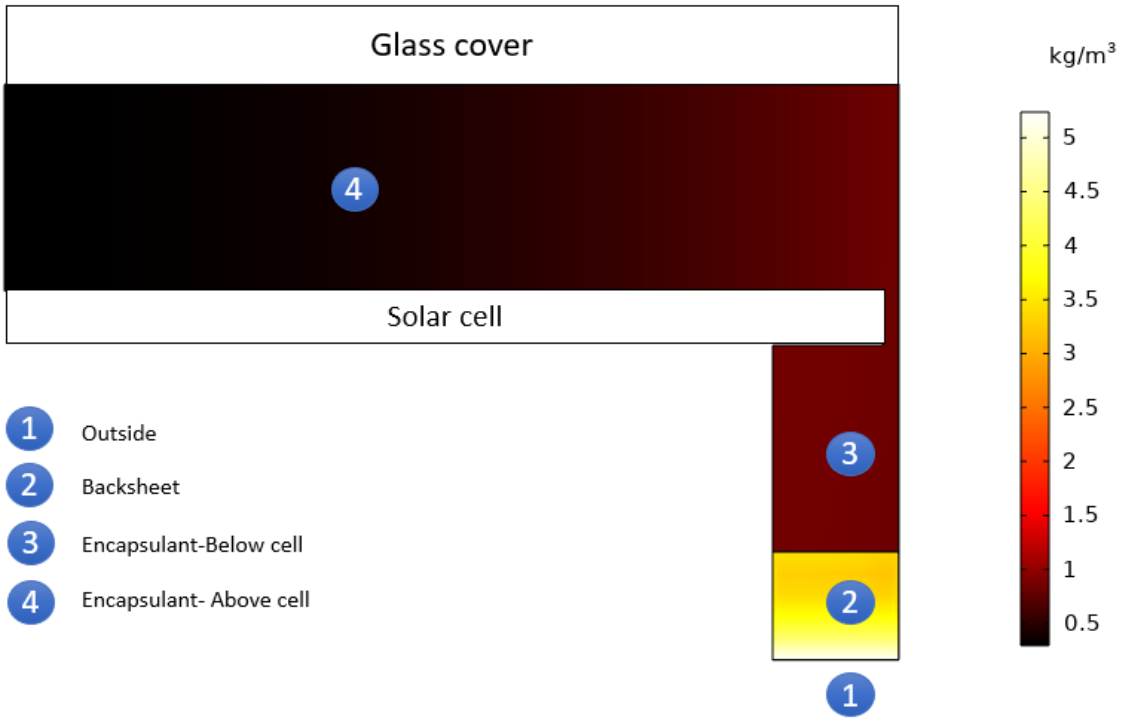

Figure 2.5: Representation of the 2D model in COMSOL. 1: External environment, 2: Backsheet, 3: encapsulant below solar cell, 4: encapsulant above solar cell. Simulation results for a module in Almeria after 1.5 years of simulation are shown as heat map.

The moisture ingress into glass-glass modules is treated as a 1D problem. The moisture ingress is calculated until the middle point of the module (from the shorter side). A representation of the glass-glass model is shown in figure 2.6. The environment would be on the left of the figure and the right of the image goes until the middle of the encapsulant.

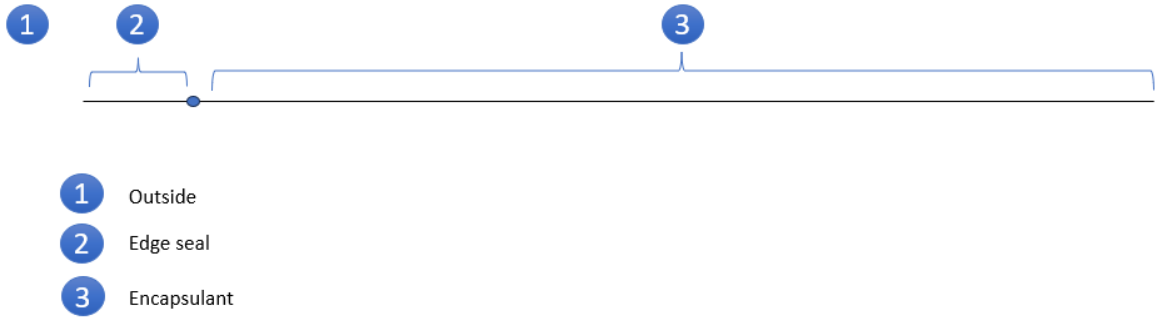

Figure 2.6: Representation of the 2D model in COMSOL. 1: External environment, 2: Backsheet, 3: encapsulant below solar cell, 4: encapsulant above solar cell

2.5. Model validation

Validation of the model should be done by using an experimental method that allows to measure the amount of water that enters the module as a function of time. Permeation based techniques measure the transient

Water vapour transmission rate (WVTR) which allows to determine the diffusion coefficient and saturation concentration of a given material at fixed temperature and RH [51]. These techniques allow to determine the parameters for individual materials not at module level. With those parameters it is possible to determine the permeation and solubility coefficients. If the measurements are carried out at different temperatures, the temperature dependency of these parameters can be determined [51]. Gravimetric techniques are based on measuring the weight change of a sample when it is exposed to a given temperature and RH [45]. These measurements are also usually carried out for individual materials [7]. Techniques based on the presence of degradation products use chemical analysis (some form of spectroscopy) to determine the concentration of degradation products formed by the reaction of water and the encapsulant [52]. It is also possible to use digital humidity sensors to directly measure the amount of water in the modules [53]. These sensors are generally designed to detect RH levels in air. Therefore, a re-calibration step is necessary to use them to measure the amount of moisture in PV module components.

In order to validate the model it will be compared to results found in literature. In order to make a valid comparison to results found in literature the same conditions should be used. This means that the same input parameters must be set: climatic conditions used (RH and Temperature), material parameters for the encapsulant and backhseet (Diffusion and Solubility) and sizing of the module (thickness of all layers, width of module). Not all parameters are always given in literature when results are presented, this makes the comparison harder to carry out.

2.5.1. Damp Heat conditions

During Damp-Heat tests the module is exposed to a fixed relative humidity and temperature [7]. This makes the comparison between results easier as the climatic conditions are known. Additionally, the temperature is fixed, meaning that the material parameters can be considered constant.

One example found in literature is shown in figure 2.7 [54]. In their research they give results for measured and simulated moisture ingress into a breathable backsheet module. The moisture ingress is measured using digital humidity sensors. The values needed to run the simulation are shown in table 2.3. The diffusion coefficient for the encapsulant and the backsheet are given, the thickness of the two materials, the initial concentration of water in the module (C_0) and the concentration at the interface (C_{Amb-BS}) and the module temperature.

D_E	$1.5 \cdot 10^{-10}\ m^2/s$	t_E	0.92 mm	C_0	26.86 mol/m^3,	T	323.88 K,
D_{BS}	$4.32 \cdot 10^{-12}\ m^2/s$	t_{BS}	0.295 mm	C_{Amb-BS}	102.56 mol/m^3		

Table 2.3: Input parameters for the simulation to replicate the results obtained by Kyranaki et al

The model presented by Kyranaki et al. [54] is a 2D model for the backsheet and encapsulant without the presence of solar cells. Our model was adapted to simulate this as well. They also run their model in COMSOL. The results are reported as relative moisture concentration (RMC) [%] which is obtained by dividing the actual concentration inside the encapsulant by the saturation concentration and expressing it as a percentage or fraction.

$$RMC = \frac{C_{encap}}{S_{encap}} \tag{2.9}$$

This quantity is proposed to be a better suited to represent the amount of degradation compared to water concentration [41]. This is because an encapsulant which has a high water concentration but has a very low value for RMC is far from its saturation point. This means that the water in that encapsulant is less likely to cause harmful reactions. For this reason, special focus will be placed on the RMC in the next chapter when analyzing the results of the model.

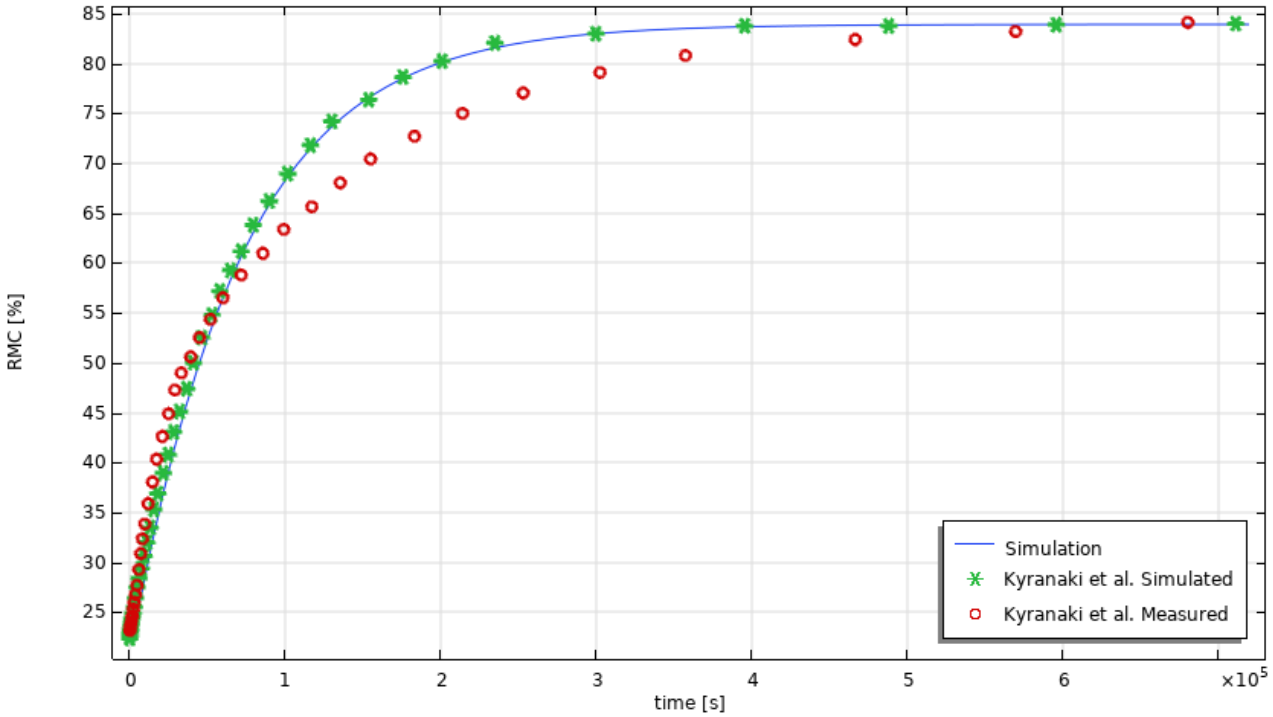

Figure 2.7: Comparison of experimental and simulated results from Kyranaki et al. [54] and results of the model presented in this thesis.

The results obtained from both simulations are relatively close to each other. In the results reported by Kyranaki et al, the moisture ingress into the encapsulant is faster initially. The results are also plotted on a logarithmic time scale so tha the difference between the models at the beginning is more noticeable (Figure A.3). The simulated values converge and reach equilibrium faster than the measured values. The three results converge at the saturation value when the driving force for moisture ingress disappears.

The difference between the simulated and measured can lead to the conclusion that one of the underlying assumptions of the model is not accurate. As already discussed, the Fickian model is not always the most suitable model for the diffusion process that takes place in polymers used in PV modules [42, 54]. Moreover, the sensors themselves are based on a different (unknown) polymers whose behaviour might be affecting the results [54].

Hulsmann et al. [17] developed a similar model to the one presented in this work. The model is set out in a similar way to the one that is shown in figure 2.4 for the breathable backsheet. The dimensions used by them are 350 μm, 450 μm and 200 μm for the thickness of the backsheet, encapsulant layers and solar cell. The width of the solar cell is taken to be 16 cm. In their paper they simulate the moisture ingress for 3000 h of a damp-heat test (fixed RH and temperature) at a RH of 0.85 and temperature of 85 $^{\circ}C$. The material parameters are read from the Arrhenius plots provided in the paper. These parameters are given in the paper with an accuracy of 20% [17]. The solubility of the backsheet is fixed so the same saturation concentration is achieved, the value taken is still within the 20% range accuracy. The solid lines represent two different simulations with our model with the lowest and highest diffusion coefficient within the reported range. The circles represent the data reported by Hulsmann et al. [17]. The blue line represents a point in between the solar cells and the red lines represent a point in the encapsulant on top of the middle of the solar cell.

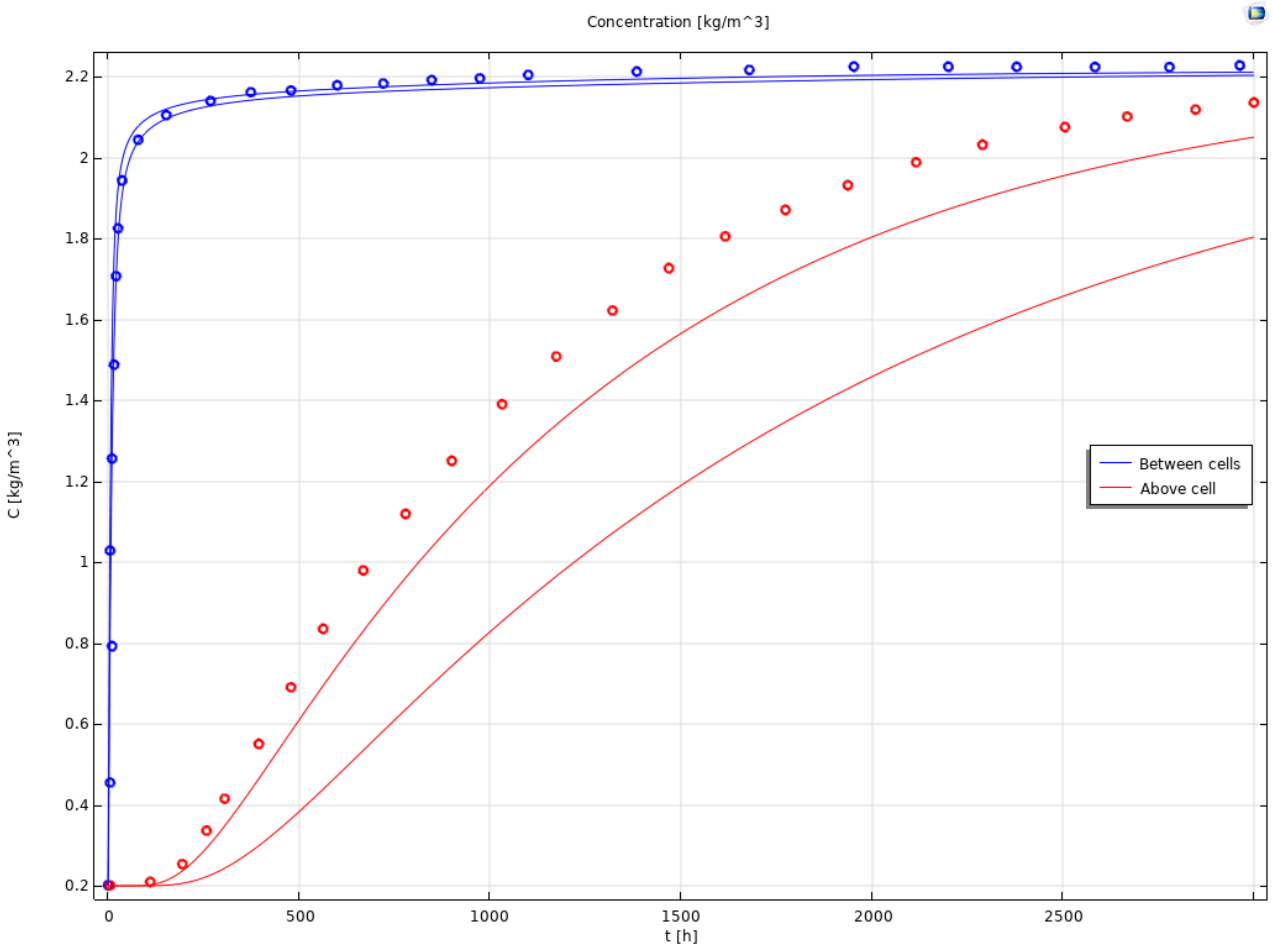

Figure 2.8: Comparison of results of a similar model from from literature [17] and results of the model presented in this Thesis. Solid lines are the results given by our model, the two lines represent results for the model using the upper and lower values for the diffusion coefficient in the range reported in the paper.

The results obtained for the point in between the solar cells are pretty close to the values presented in the paper. For the point on top of the middle of the solar cells the values presented by Hulsmann et al. show a faster increase in the water concentration than even the highest reported value for the diffusion coefficients. Even though, it is outside the reported results it is expected that the curves reach the same saturation level. The important takeaway is that the model shows the correct behaviour when exposed to constant conditions of temperature and RH.

2.5.2. Real world conditions

One of the goals of this thesis is to model the moisture ingress into a PV module in real life conditions. It has already been discussed that measuring moisture ingress into a PV module is not an easy task in laboratory settings. It is not surprising that it is even more challenging to measure it in real life conditions. In the absence of real life measurements, one way to validate our model is to compare it to the results of other models reported in literature. For example, Mitterhofer et al. [20], reported simulation values for 10 years for a module installed in the amazonian rain forest. In this case the sizing of the module is not given [20]. The Diffusion coefficient and Solubility are taken from [40] which can be found tables 2.1 and 2.2. Miterhofer et al. also use the Sandia model to calculate the module temperature.

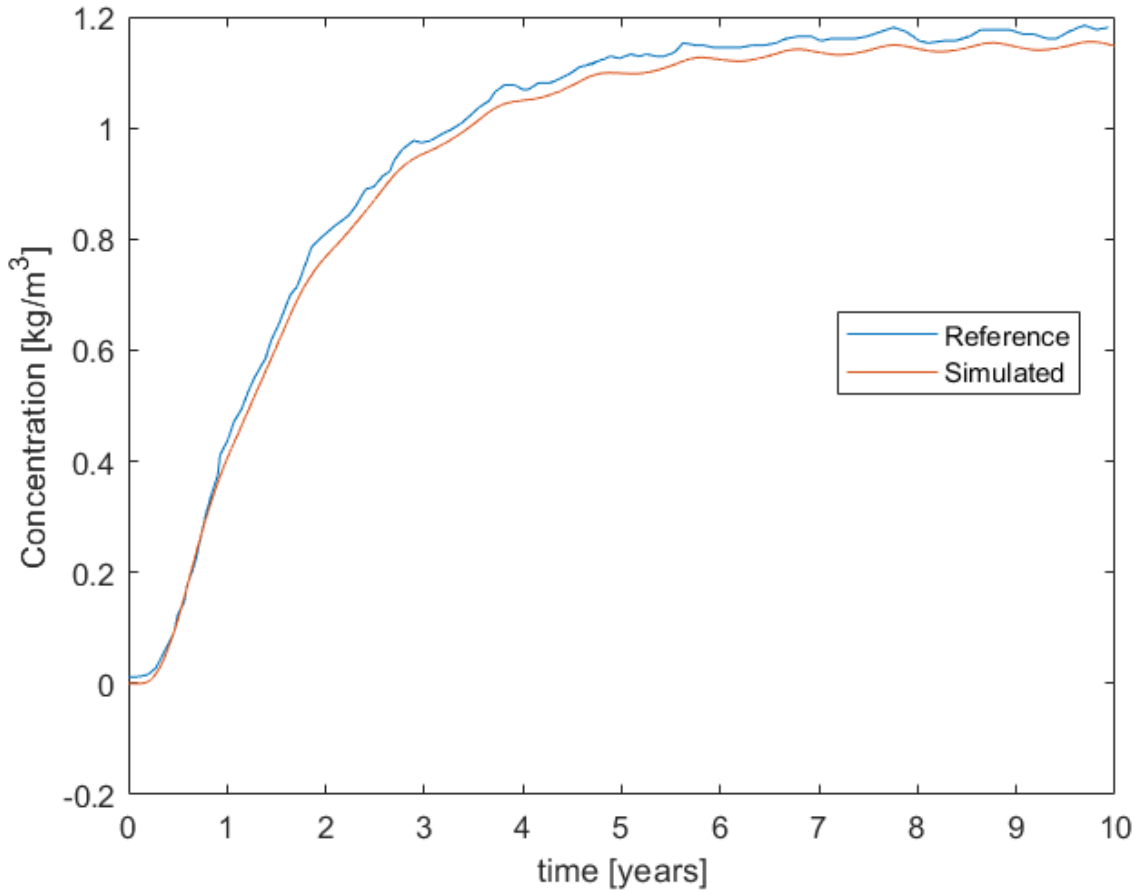

Figure 2.9: Comparison of results of a similar model from from literature [20] and results of the model presented in this Thesis. Simulation for Manaus (Brazil) for a duration of 10 years

The results show great agreement between the two models. The noise in the results reported from literature are due to the way in which the data was adapted (manual measurement). This is a very satisfactory result which confirms that the developed model gives the same results as a similar model given in literature.

2.5.3. Sensitivity Analysis to input parameters

In this subsection the behaviour of the model under different conditions is examined. A temperature range and 50 °C 95 °C is taken. A RH between 0.5 and 0.95 is examined. This is done to understand the behaviour of the model under different conditions to facilitate the analysis of the results in the next section.

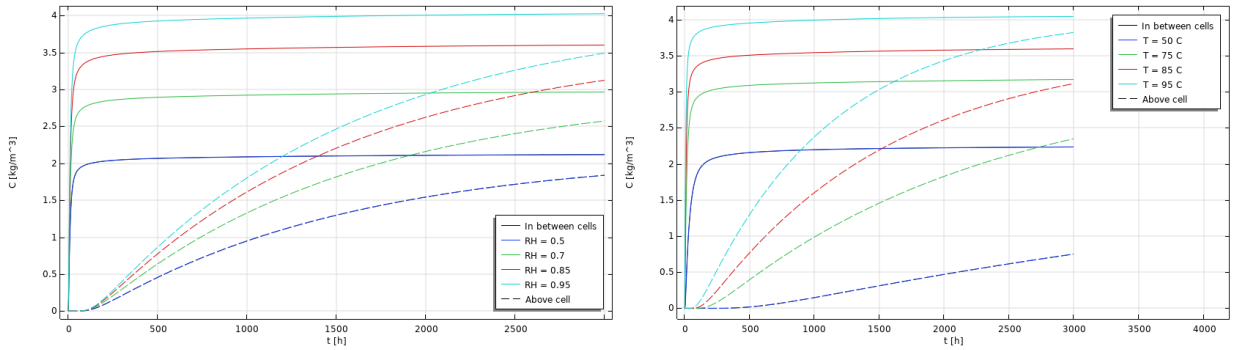

Figure 2.10: Left: Water concentration for different values of RH at a temperature of 85 °C. Right: Water concentration for different temperatures at a RH of 0.85. The results are shown for the point in between solar cells and the point above the middle of the solar cell.

In figure 2.10(left) the results are shown for a range of RH. As is expected, RH has an effect on the equilibrium reached by the moisture in the module. A higher RH will result in a higher water concentration in the module. Interestingly, the RH also has an effect on how quickly water reaches the middle of the solar cell even though it has no effect in determining the diffusion coefficient. This is because a higher RH will result in a higher concentration gradient curvature which will in turn result in faster diffusion. In figure 2.10 (right) the results at different temperatures are plotted. It can be seen that the temperature has a bigger effect on the diffusion speed as the lines between different temperatures are further apart than the ones for different RH. Temperature also affects the equilibrium concentration reached. This is because the solubility increases with temperature. In figure 2.11 the results are shown expressed in RMC instead of concentrations. The results show exactly the same trend for the different RH as the ones for the concentrations. This is because the solubility is the same for all the curves. This is because 2.11 (left) is 2.10 (left) divided by a constant (the solubility of EVA at 85°C). On the other hand, the trends are quite different when different temperatures are examined. This is because in figure 2.11 (right), all curves tend to the same value. That value is the RH of the environment. The difference is expected as the dependence on the solubility is removed, therefore the RMC will always tend to the value of the ambient RH. These insights help us understand the results in the next chapter.

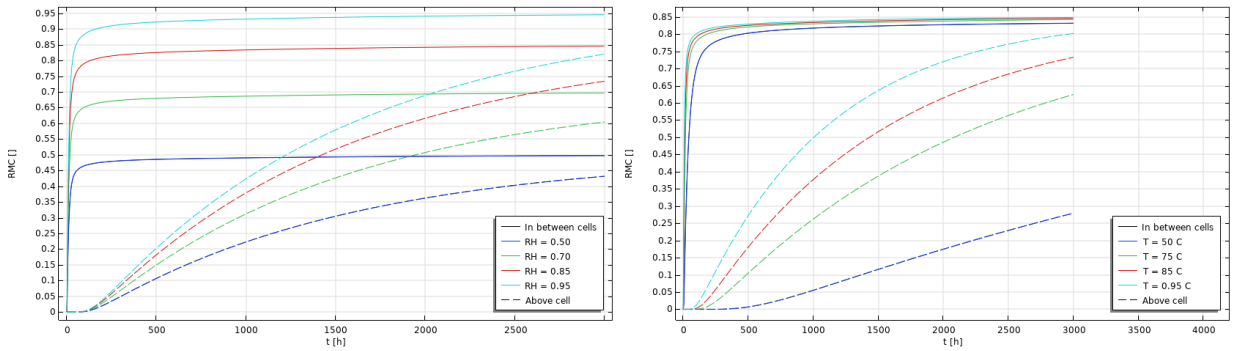

Figure 2.11: Left: RMC for different values of RH at a temperature of 85 °C. Right: RMC for different temperatures at a RH of 0.85. The results are shown for the point in between solar cells and the point above the middle of the solar cell.

2.6. Alternatives to FEM

A FEM analysis is considered the most realistic way to evaluate the moisture concentration inside the PV module [22]. However, it is also the most computationally expensive. There are some alternatives. The first one is to use an analytical expression [22, 55]. These functions take as input ambient conditions and material parameters and can return the moisture concentration in the module at a given position and time. There are

different analytical functions to represent the different geometries. One example of these analytical expressions was proposed by Marwaha et al [55] for a breathable backsheet module. This model consists of equations 2.10 and 2.11.

$$C_{BS}(x,t) = C_{Amb-BS} + \frac{2}{l_{BS}} \sum_{n=0}^{\infty} e^{-\frac{D_{BS}(2n+1)^2\pi^2 t}{4l_{BS}^2}} cos(\frac{(2n+1)\pi x}{2l_{BS}})(\frac{2l_{BS}(-1)^{n+1}C_{Amb-BS}}{(2n+1)\pi}) \tag{2.10}$$

Equation 2.6 gives the concentration of water in the backsheet as a function of time and depth in the backsheet. In this equation, l_{BS} is the thickness of the backsheet. This form of the equation is valid when the module is dry initially. If the module has some moisture present at the beginning, the formula needs to be expanded to account for this. The expansion is given in [55].

$$C_E(t) = \frac{S_E}{S_{BS}} \cdot C_{BS}(l_{BS}, t) \tag{2.11}$$

Equation 2.11 returns the concentration in water in the encapsulant as a function of time. The first thing that can be noticed from this equation is that the concentration in the encapsulant does not have a dependence on position. In other words, the concentration of water in the encapsulant is considered to be homogeneous. The justification for this assumption is that the diffusion coefficient of the encapsulant is orders of magnitude larger than the one of the backsheet [55]. This assumption is valid for the part of the encapsulant between the backsheet and the solar cell. However, for parts of the encapsulant above the solar cell where the diffusion length is much larger this assumption should be revised.

Kempe et al [22] proposed analytical models for glass-glass modules both for 1D and 2D approaches. One limitation of the proposed expressions is that they can only be applied to constant environmental conditions. These expressions have been developed to be used with fixed conditions [22]. Applying them to changing conditions such as the ones that affect a PV module in the real world, results in an over estimation of the daily/seasonal fluctuation of the moisture concentration in the module.

A different approach would be to use a simplified numerical model. Kempe et al [22] proposed a simplified model for the concentration in the encapsulant by assuming that the concentration is uniform in the encapsulant. This is a reasonable assumption if the Diffusion coefficient of the encapsulant is larger than the Diffusion coefficient of the backsheet. The mass balance presented by Kempe et al, is based on the WVTR, this expression can be adapted to include the diffusion and solubility coefficients [49].

$$\frac{\partial C_E}{\partial t} = \frac{D_{BS}}{l_e \cdot l_{BS}}(S_{BS} \cdot RH - C_E \cdot \frac{S_{BS}}{S_E}) \tag{2.12}$$

This simplified model will lower the computational time needed. However, it is only valid for the section of the encapsulant that is between the backsheet and solar cell. On the other side of the solar cell the concentration can't be regarded as uniform. For the same reason, this approach can not be applied to a glass-glass module.

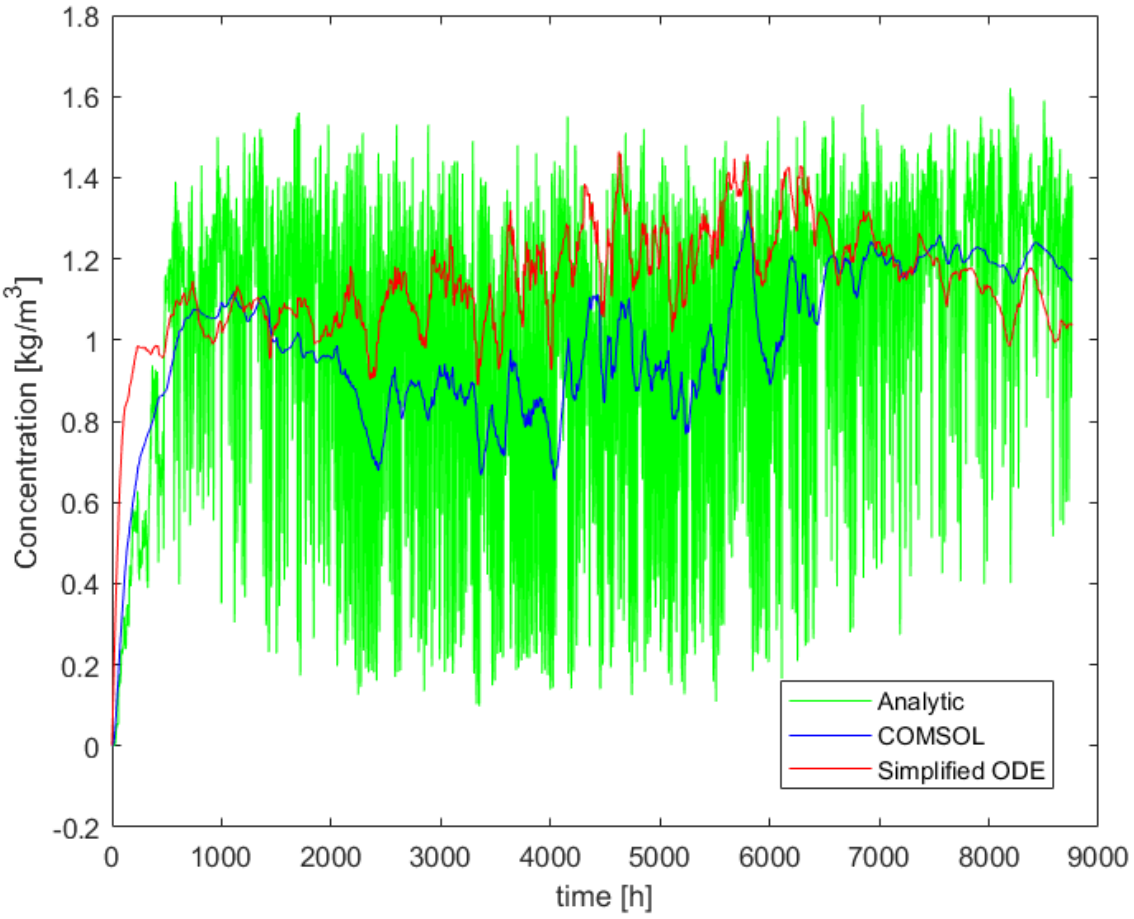

Figure 2.12: Comparing the results for three different models (FEM-COMSOL, Analytic and simplified ODE) for the location of Delft for 1 year

In figure 2.12 the results using the developed FEM model and the two alternative models presented in this section are shown. The simulations are carried out for the location of Delft for one year. It is also important to emphasize that these simulations represent a point at the interface of the solar cell and encapsulant at the back of the solar cell (in between the backsheet and the solar cell). The results of the analytical model stand out as they show a much larger variability than the other two. This is not surprising as the analytical model has been developed to deal with fixed conditions. Applying it to changing conditions over time results in large jumps in concentration. For example, consider the arbitrary situation in which the module is kept dry (not exposed to any humidity) for 3000h and after that it is exposed to an atmosphere of RH = 0,85. The result when time = 3001h will be the concentration of water in the module after 3001h of exposure to an atmosphere of RH = 0.85. This is of course not representative of the situation that is explained above. This effect is quite important as both temperature (affects the material parameters) and ambient RH are changing in real life conditions. One possible way to overcome this difficulty is to take a moving average of the solution.

The results for the FEM model and the simplified ODE model show a similar degree of variability and in general the trend is similar. However, there is a noticeable difference in the values of the concentration. At around 2000h the FEM model predicts that the module will dry more than the simplified model, this gives rise to an offset between the two results. The opposite happens at the end of the simulation where the FEM model predicts a larger moisture ingress than the simplified model. Additionally, the simplified model reaches equilibrium faster at the beginning. These differences could be caused by a large number of things. The models are inherently different, the diffusion coefficient for the encapsulant does not play a role in the simplified

model (It just needs to be larger than the one of the backsheet to justify assuming the concentration is uniform in the encapsulant). The simplified model also ignores the presence of a solar cell and the fact that moisture can diffuse in between the gaps of the solar cells.

2.7. Discussion

2.7.1. Assumption discussion

Some of the assumptions used in the development of the model are extremely robust and there is no reason to doubt them. For example, the glass and solar cell being treated as impermeable [21, 22]. Assuming that the ambient pressure is equal to 1 atm seems also pretty reasonable under most operational conditions of PV modules. Assuming that the temperature is uniform in the whole module is an inherent assumption of using the Faiman model to obtain the module temperature. This model is widely used in papers which carry out similar simulations [45, 20]. Using Henry's law to predict the adsorption at the interface is also a common approach in literature [5, 41].

Other assumptions are a clear simplification of the reality. For example, assuming that water does not react is clearly not true as the presence of degradation caused by water depends on water causing harmful reactions. This assumption just means that the amount of water that reacts is much smaller than the water that diffuses through the encapsulant. If the reaction speed parameters were available for the relevant reactions were available these reactions could be included in the model. The assumption that no material ageing takes place is one of the assumptions that is furthest away from reality. However, no data is available to implement ageing in the model. Assuming that the backsheets are one homogeneous phase is also clearly false. However, this can be justified as the moisture permeation properties are measured for backsheets as a whole. The doubts about Fickian diffusion being an adequate model have already been expressed before. More information is given in the next subsection about a possible alternative.

2.7.2. Limitations of the model and possible improvements

The model presented in this section presents a fair representation of the physical processes that are responsible for the moisture ingress into a PV module. The assumptions made in the model development are in good agreement with what is found in literature. There is a lack of replicable data in literature. The papers that have been discussed that give the necessary data to run the simulations have shown that the results obtained by the model developed in this research is in good agreement with what is reported in literature as is discussed in section 2.5. However, this does not mean that there are no possible improvements that could added to the model to be more realistic.

Supersaturation: One aspect that is relevant in real-life moisture ingress which is not present in this model is that of supersaturation [22]. Supersaturation occurs when the concentration of water is higher than the saturation concentration of water in a given media. This occurs in general when temperatures drop (causing a decrease in saturation concentration) [56]. This is the same process that causes the formation of dew at night. Whether supersaturation occurs or not is determined by the actual concentration of water in the module compared to the saturation concentration at a given time. In particular an important aspect is given by the temperature dependence of the saturation concentration [41]. A module whose solubility is highly dependant on temperature is more likely to experience supersaturation than a module with a less variable saturation concentration. This is because a temperature drop could result in a considerable decrease in saturation concentration. Supersaturation of water in the module can result in faster degradation and loss of optical performance of the module if it happened in front of the solar cell [7]. Another way in which supersaturation is relevant is that it can happen on the surface of the module during the night [22]. The condensation of water on the surface can be a cause of moisture ingress. This is in general not taken into account in moisture ingress models. Kempe et al [22], proposed an approach to factor this into moisture ingress modules by calculating a weighted average in which the driving force of moisture ingress could increase above the allowed limit of saturation. However, this is considered to be outside of the scope of this research.

Material ageing and degradation: Another way in which the model does not reflect the reality of moisture ingress through the lifetime of a module is that it assumes that the moisture ingress is homogeneous for the

whole lifetime of the module. This does not mean that the moisture ingress is constant through the lifetime of he module. As has been shown, it is dependant on temperature and relative humidity which are time dependent parameters. It rather means that there is no difference between the moisture ingress behaviour through the lifetime of the module. For example, the module does not distinguish between moisture ingress between a day in the first year of lifetime and the 19th year if the environmental conditions are the same. This is not realistic, as we have seen that modules experience various degradation modes that can compromise the physical insulation of the modules (delamination,cracking...) [4, 16]. This will mean that moisture can follow different paths as the module degrades. This could be taken into account by defining a second path that ”opens” as the module ages. This would reflect the loss of physical insulation. However, it is not possible to predict the rate at which moisture would enter through this alternative path as there is no data to validate such a phenomenon. A simplification could be made by which the parameters that determine the moisture ingress (D_0,S_0) could be made time varying representing the expected degradation of the insulating capabilities.

COMSOL model optimization: The COMSOL model has been developed to reflect the physical processes with reasonable assumptions. However, the model can still be optimized. In particular, in terms of computation time. For reference, the backsheet model takes around 2 hours to calculate the moisture ingress for 20 years. In order to decrease the computation time two suggestions are given. Firstly, the meshing should be optimized. The regions in which the concentration gradient is less pronounced a larger mesh could be used. In our model, the mesh is uniform for the whole model. Secondly, a combination of geometries could be used. As has been explained, the moisture ingress into a breathable backsheet module can has to be described by a 2D model. However, the part above the solar cell could be simplified to a 1D equation. The water concentration becomes uniform in one of the directions due to the scale difference (thickness vs length of encapsulant). In comparison, the glass-glass model, takes around 40 minutes to make the same calculation thanks to its simpler geometry. Nevertheless, this could still probably be optimized by changing the mesh size.

Non-fickian diffusion: As already mentioned earlier, Fickian behaviour is not always a good fit to simulate moisture diffusion through polymeric materials. This is because these materials can be non-homogeneous resulting in different regions with different moisture transport properties [57]. The main alternative to a Fickian diffusion model are dual transport models. These models take into account two transport mechanisms[42, 57]. Mitterhofer et al [42], proposes a dual transport model to be used in FEM. This model consists of dividing the bulk of the polymer into two regions. The bulk of the material and micro-channels. Diffusion through the microchannels is faster than through the bulk region. The moisture transport is then calculated in the two regions according to Fick’s law using two different diffusion coefficients. The moisture transport between the two regions is also included in the calculation. As acknowledged by the author, this model is only a mathematical model for FEM simulations. It does not have an origin in the material properties. However, it can still reflect the reality of diffusion through polymers [42]: The so called micro-channels could be the free volume in between the polymer matrix. The moisture transport through the free volume is faster than through the polymer matrix. Alternatively, the definition of two distinct regions could be the reflection of the heterogeneity of the polymeric materials. For example, EVA is a copolymer composed of two different polymers vinyl-acetate (VA) and ethylene. VA is more polar than ethylene which can lead to faster diffusion. Additionally VA decreases the crystallinity of EVA which also results in faster diffusion. The different properties of the copolymers can give rise to different regions with different transport properties. The model improves the fitting to moisture ingress measurements. However, it is a mathematical fit of some extra parameters. There does not seem to be one dual transport model that can predict the moisture transport behaviour of all materials in different conditions [42].

2.8. Conclusion

In this chapter, the developed moisture ingress model is presented. In section 2.1 the moisture transport mechanism that is behind the ingress of water into the module are explained. In section 2.2 the different material properties that determine the rate and amount of water that enters the module are presented. Namely, these are the diffusion coefficient and the solubility of the materials. Values found in literature are presented and discussed as they are used as input for the module. In section 2.3 differences in approach when modelling a breathable backsheet module and a glass-glass module are presented. The main difference is the moisture ingress path. For a breathable backsheet module moisture enters through the backsheet which is exposed to ambient conditions. For a glass-glass module moisture enters through the side passing through the edge seal.

In section 2.4 the relevant equations that constitute the model are presented.

In section 2.5 the model is validated with experimental and simulated data from literature. The model gives a good agreement with the results presented in literature. This is proof that the developed model is up to the standards of what is presented in the current literature to model moisture ingress into PV modules. In section 2.6 alternatives to FEM models are quickly presented. These are and analytical model and a simplified model consisting of one ODE. The analytical model shows difficulty in treating time varying data as input as it was not developed to do so. The simplified ODE model provide results in accordance with the results given by the FEM model. However, it is only useful for the encapsulant between the solar cell and the backsheet. It can not be used for the part of the encapsulant that lies between the cell and the glass sheet. Finally a thorough discussion of the limitations and possible improvements for the model are presented in section 2.7.

3

Moisture ingress model results

In this chapter the developed moisture ingress model and moisture induced degradation will be used to asses performance of PV modules under different climatic conditions. Using the moisture ingress model, the amount of water entering a module through its lifetime will be modeled. These results will be used in the next chapter to assess the moisture induced degradation that can be expected under those conditions. Additionally, the different materials that can be used to influence the moisture ingress will be studied. Four different encapsulants and four different polymeric backsheets will be analyzed. Moreover, the effect of using a impermeable backsheet will be modeled.

3.1. Location dependence

The location in which the module is located will determine the climatic conditions it is exposed to. In this section the effect of installing modules in different climates will be investigated. Climates can be classified according to their characteristics using the Koppen-Geiger climate classification [10]. The Koppen-Geiger classification consists of five major climate types [58]:

- Tropical: Have average temperatures above 18 $^{\circ}C$ for the coldest month and generally high precipitation. The chosen locations for Tropical locations are Gran Canaria (Spain), Manaus (Brazil) and Jakarta (Indonesia)
- Arid: Have very low precipitation (below a certain threshold relative to the worldwide precipitation levels). There can be hot and cold arid climates. The chosen locations for this type of climate are Negev (Israel) and Almeria (Spain) and Puno (Chile)
- Temperate: Have temperatures between 0 and 18 $^{\circ}C$ for the coldest month. There are Temperate climates that experience high and low precipitation. Los Angeles (USA) and Freiburg (Germany) are analyzed
- Continental: Temperature above 10 $^{\circ}C$ in the warmest month and below 0 $^{\circ}C$ in the coldest month. Portland (USA) and Oslo (Norway) are chosen to be studied further
- Polar: The hottest months have a temperature below 10 $^{\circ}C$. Zugspitze (Germany) is chosen to represent polar climates

It is important to note that the climates are classified mainly according to temperature. Only arid climates are classified according to the amount of precipitation that they experience. The climate types discussed above are only the first level of classification. The whole classification is made of one or two more subcategories for each climate type [58].

The climate data is taken from the ASHRAE 2017 database. This database is already available within the simulation software COMSOL. The necessary climate data is: Ambient temperature, ambient relative humidity, wind speed and Global horizontal irradiance (GHI). The GHI is taken as the incident irradiance on the modules, this means that it is assumed that the modules are installed horizontally. When looking at the input data, it was noticed that the ASHRAE database does only includes a daily value for the GHI (the value at noon), this data does not have the daily fluctuation in irradiance that the module will experience in real life application. Therefore, the GHI is taken from Meteonorm database for all locations.

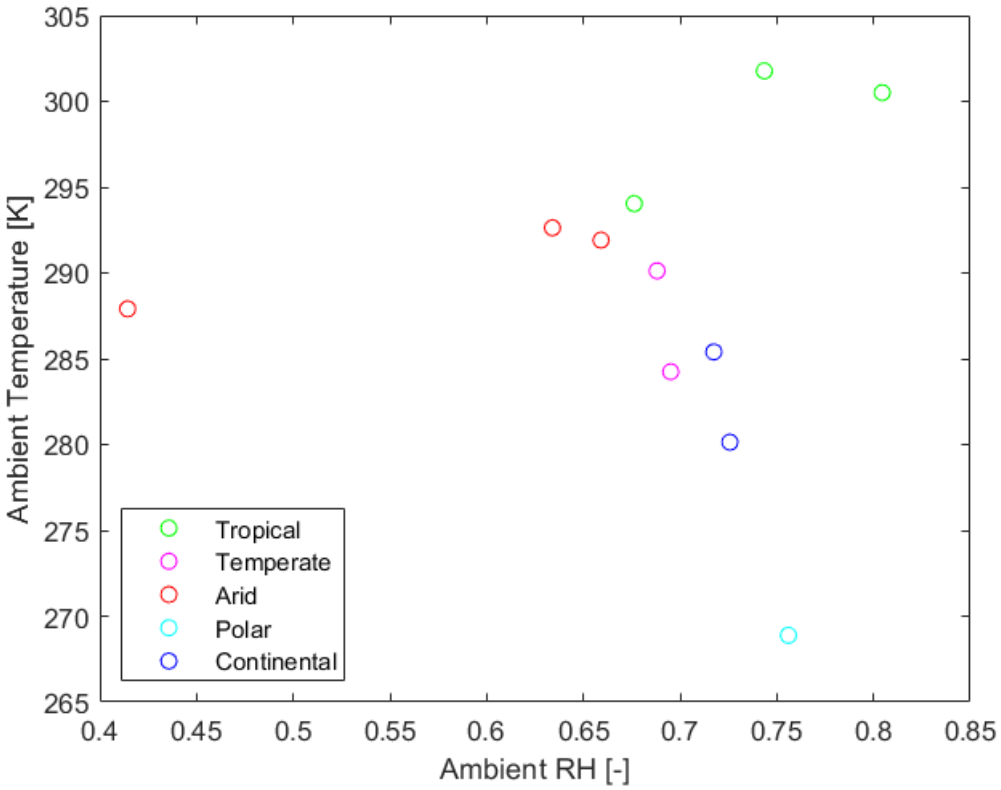

Figure 3.1: Average RH and ambient temperature for each location

Figure 3.1 shows the average ambient RH and temperature. It can be seen that while some of the locations have climates that fall within what would be expected for that climate type the distinction is not so clear for other climates. The tropical climates have the highest temperatures with high relative humidity. Among the tropical climates, Gran Canaria stands out as it has a relatively lower RH and temperature. This could be due to the fact that the interior of the island presents characteristics of arid climates. Temperate and continental climates show similar characteristic ambient conditions. Continental climates have in general lower temperatures and higher relative humidity than temperate climates. The Polar climate has the lowest temperature and a relatively high relative humidity. Arid climates are characterized by a high temperature and low humidity. This is the case for the location of Puno. However, the other two arid locations (Almeria and Negev) have a higher humidity than expected. This is likely caused by the proximity of both locations to large bodies of water. The proposed climate classification will be used for the rest of the section. However, it has to be understood that the classification is not clear cut when it comes to certain locations. Therefore, the results will be analyzed in terms of average climate conditions rather than according to the climate classification.

Another interesting factor that is important to understand the results for moisture ingress is the range of temperatures and humidities that the module will experience. The temperatures and humidities can vary during the day and during the year. Figure B.1 shows the same data as Figure 3.1 but it includes the averages for the hottest/coldest and most/least humid months as error bars on each point. What stands out from this data is the small variation in temperature experienced by some locations (Manaus, Jakarta and Puno), this is due to the proximity of these locations to the equator. Also interesting is the broad range of RH experienced in the arid location of Puno. This information will enable us to understand the results for the moisture ingress model.

3.1.1. Moisture ingress in different climates

The results for the moisture ingress model for the different climates is shown in figure 3.2. The plots show the RMC averaged over one day. The actual results without averaging over one day can be found in the appendix

in figure B.2, this data show the daily fluctuation due to the temperature difference between day and night. This difference in RMC is not due to an actual change in the concentration of water but rather to a change in water solubility due to the effect of the change in temperature through the day. This makes it harder to interpret the overall trend. The results for the concentration over time for the different climates can be found in the appendix in figure B.3.

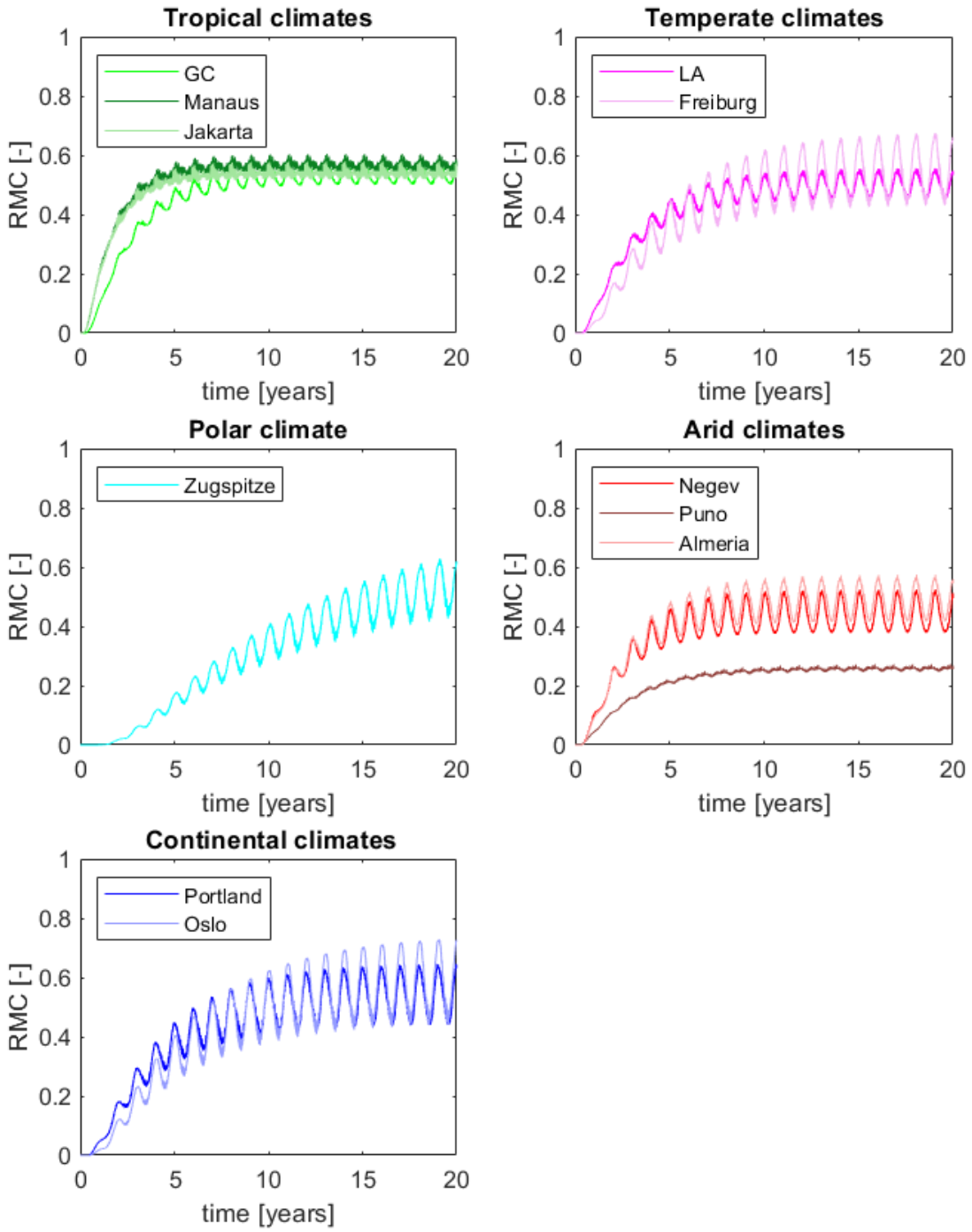

Figure 3.2: Daily averaged RMC for the different climates

The results for tropical, temperate and continental climates agree well within their respective climate types. In the arid climates, the results for Puno differ a bit from the other two in two ways mainly: the RMC shows a much smaller seasonal variation and the saturation level is significantly lower. This is caused by the more stable temperature through the year and the lower RH values that were highlighted above. The locations that show the least seasonal variation for the RMC value are the locations with the least variation in temperature. Similar results are obtained for the concentration of water inside the module. With the difference that the seasonal variation disappears almost entirely. This is due to the fact that the seasonal variation in the RMC is accentuated by the seasonal difference in temperature.

In order to analyze in more detail these results and find what correlations exist between the moisture inside the module and the climatic conditions, the following aspects will be studied:

- **Lifetime moisture ingress**: the average values for the RMC and moisture concentration through the life of the module. This is an indication of the overall effect of moisture ingress through the lifetime of the module.
- **Equilibrium moisture ingress**: this is the average values for RMC and moisture concentration for the 20th year that is simulated. This is analyzed to establish which climatic conditions have an effect on the equilibrium level reached by the module independently of the time it takes for the module to saturate. This is termed equilibrium because for most modules at the 20th year of simulation the value has stabilized.
- **Moisture ingress time**: This is defined as the time it takes for the RMC of water in front of the cell to reach a value of 0.05. This will give us information about the dynamics of moisture ingress in relation to the ambient conditions. In particular, how much time the module remains dry under different conditions.
- **Moisture saturation time**: This is defined as the time it takes for the RMC of water in front of the cell to reach a value of 95% of the equilibrium value obtained in the 20th year. This of course is an indication of how fast the equilibrium value is reached.

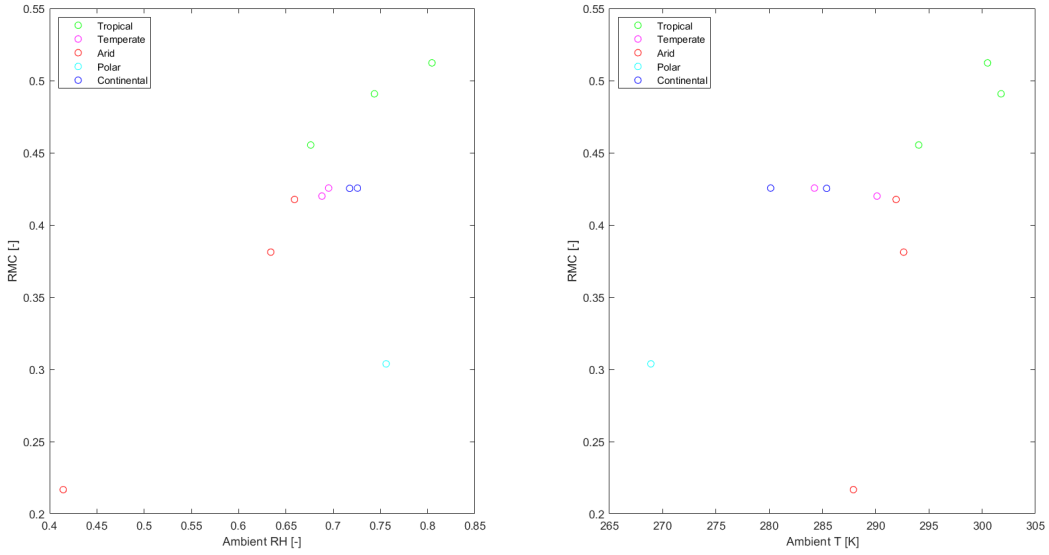

Figure 3.3: Average RMC through the lifetime of the module as a function of the ambient conditions.

The results shown in Figure 3.3 show the averaged RMC through the lifetime of the module as a function of the average ambient temperature and relative humidity of each climate. Figure 3.3 shows that there is a clear correlation between the ambient RH and the RMC of the module. Nevertheless, there is one point that does not follow this trend, the polar location has a relatively high RH but has one of the lowest RMC. This is due to the fact that moisture diffuses more slowly in the polar climate due to the lower temperatures. This causes the average RMC to be lower than the saturation RMC. The connection is less clear when it comes to temperature and RMC. However, there is a trend that indicates that higher temperatures result higher RMC. Again, this

is likely due to higher temperatures causing higher diffusion speed which results in a higher RMC when the average through the lifetime is taken.

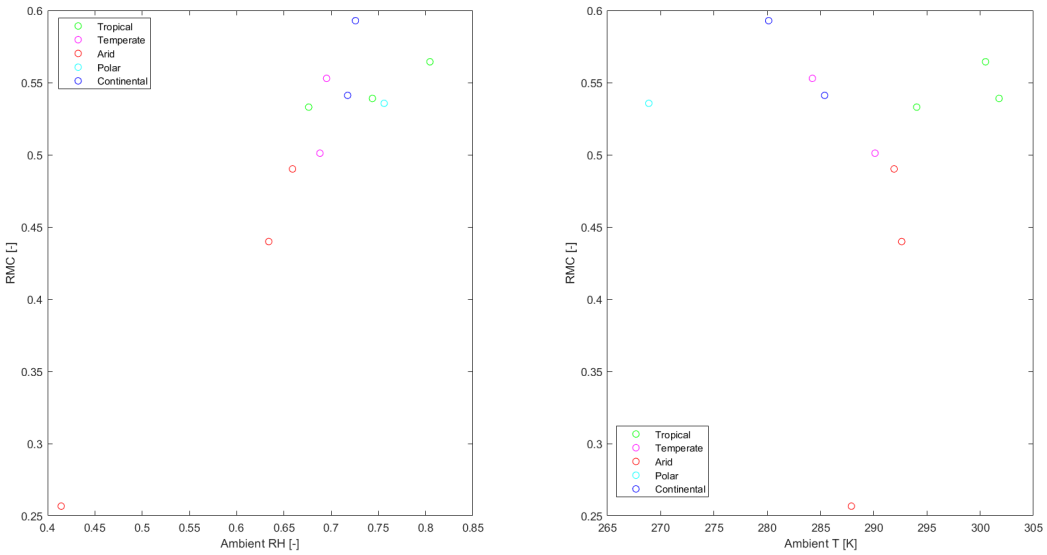

Figure 3.4: Average RMC of the 20th year of simulation as a function of the ambient conditions.

In order to study the connection between the climate conditions and the equilibrium RMC, the average of the RMC is taken only during the 20th year of simulation. The results are shown in Figure 3.4. The trend connecting the RMC level to the ambient RH remains and the outlier of the polar climate observed before conforms to it. On the other hand, when one looks at the results plotted against the average temperature the appearance of a trend is completely gone. This confirms that the climatic stress that determines the RMC equilibrium point that is reached is the ambient RH. However,the trend observed in Figure 3.4 (left), raises another question: what determines the disparity between the equilibrium RMC and the average ambient RH? One possible source of this discrepancy is the definition of the effective relative humidity in the model.The effective RH is defined to take into account the difference between the ambient RH and the RH at the surface of the module. The results are shown in figure 3.5, it can be seen that the effective RH at the surface of the module is closer to a 1 to 1 equivalence to the module RMC than the ambient RH. However, there is still a mismatch present.

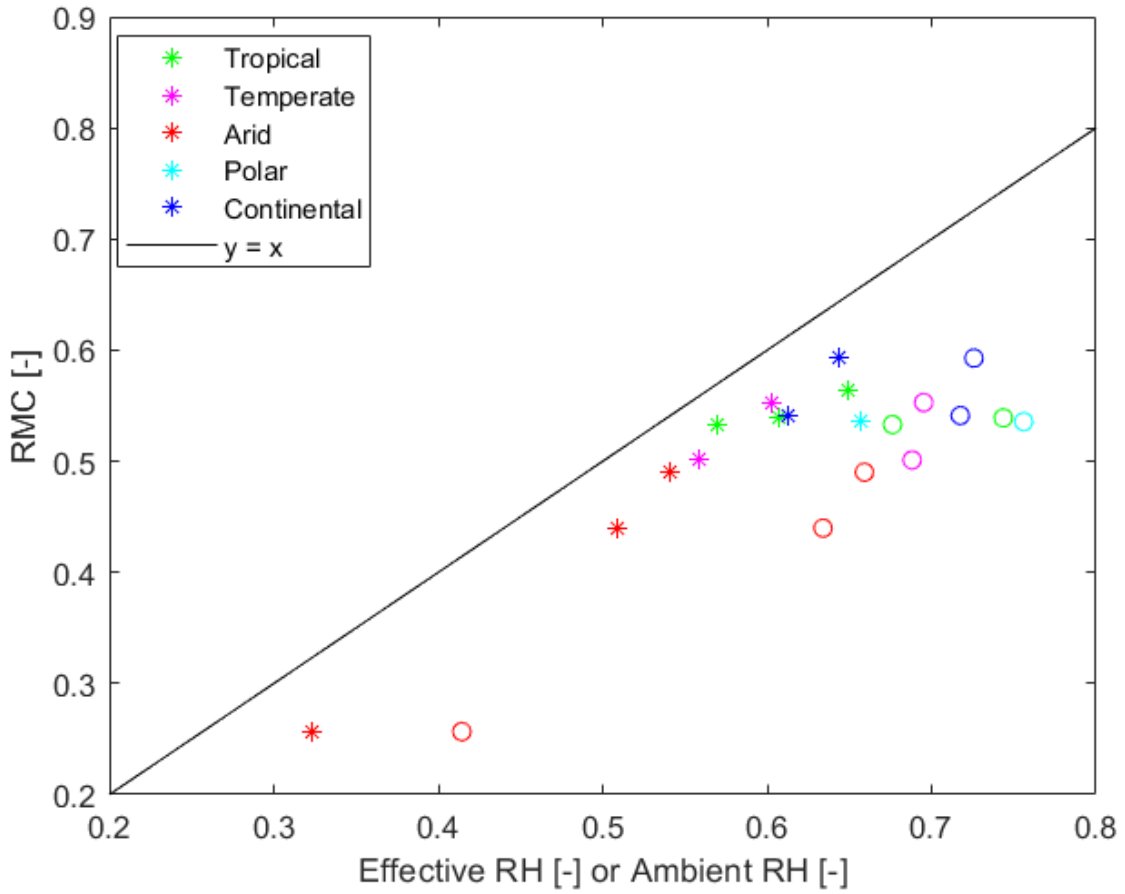

Figure 3.5: Average RMC of the 20th year of simulation as a function of Effective RH (*) and Ambient RH (○).

The same analysis is carried out for the average water concentration through the 20 years and in the last year. The results can be found in the Appendix in figure B.4 and figure B.5 respectively. The major difference is that when looking at the concentration, a connection to the temperature also appears due to the dependence of the solubility on temperature.

The results indicating that it is possible to predict the RMC at equilibrium prompt the question of whether it is possible to do the same with the water concentration. The same approach is followed as for the RMC. In this case the average equilibrium concentration of water in EVA is taken. The average equilibrium concentration is given by the effective relative humidity multiplied by the average solubility of the encapsulant. The results are given in figure 3.6. Again, it can be seen that the average equilibrium concentration of the encapsulant is a good predictor of the average concentration in the 20th year of simulation.

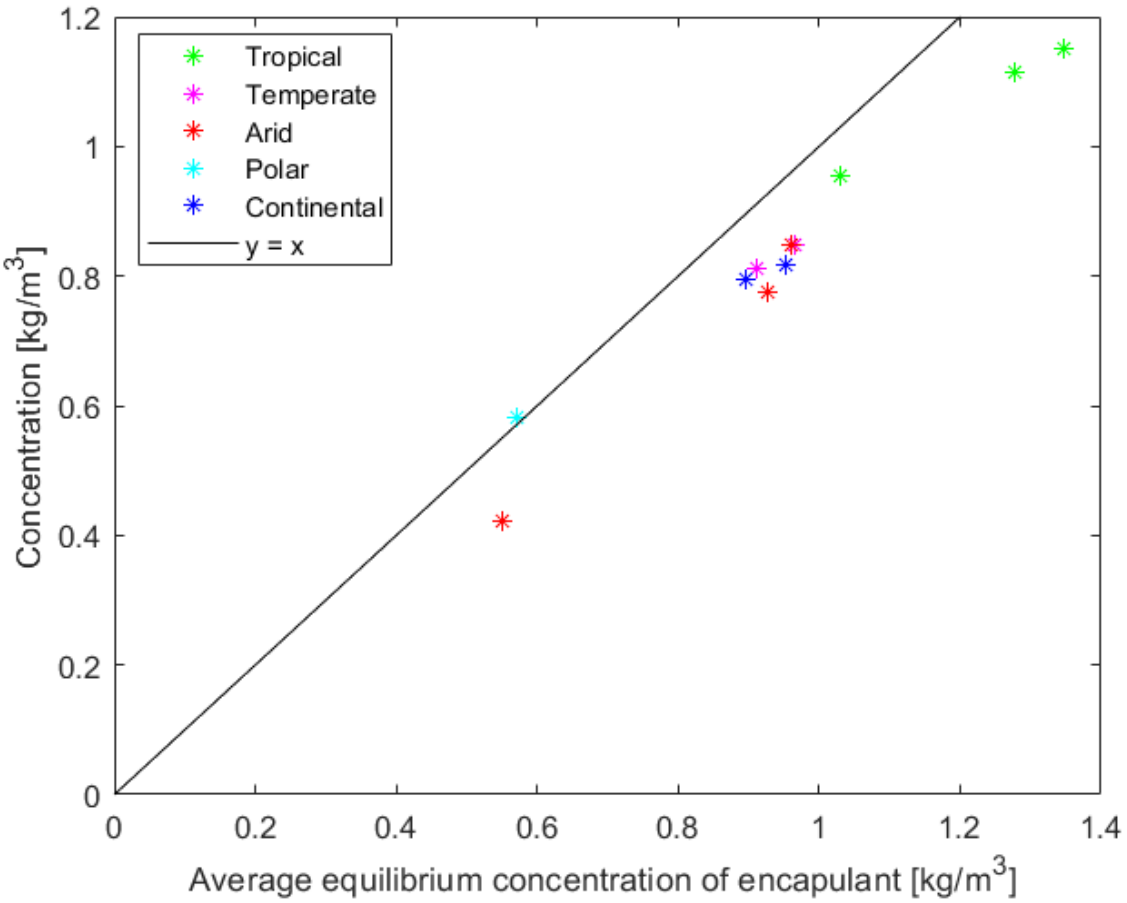

Figure 3.6: Water concentration in the 20th year of simulation vs the average equilibrium water concentration in the encapsulant for the different locations

The above results mean that it is possible to predict the equilibrium concentration or RMC of moisture that is reached without the need for a FEM analysis. These quantities can be approximated by the effective ambient RH and the equilibrium concentration of the encapsulant. Still, the big advantage of a FEM analysis over using such approximations is the ability to predict the time evolution of these quantities. That is why the next step is to analyze the moisture ingress time and in particular the moisture saturation time.

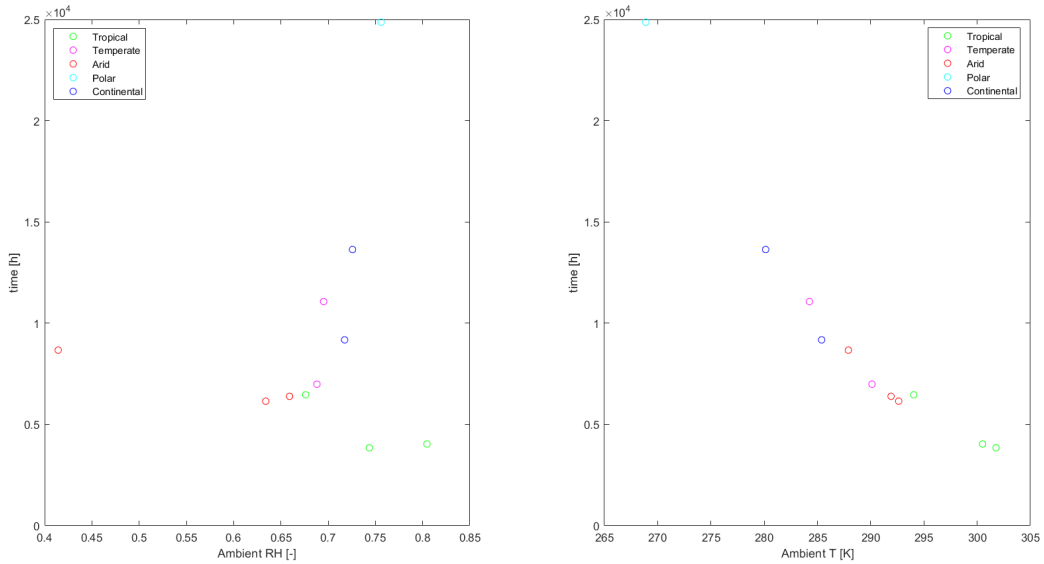

Figure 3.7: Time elapsed before a RMC of 0.05 is reached inside the module as a function of average ambient RH and temperature.

In order to study the connection of the climate conditions to the dynamics of moisture ingress, the time that it takes for each climate to reach a RMC of 0.05 at the front of the cell is plotted against the RH and temperature. The results are shown in Figure 3.7. There does not seem to be a correlation between the time that it takes to reach the indicated concentration and the ambient relative humidity. On the other hand, there is a clear trend when it comes to the temperature. At higher temperatures it takes less time to reach a given RMC. The results are plotted for the time it took to reach a different concentration (RMC = 0.01), this can be found in Figure B.6. The results are in accordance with what has been stated. This indicates that it is temperature that determines the dynamics of moisture ingress. In other words, how quickly the moisture penetrates into the module. The analysis is repeated for concentrations instead of RMC and the same conclusions are drawn. The results for concentration can be found in Appendix in Figure B.7 and Figure B.8 for the time it takes to reach a concentration of 0.05 and 0.01 kg/m^3 respectively.

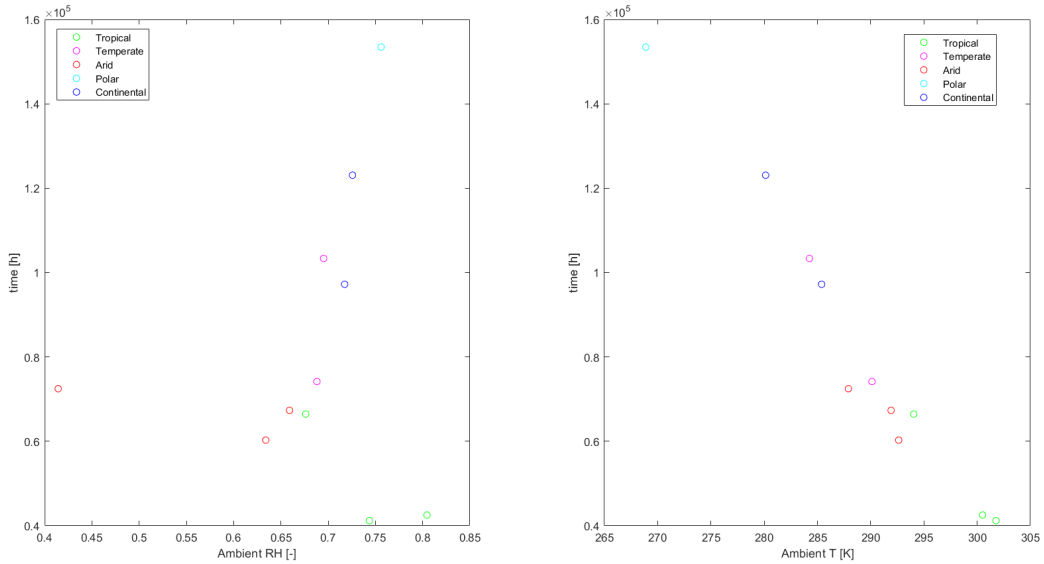

Figure 3.8: Time elapsed before a 95% of the equilibrium value for RMC is reached inside the module as a function of average ambient RH and temperature.

Figure 3.8 shows the time that it takes for the value of the of the RMC reaches a value of 95% of the value in the last year of simulation. The same conclusions can be drawn as when the penetration time was studied, temperature is the climatic stress that determines the time it takes for the module to reach equilibrium value. In this case the relationship seems to follow a more linear trend than for the penetration time. If the trend is analyzed for the time it takes to reach 99% of the saturation value the data point for the polar climate no longer follows the linear trend. That is simply because the linear trend would predict that it takes longer than 20 years and the simulation time stops at 20 years. The polar climate does not reach equilibrium in the 20 years of simulation. The time it takes for the concentration to reach 99% of the value in the last year can't be taken as the time that it takes to reach equilibrium.

The dependence on temperature of the time it takes for moisture to diffuse into the module is caused by the dependence of the diffusion coefficient on temperature. At higher temperatures the diffusion coefficient is higher therefore the diffusion is faster. To try to predict, the time it will take to reach steady state a new quantity has to be introduced. The characteristic diffusion time. This is the time it takes for moisture to break-through a membrane [22]. It is proportional to the square of the thickness through which moisture has to diffuse divided by the diffusion coefficient. Therefore, we will try to equate the saturation time to the following expression:

$$t_{eq} = A\frac{l^2}{D} = 2.003\frac{l^2}{D} \tag{3.1}$$

Here A is a constant that will be used to fit the above expression to the simulated saturation times. Only the modules that have reached equilibrium will be used to fit for A. Therefore, Oslo and Zugspitze are excluded from the fit. The value for the parameter A that gives the best fit is 2.003. The results are shown in figure 3.9. This shows that a linear relation exists between the saturation time and the characteristic diffusion time. However, expression 3.1, relies on fitting of the parameter A. It is unclear if this parameter changes depending under different conditions.

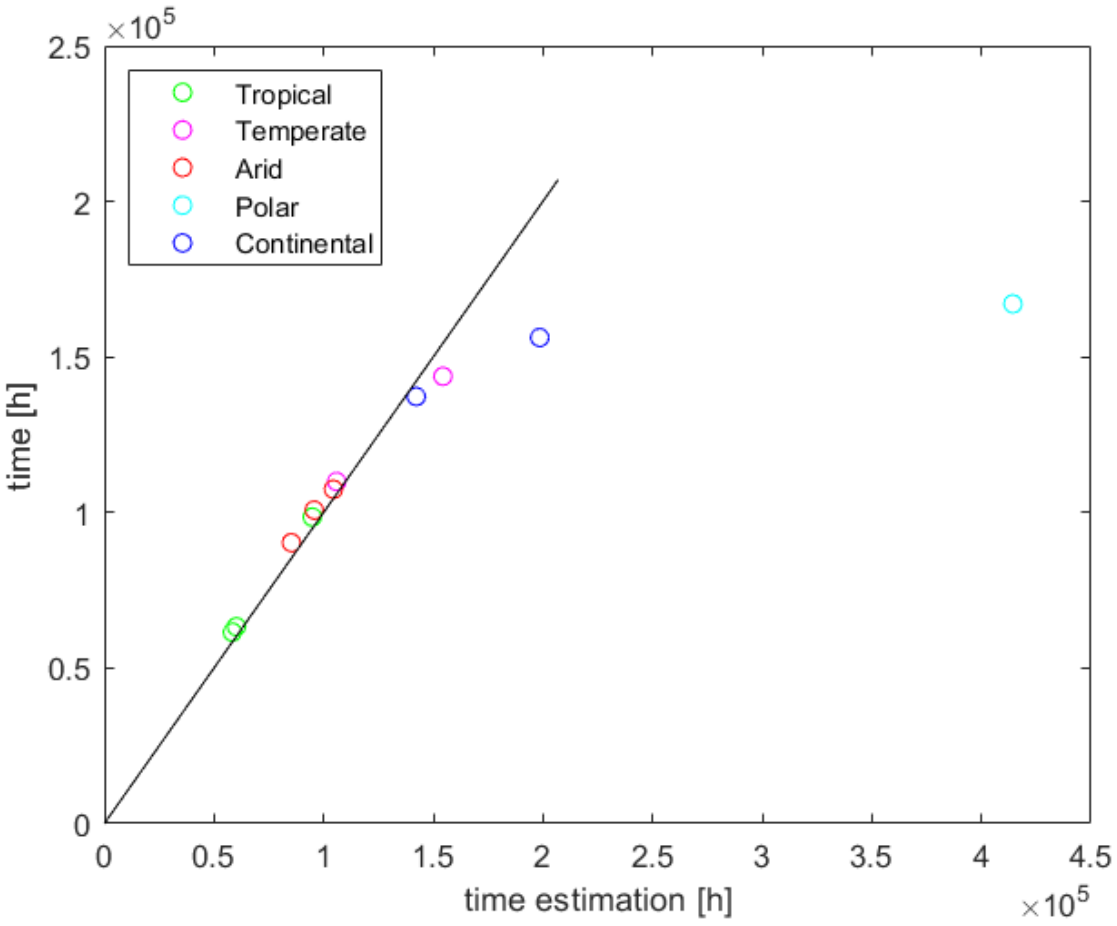

Figure 3.9: Saturation time vs the predicted saturation time with equation 3.1

3.2. Module materials dependence

In the previous section, the materials of the module that was studied remained constant. The encapsulant is EVA and the backsheet is a PET based backsheet. One of the objectives of this project is to deliver a model that can be used to predict the moisture ingress into different modules depending on the respective materials that are used. Therefore the effect of using different encapsulants and backsheets will be modeled.

3.2.1. Encapsulation material dependence

As already mentioned, EVA has been the main encapsulant used in commercial PV modules [9]. It has remained the most popular encapsulant because it has a good ratio of performance/costs [59]. This is due in part to the ease in which it can be processed and applied to the modules. However, it has some properties that are not ideal for the long-term stability of the PV module. Its degradation gives rise to the formation of acetic acid which can be harmful to the performance of the module. For this reason, there are new materials that are being considered. The materials considered for encapsulation of PV modules can be classified in three different categories [59, 60] according to their physical properties:

- Elastomers: Elastomeric materials need cross linking during the lamination step in order to achieve the desired mechanical properties. Elastomers are flexible materials which makes them suitable to be used as encapsulants. The most common elastomers used as encapsulants are EVA and silicone encapsulants
- Thermoplastics: Thermoplastics on the other hand do not need additional steps to reach the desired physical properties. They are more brittle than elastomeric materials. Examples of thermoplastic materials used as encapsulants are Ionomers and polyvinylbutyral (PVB)

- Thermoplastic elastomers: Thermoplastic elastomers are materials that combine thermoplastic and elastomer polymers in order to give a material with the advantages characteristic of both types of polymers. Thermoplastic polyolefins (TPO) and polyolefin elastomers (POE) are examples of the thermoplastic materials considered for the encapsulation of PV modules

Polyolefin based thermoplastic elastomers such as POE and TPO are projected to be the first encapsulant type that achieve a significant market penetration [59]. Ionomers in particular show great promise for their application in areas where a higher resistance to water penetration is needed compared to EVA such as thin film technologies [61]. This is due to the lower diffusion coefficient that these materials exhibit. Therefore, TPO and Ionomers will be the materials that will be studied further. Additionally, an alternative silicone based elastomer to EVA will be studied: PDMS. In order to model the moisture ingress into a PV module with this materials as encapsulant their respective diffusion coefficients and solubilites are needed.

	$D_0\,[m^2/s]$	$E_a\,[kJ/mol]$	$S_0\,[g/m^3]$	$E_a\,[kJ/mol]$
EVA	2.31×10^{-4}	38.1	1.81×10^{6}	16.7
TPO	5.22×10^{-2}	52.9	1.56×10^{6}	24.6
Ionomer	1.5×10^{-3}	55.6	1.78×10^{7}	19.5
PDMS	3.43×10^{-5}	26.8	8.05×10^{4}	11.2

Table 3.1: Arrhenius expression parameters for different encapsulation materials [36]

To be precise, Kempe et al [36] uses a cured EVA ethylene-co-vinyl acetate with approximately 33 wt% vinyl-acetate. The Ionomer is a thermoplastic poly(ethylene-co-methacrylate) with Na^+, and Zn^{2+} counter ions. No information is given about the detailed composition of the TPO. PDMS is a Pt catalyzed addition cure polydimethylsiloxane.

In figure 3.10 the Diffusion coefficients for the different materials are shown as a function of the inverse of temperature in what is called an Arrhenius plot. The Ionomer encapsulant has the lowest diffusion coefficient by more than an order of magnitude. EVA and TPO have pretty similar values for the diffusion coefficient. Finally, PDMS has the highest diffusion coefficient.

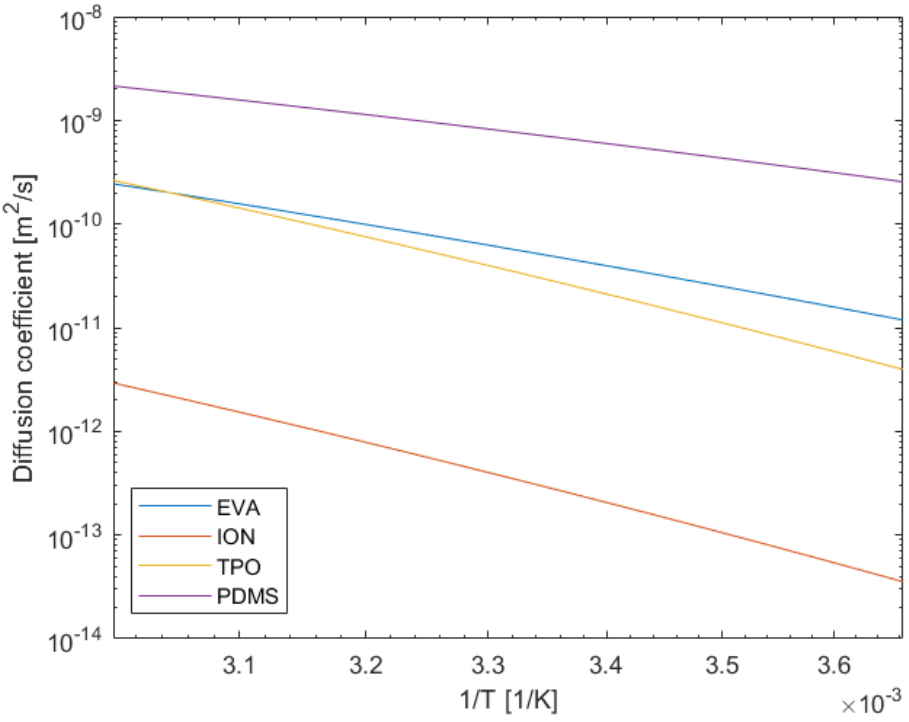

Figure 3.10: Diffusion coefficients for different encapsulants as a function of the inverse of temperature (0-60 $^{\circ}C$). Based on data from[36]

In figure 3.11 the solubility of the encapsulants as a function of the inverse of the temperature is given. The Ionomer has the highest solubility value. This could be due to the highly polar nature of the encapsulant since water is also a polar molecule. The second highest is EVA with PDMS having the third highest solubility. Finally, TPO has the lowest solubility of water. Interestingly, the order is the same at all temperatures. This can be attributed to a reasonably similar activation energy for all materials.

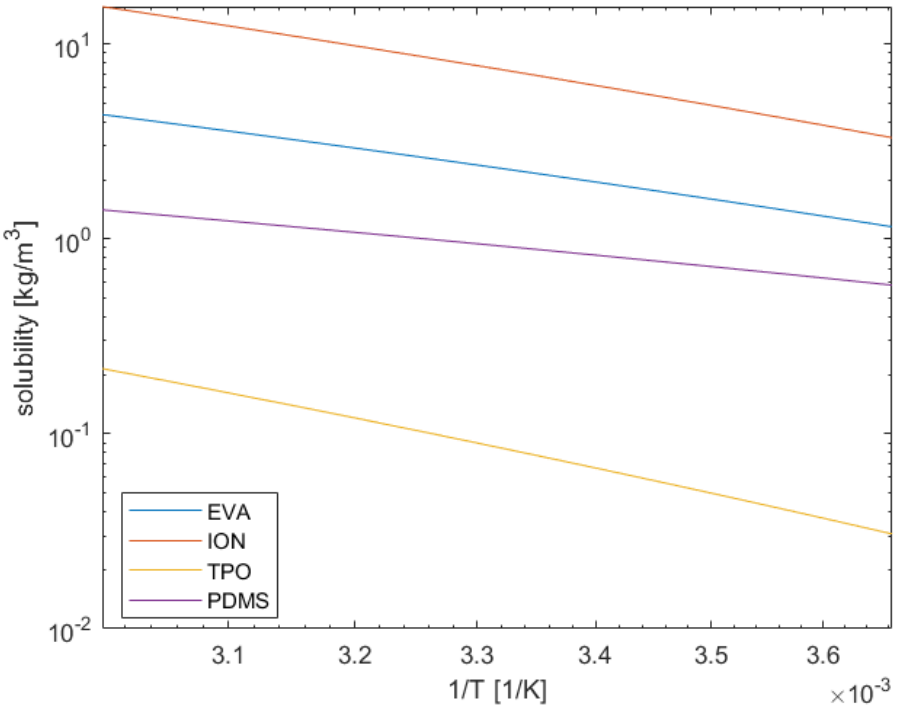

Figure 3.11: Solubility for different encapsulants as a function of the inverse of temperature (0-60 $^\circ C$). Based on data from [36]

The parameters above are compared to parameters from another source in figure B.9 and in figure B.10 for the diffusion coefficient and the solubility respectively. The main takeaway is the difference the difference between the values given by the two sources. The results for EVA show the best agreement between the different sources. The results for Ionomer and TPO encapsulant differ greatly between the two sources. Two main possible reasons for the disagreement are proposed. Firstly, the two sources use different methods to measure moisture ingress. Kempe et al [36] uses water vapour transmission rates measurements using the MOCON Permatran in combination with a visual method relying on the reaction of water with Ca films. Mitterhofer et al [40] uses digital humidity indicators and in-situ gravimetric techniques to measure the moisture ingress into the PV modules. Secondly, the materials could be different. EVA samples could be different due to composition (different percentages of ethylene and vinyl acetate), different additives, curing conditions (determines degree of cross-linking). Ionomers and TPO are categories of chemical species. Mitterhofer et al [40] does not provide information about the detailed composition of the samples they analyzed.

Additionally, there is a very surprising result which is the diffusion coefficient that decreases with temperature for TPO. This is the only measurement that behaves in this way. At higher temperatures higher chain mobility and free volume are expected making the diffusion of species easier making this result unrealistic. This data is shown to convey the degree of uncertainty that is tied to the measurement the parameters. Additionally, both authors express doubts about the Fickian behaviour when it comes to Ionomer (at high temperatures) and TPO. This is one of the key assumptions of the model. The simulations for the different encapsulants will be carried out with the data given by Kempe et al [36] as they provide more details about the materials used and there is no unexpected behaviour of the parameters. It is important to note that regarding the dependence on climatic conditions, the simulations were carried out with different values for the Diffusion and solubility. That is why the results for the EVA encapsulant differ from the previous section.

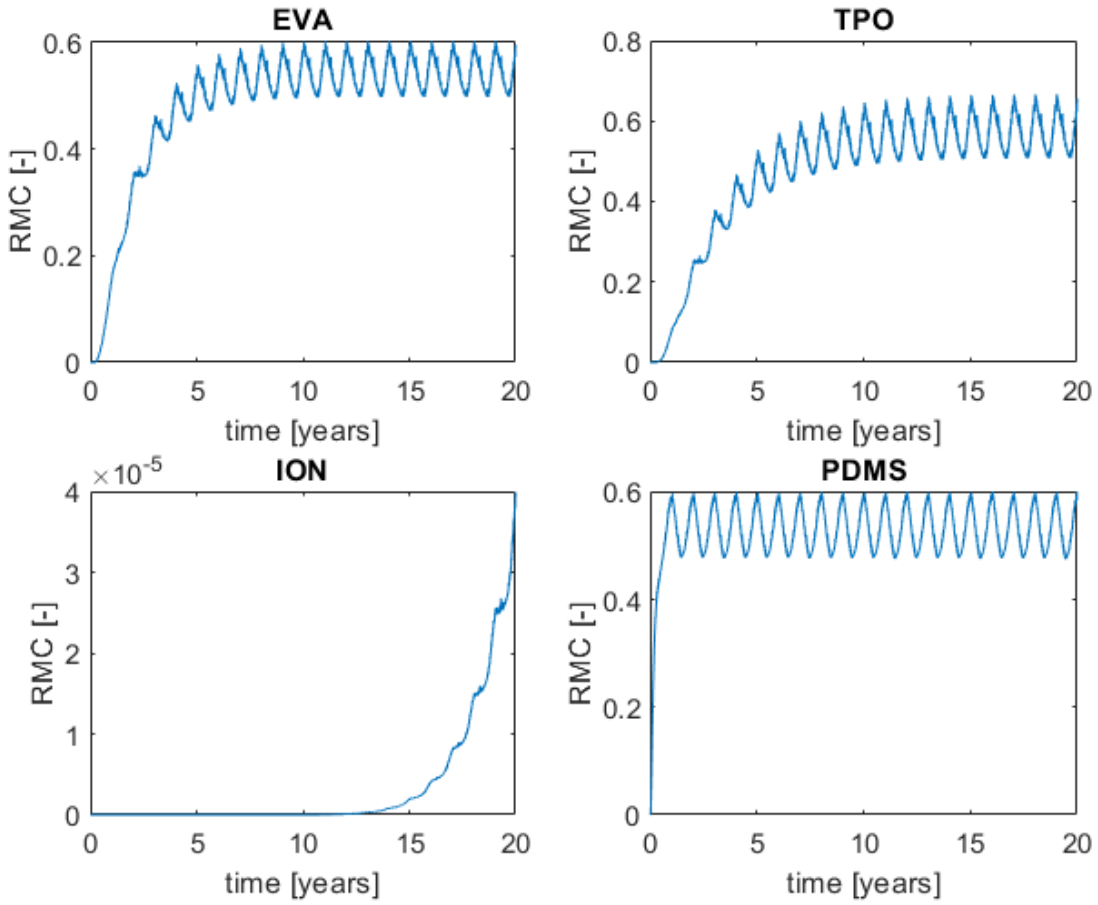

Figure 3.12: Averaged RMC using different encapsulants

To compare the performance, the moisture ingress into PV modules has been modeled using the four different encapsulants. The simulations were carried out for one specific location (Gran Canaria). Figure B.11 shows the results of the evolution of the moisture concentration at the front side of the cell while figure 3.12 shows the results for the RMC at the front of the solar cell. The results that stands out is the simulation for the Ionomer where the module is basically kept dry (the front side of the solar cell). This is due to the lower diffusion coefficient that characterizes this material. PDMS takes the least time to reach the saturation point due to having the highest diffusion coefficient. TPO and EVA have similar diffusion times due to the similar diffusion coefficient. Moisture takes less time to enter in EVA due to the higher diffusion coefficient of EVA at lower temperatures which is when moisture enters the module. The results for the moisture concentration follow the same trend but are scaled with the solubility of each encapsulant. Meaning that the encapsulants with a higher solubility will have a higher concentration. This does not apply to the encapsulant with the highest solubility (Ionomer) as it remains dry due to the low diffusion coefficient.

The modules (except Ionomer) reach roughly the same RMC at equilibrium. The average values for the last year are 0.542, 0.532, and 0.573 for EVA, PDMS and TPO respectively. The average RH for GC is 0.676. As already discussed, the mismatch between those values can be attributed to the definition of an effective relative humidity that is included in the model to simulate the dynamics at the interface by taking the ratio of the saturation pressures between the module and the surrounding climate. However, the variation between the results indicates that the material properties of the encapsulant do play a small role in determining the equilibrium RMC that is reached. The equilibrium concentration that is reached changes due to the different solubilities. As has been done in the previous section, the average equilibrium concentration of the encapsulant is plotted against the average concentration in the last years that is simulated. The results can be seen in figure 3.13. As can be seen the average equilibrium concentration in the different encapsulants is a good

predictor for the equilibrium concentration reached by the different encapsulants.

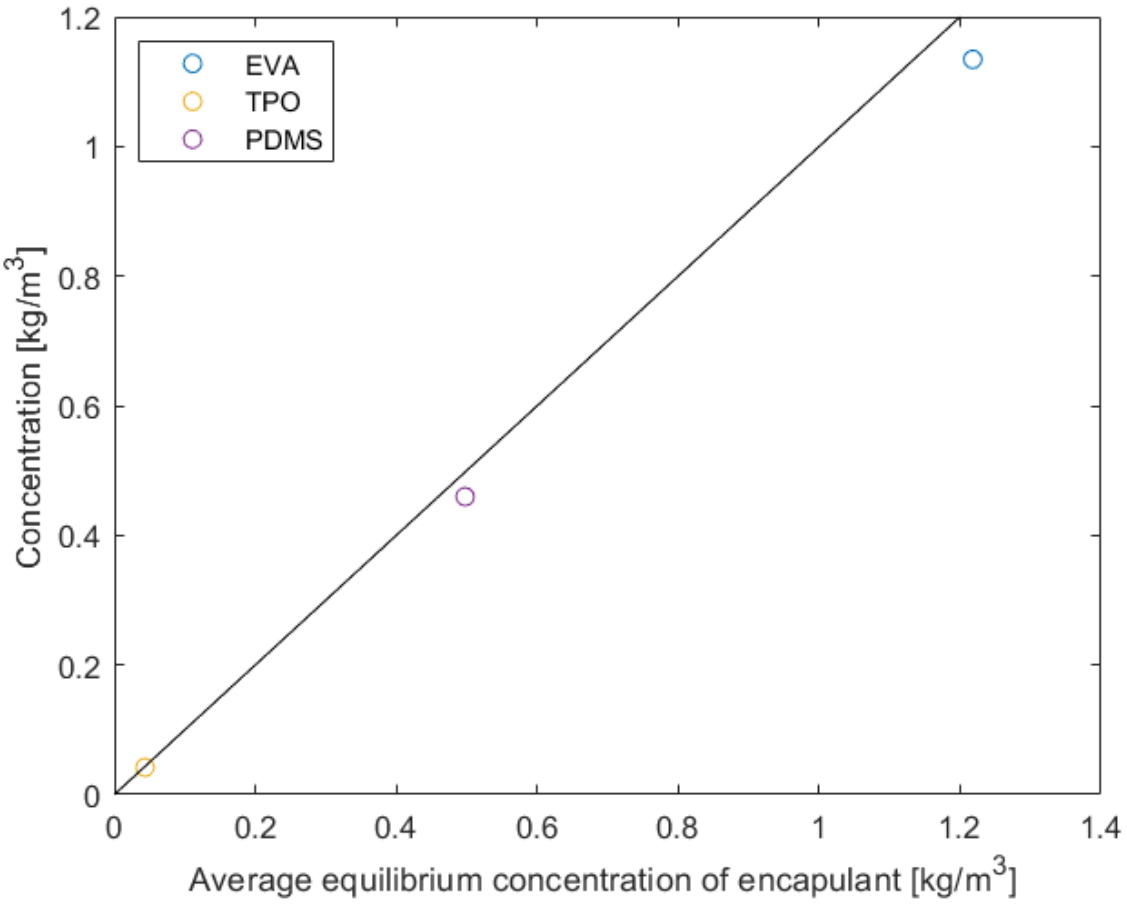

Figure 3.13: Water concentration in the 20th year of simulation vs the average equilibrium water concentration in the encapsulant for the different encapsulants

The next step is to find out if the dynamics of moisture ingress can be predicted using equation 3.1. The results are shown in figure 3.14. This also confirms that the equilibrium time can be approximated using this approach. The same value for the parameter A is used as was used for the different climates. This means that this parameter is applicable to different encapsulation materials. The parameter A is likely dependant on other factors. One example is the geometry of the solar module that is looked at. For example, the spacing between the solar cells.

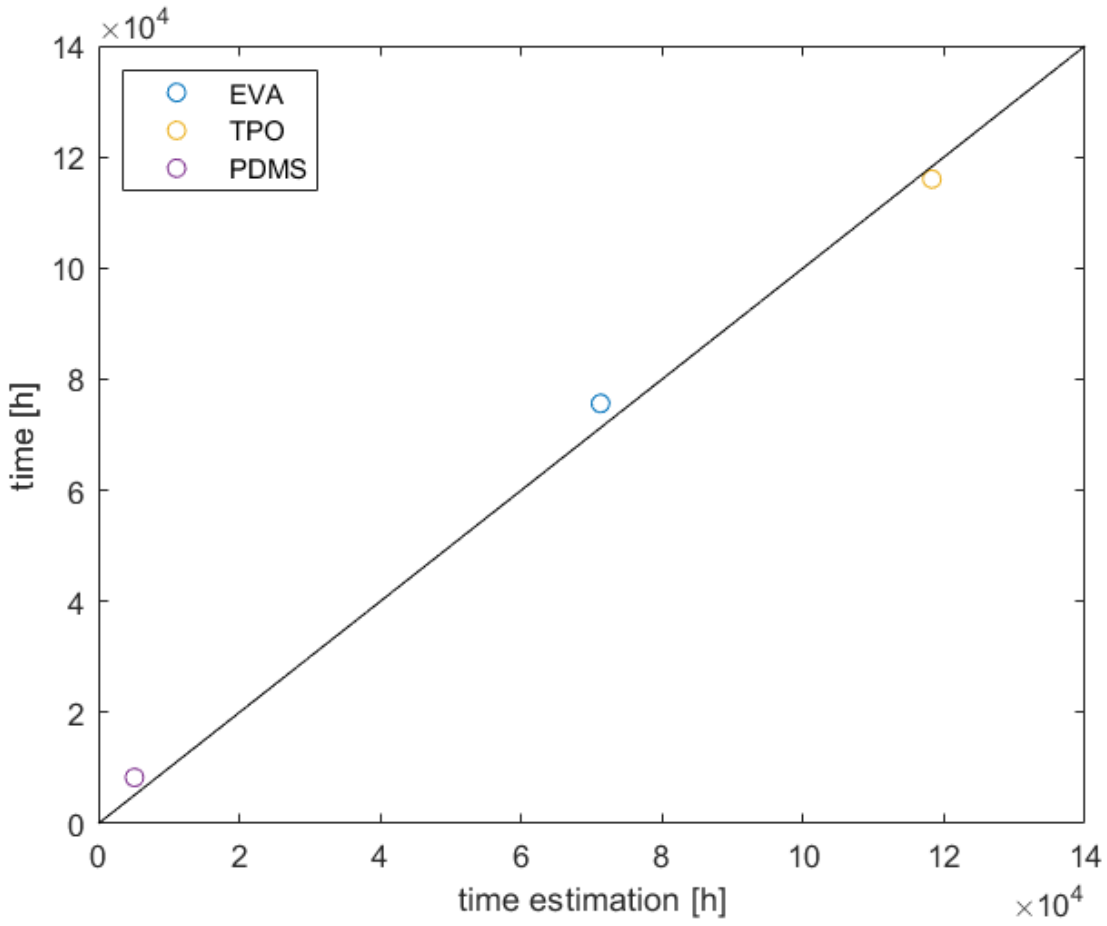

Figure 3.14: Saturation time vs the predicted saturation time with equation 3.1 for the different encapsulants

3.2.2. Backsheet materials

Together with the water transport properties of the encapsulant, the insulating properties of the backsheet are the other parameter that can determine the amount of moisture ingress when a breathable backsheet is used. The moisture present in the environment has to travel through the backsheet to reach the encapsulant. The backsheets are generally comprised of different layers but their properties are reported as one value valid for the whole backsheet and not different values for the different backsheets [44]. In this work, four different backsheets will be studied. Three PET based backsheets: PET backsheet (three layers of PET), TPT backsheet (PET layer in between two polyvinylfluoride (PVF) layers), TPSiO$_x$ backsheet(Core PET layer coated by SiO$_x$ with one PVF protection layer and a polyethylene adhesion layer). For clarification, PVF is also known as Tedlar, this gives the initial T in the TPT and TPSiO$_x$ backsheets. Finally, a polyamide based (PA) based backsheet will also be studied. It is important to note that the parameters for the PET backsheet are different than the ones used in the previous section as they have been taken from a different source and has already been explained, there can be a great difference between the different parameters between different PET backsheets measured in different ways. Therefore, the data from the same source will be used in order to compare the performance of the different backsheets. The simulations are carried out for the location of Gran Canaria and an EVA encapsulant.

	$D_0\,[m^2/s]$	$E_a\,[kJ/mol]$	$S_0\,[g/m^3]$	$E_a\,[kJ/mol]$
PET	6.02×10^{-6}	39.16	7.08×10^{9}	43.17
TPT	5.97×10^{-7}	33.11	3.03×10^{10}	44.82
TPSiO$_x$	1.01×10^{-9}	17.15	1.01×10^{14}	69.96
PA	2.27×10^{-3}	53.94	2.98×10^{9}	41.59

Table 3.2: Arrhenius expression parameters for different backsheet materials: PET, TPT, TPSiO$_x$, and PA [39]

The diffusion coefficients for the different backsheets are plotted in figure 3.15. Unlike what was observed with the different encapsulants, the backsheets do not present an established order for which has the highest diffusion coefficient. Instead they present inverse order at higher and low temperatures. PA has the highest dependence on temperature. At high temperatures it presents the higher diffusion coefficient while at low temperatures it has the highest. The opposite is true for TPSiO$_x$. Another interesting feature of the temperature dependence of the diffusion coefficient is that the values converge at around 300 K.

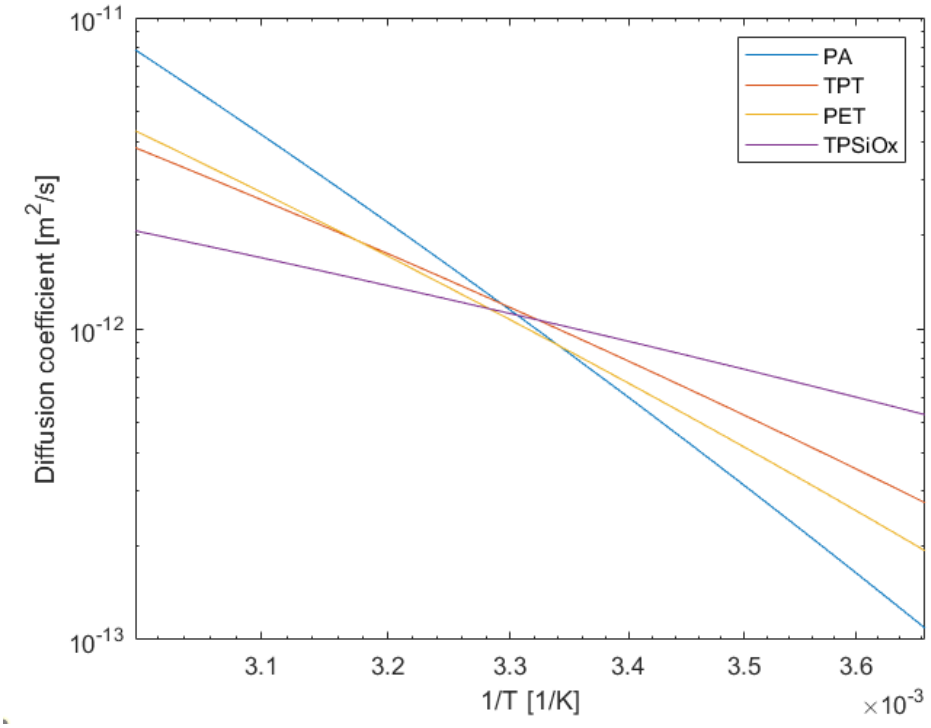

Figure 3.15: Diffusion coefficients for different Backsheets as a function of the inverse of temperature (0-60 $^{\circ}C$). Based on data from [39]

The solubility for the different backsheets are plotted in figure 3.16. The solubility maintains a constant order for most of the observed temperature range. In order from highest to lowest solubility: TPT, PET, PA and TPSiO$_x$.

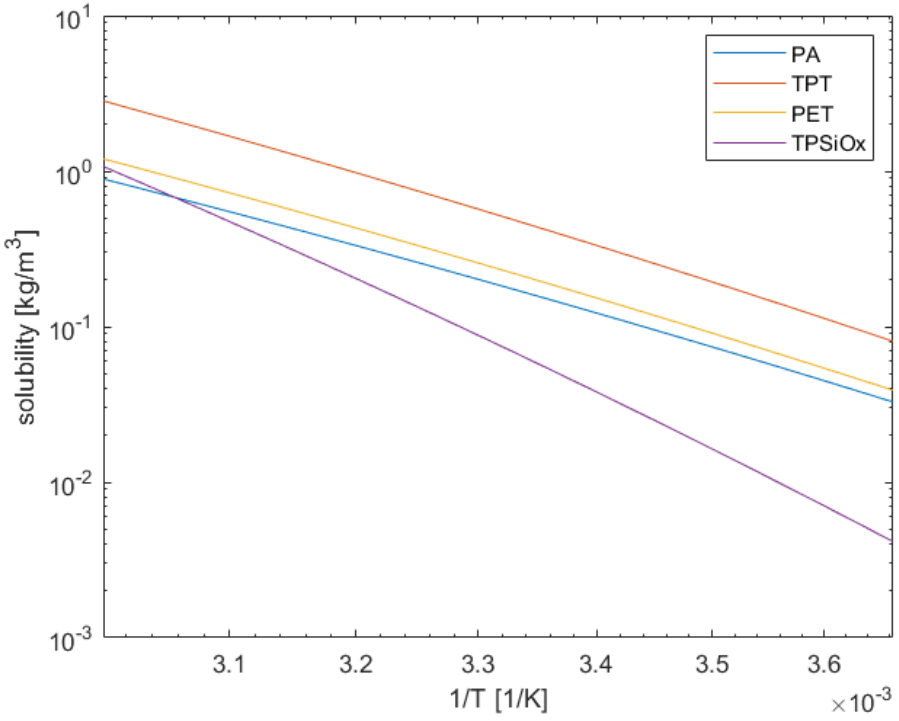

Figure 3.16: Solubility for different Backsheets as a function of the inverse of temperature (0-60 $°C$). Based on data from [39]

In the previous two sections the analysis of the results is done in terms of the ambient conditions and the material properties of the encapsulant. If these parameters are the only parameters that determine the moisture ingress, the results for modules with different backsheets but with the same encapsulant and installed in the same location should be equal. In figure 3.17 the results for the averaged RMC for modules with different backsheets are plotted. These results show that the curves are not exactly the same. Therefore, the choice of backsheet does have an effect on the moisture ingress. It can be seen that the equilibrium RMC value is the same for all the simulations. However, there is a noticeable difference in the rate at which moisture enters the module between the different backsheets. In particular, the moisture ingress for the TPSiO$_x$. backsheet is slower than the other three. To incorporate the effect of the backsheet equation 3.1 is adapted in the following way:

$$t_{eq} = A(\frac{l_e^2}{D_e} + \frac{l_{BS}^2}{D_{BS}}) \tag{3.2}$$

However, this did not improve the results as the added time from the second term (the time corresponding to the diffusion through the backsheet) is much smaller than the first term. The next attempt was made with the minimum value of the diffusion coefficient. This is done because the lowest value for the diffusion coefficient corresponds to the lowest temperature which is when moisture should be entering the module. This did not improve the results. A link between the different backsheet properties and the equilibration time has not been found. One conclusion that can be drawn here is that the parameter A is also affected by the properties of the backsheet. This is because equation 3.1 does not give accurate results for any of the backsheets. Remember that the data for the PET backsheet in this section and the previous sections comes from different sources. That means that they can be effectively treated as different backsheets. Whereas in the section where different encapsulants are analyzed the same backsheet is used as in the section examining different climates.

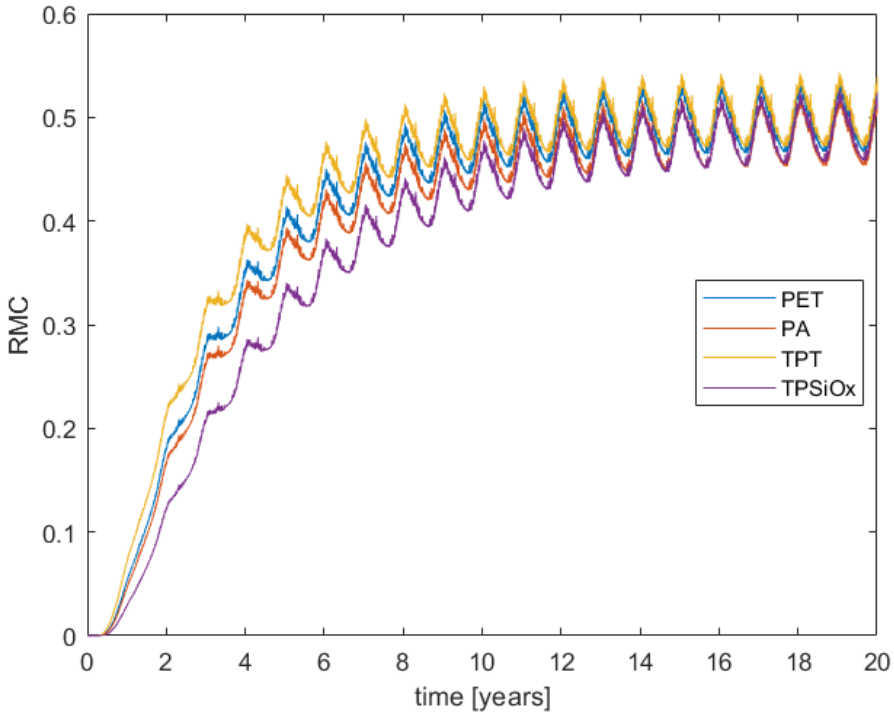

Figure 3.17: Averaged RMC of modules with different BS materials

3.3. Impermeable backsheet

A key aspect that determines how much moisture enters a PV module is the backsheet that is chosen. There is two main categories when it comes to backsheets. Breathable polymeric backsheets and non-breathable glass backsheets. The latter are impermeable to moisture ingress. This means the moisture penetrates through the edge seal on the side. In order to model the ingress through the edge seal the necessary parameters are needed, they are given in Table 3.3. It is important to note that edge seals often have dissecants and other additives that interact with water [62]. This means that the materials they are not Fickian materials. Therefore, the proposed parameters can only be taken as effective parameters used as an approximation of the real moisture ingress parameters of the material. The two encapsulants that are most commonly used for glass-glass modules are EVA and polyvinyl butyral (PVB) [5, 63]. The plots of the material properties as a function of temperature can be found in Appendix B.4. Therefore the simulations will be carried out for those two encapsulants with PIB edge seals for five different locations: Gran Canaria, Zugspitze, Freiburg, Almeria and Oslo. One location per climate type is chosen to ensure variability of environmental conditions.

	$D_0\ [m^2/s]$	$E_a\ [kJ/mol]$	$S_0\ [g/m^3]$	$E_a\ [kJ/mol]$
PIB	$1.7 \cdot 10^{-3}$	54.8	$3.26 \cdot 10^{4}$	5
PVB	$2.81 \cdot 10^{-8}$	9.39	$1.43 \cdot 10^{8}$	34.03

Table 3.3: Arrhenius expression parameters for polyisobutylene based (PIB) edge seals [62] and PVB [5]

The results for the averaged RMC for a module with EVA encapsulant and PIB edge seals for the five locations can be seen in Figure 3.18. The results are consistent with what has already been discussed in the first section of this chapter. The locations with higher temperatures (and therefore higher diffusion coefficients) have a higher degree of moisture ingress. The coldest location (Zugspitze) remains practically dry. This is not in the case when a breathable backsheet is used. This is because with a glass-glass backsheet the area through which the moisture can penetrate is reduced significantly and the diffusion coefficient of edge seals is smaller than the one of the backsheets. Comparing the two different encapsulants we can observe that the

encapsulant with a lower diffusion coefficient, EVA, limits the moisture ingress more compared to PVB, which has a higher diffusion coefficient.

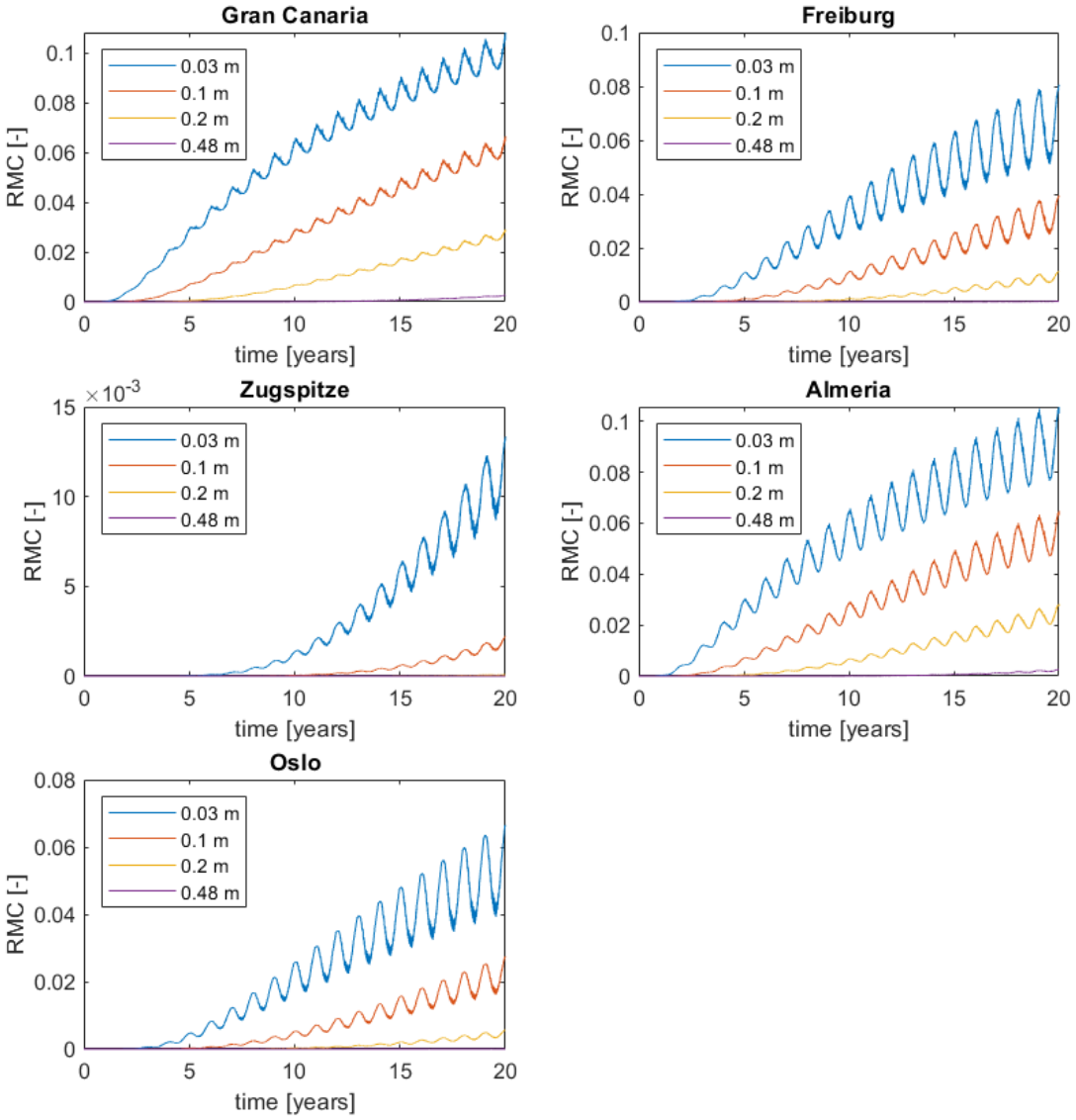

Figure 3.18: Averaged RMC for glass-glass modules with EVA encapsulant and PIB edge seals in the five different locations

In figure 3.19, the results for the simulations of a glass-glass module in different location are shown. These results again conform what has been observed previously. PVB has a higher diffusion coefficient than EVA which results in a faster moisture ingress. Still, the modules do not reach equilibrium even with an encapsulant with a higher diffusion coefficient in glass-glass modules.

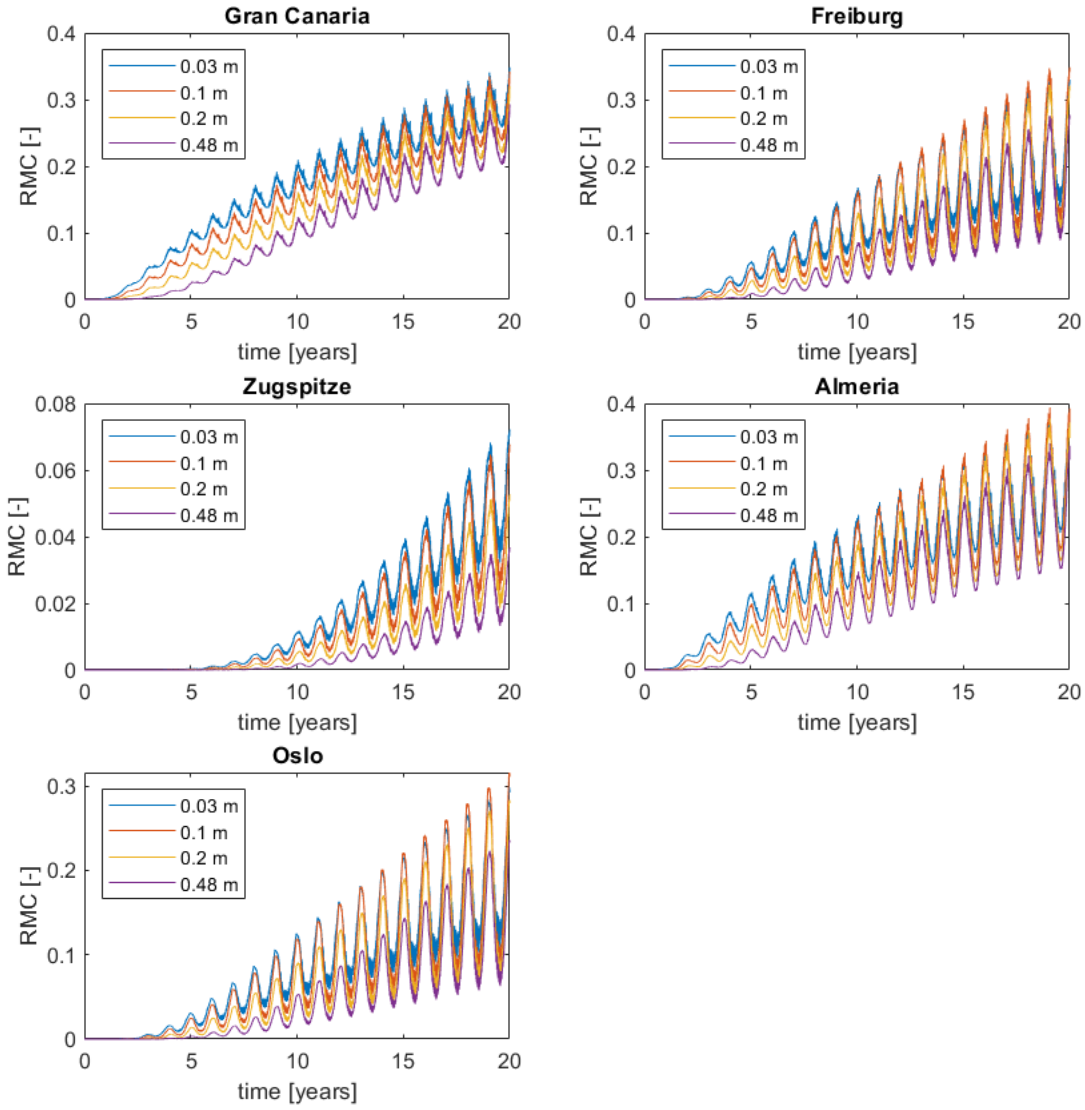

Figure 3.19: Averaged RMC for glass-glass modules with PVB encapsulant and PIB edge seals in the five different locations

Due to the difference in geometry of the impermeable backsheet simulations with the other breathable backsheet model, it is difficult to compare the two. What is clear is that an impermeable backsheet limits the moisture ingress into the module. The results show that the modules are far from reaching equilibrium. This is due to the limited moisture ingress thanks to a lower inlet area and low diffusion coefficient of the edge seal. Therefore, analyzing the equilibrium concentration/RMC or the time that it takes to reach those values is not possible.

3.4. Conclusion

The goal of this section was to analyze the results of the moisture ingress model under different conditions. Results analyzed for different climates extensively. In doing so, a relationship between the environmental conditions and material parameters to the results given by the model is found. This relationship can predict the equilibrium value attained in the simulations both in terms of the RMC and water concentration relatively accurately. A relationship is also found between the diffusion coefficient and the time that is necessary for the

system to reach equilibrium. These relationships also hold for system that deal with different encapsulants. These results give reason to believe that it is possible to use these simplified relationships to predict the results of the FEM analysis.

However, the relationship for the time needed to reach equilibrium does not hold for the simulations using different backsheets. This is reminds us that this is a complicated system with variables that change in time and affect each other. The FEM analysis carries out a detailed calculation of all the relevant water flows through the necessary equations. Therefore, it is not surprising that the simplified relationships do not provide an accurate prediction of all the results. Finally, results for simulations involving impermeable backsheet models are carried out. However, these models are far from reaching equilibrium. Therefore a different analysis is needed to better understand these results. The results obtained in this chapter are used as input for the next chapter where the degradation due to moisture ingress is simulated.

4

Modelling power degradation caused by moisture ingress

4.1. Introduction

Now that the moisture ingress has been successfully modelled and results are available for different conditions (climates, materials) this chapter will study how those results can be converted to results for the power degradation of the module through its lifetime. In order to do this the origins of power degradation due to the presence of moisture and the expected degradation behaviour are studied. Following, the possible approaches proposed in literature in order to model the degradation caused by moisture are explored in order to assess which gives the best results in combination with the moisture ingress model. The different models will be used to fit to available degradation data during accelerated lifetime tests. Finally the models will be evaluated based on their capacity to model power degradation during the lifetime of the module.

4.2. Origin of power degradation in DH tests

Understanding the origin of the degradation in performance of PV modules is a complicated issue due to the wide array of materials used in PV modules [64]. Published literature is mainly focused on the degradation of EVA encapsulated solar modules during Damp-Heat tests [64, 65, 66]. Other papers focus on different encapsulants such as polyolefin elastomers (POE) or thermoplastic olefins (TPO) [67], the composition of the encapsulant has an effect on the underlying mechanism behind the degradation. Different encapsulants will result in different degradation products and in different quantities, these different products can be more or less harmful to the PV module components resulting in different degradation behaviour [68]. Other papers focus on other aspects of the PV module design. For example, Karas et al [68], studied the difference in degradation between traditional Ag-based contacts and alternative Cu-based contacts.

4.2.1. Degradation reactions

To understand degradation caused by moisture ingress, the reactions in which water takes part need to be understood. The reaction investigated in literature can be separated into two categories [64]: Reactions with the encapsulation material and reactions with ”active” elements of the PV module. These active elements are given this name because they are directly related to the performance of the module unlike the encapsulant [69]. In the reactions with the encapsulant , water reacts with the material through a hydrolysis reaction that will result in smaller chain hydrocarbons [66]. Among these reactions, the most commonly reported is the hydrolysis of EVA to give acetic acid. The reaction is given by equation 4.1. The acetic acid can then react with other elements of the PV module which eventually results in the loss of performance.

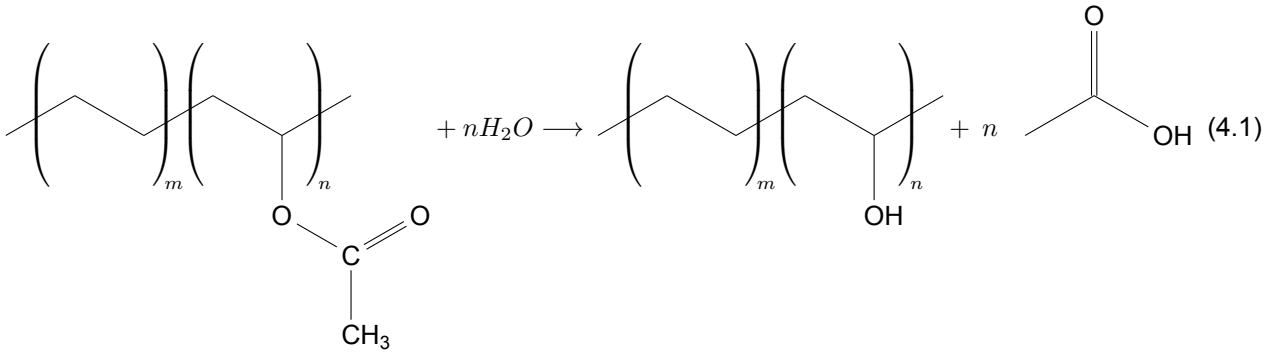

(4.1)

Other encapsulants such as polyolefin elastomers don't degrade into harmful chemicals for the PV module which makes them an interesting material for encapsulation [67]. The degradation of the encapsulation material is not directly related to a loss in power output but can lead to loss of optical properties or a breach in the physical insulation of the module [7]. This also compromises the durability of the module. Water can react with elements of the module that play an active role in the performance of the module. These elements are the solar cell, the anti-reflective coating, the solder bonds and grid fingers [69]. The degradation of the solar cell and the anti-reflective coating is not well understood [64]. When investigating this issue, Peike et al [64] did not observe any degradation of the solar cell or the anti-reflective coating. This led to the conclusion that the degradation of the solar cell or the anti-reflective coating is not at the origin of loss of performance during damp heat tests. This is in accordance with other papers, where the loss in performance is often attributed to the corrosion of the metallization elements (solder bonds and grid fingers) [66, 70]. The reaction of the metallization elements is given in equation 4.2. However, in other studies, the parameters corresponding to solar cell performance also show degradation of the solar cell [68]. Overall, the results found in literature show that the degradation in performance is most likely caused by the degradation of the metallization elements but the exact mechanism still needs to be investigated [64, 69]

$$Me + XH^{+} \rightarrow Me^{X+} + \frac{X}{2}H_2 \tag{4.2}$$

There is a number of metals used in solar cells: Ag, Cu, Sn, Pb and Al [66]. All these metals can react with water or acetic acid as is shown in the above reaction (equation 4.2). The cation (H^{+}) can come from the dissociation of water or acetic acid. X is used as a coefficient to balance the equation depending on the oxidation number of the metallic element. Me is general term denoting a metallic element, in the real reaction this term should be replaced by the metal that is being oxidized and the corresponding oxidation number. There are some metals that get oxidized more easily, these metals have lower oxidation potentials [66]. For example, Al has the lowest oxidation potential among the metals mentioned above, therefore it will be corroded first.

The corrosion of metallization elements is generally associated to an increase in series resistance of the cells [64]. This is caused by the corrosion of the ribbon in solder joints and the grid fingers [71]. The corrosion decreases the area of electrical connection which results in an increased series resistance [66]. This is confirmed by I-V measurements [64]. I-V measurements are used to determine the performance of a solar cell, they consist of measuring the current that flows through the cell at different voltages. Some studies have reported a decrease in the current generated by the solar cells after damp heat tests [70]. However, this is thought to be related to the discoloration of the encapsulant rather than the corrosion of metallization elements. The performance of the module can be described by an equivalent circuit equation [69]. The evolution of the equivalent circuit parameters depends on the materials that are used in the module [69]. How these parameters evolve over time is also different depending on whether the backsheet is breathable or non-breathable [69]. This has an important implication for our research as it implies that a degradation model can only be used for predicting the loss of performance of a module in different conditions. It is not possible to use the model that has been calibrated using one module to predict the degradation behaviour of another module.

4.2.2. Degradation behaviour

As has been discussed, there is a lot of variation in material parameters. This will affect the amount of moisture that enters the PV module and the reactions that this moisture can cause. However, there is still behaviours that are common in the degradation during accelerated lifetime tests. The degradation process can generally be described by the same three stages [68, 69, 70]:

1. **Diffusion of moisture**: During the first stage the moisture diffuses to where it can react with elements of the PV modules. During this stage there is no degradation of performance. The duration of this stage depends on how well the module is insulated to moisture ingress.
2. **Reactions causing losses in performance**: Moisture (or other reactants like acetic acid) react with the elements of the module susceptible to degradation. The loss of performance is observed in this stage.
3. **Saturation of degradation**: In the last stage, the degradation reaches a limitation. This can be due to an exhaustion of the module components that are susceptible to moisture induced degradation or due to diffusion limitations of water/acetic acid to the reaction site.

The explanation given above is a good generalization of the degradation behaviour of PV modules during accelerated lifetime tests. However, there are instances in which the modules do not follow this behaviour [69]. For example, if the module is less permeable to moisture ingress, the modules can get through the test showing minimal degradation. Alternatively, if the module is tested at higher temperatures the module can experience complete failure. This was observed by Zhu et al [69], when testing a module with a thermoplastic silicon as encapsulant where the encapsulant melted during testing resulting in complete failure of the module.

4.3. Modelling of power degradation

The most important models used to describe the degradation effects of climatic stresses have been presented in section 1.4.2. In this section the application of these analytical models to the modelling of power degradation in accelerated lifetime tests will be presented.

This study is focused around degradation caused by the effect of relative humidity (RH), the accelerated lifetime test that reflects this effect best is the Damp-heat test [69, 70]. Damp heat tests consist of exposing the modules to a fixed high temperature and relative humidity for a certain amount of time [21]. During these tests there is no temperature cycling and the effect of UV irradiation is minimal. Therefore, the degradation caused by those stresses is neglected. The degradation rate caused by relative humidity can be expressed using the Peck equation for moisture induced degradation [33, 34].

$$k_{RH} = k_0 \cdot RMC^n \cdot exp(\frac{-E_a}{k_B \cdot T}) \tag{4.3}$$

In the equation above, k_0 is the rate constant, E_a is the activation energy that gives the dependence on temperature. This expression reflects the effect of relative humidity on degradation as well as the dependence of temperature. It has to be noted that the RH term in this expression represents the ambient relative humidity [33]. The results of the COMSOL model give the concentration of water in the module. Coyle et al [41], proposed to use the relative moisture content (RMC). That is why the ambient RH value is swapped by the module RMC in the equation above. This represents the degree to which the encapsulant around the solar cell is saturated with water. This quantity is used in microelectronics packaging literature to describe degradation [41].To obtain RMC, the concentration of water in the encapsulant is divided by the saturation concentration of water in the encapsulant. Using this value means that it is assumed that the absolute amount of water is not relevant for the degradation. Additionally, using this quantity means that in an accelerated lifetime test where the ambient RH and temperature are fixed RMC and the ambient RH will eventually reach the same value.

Using expression 4.3 with ambient RH (fixed) results in a fixed value for k_{RH}. If this is taken directly as the degradation rate, it will result in a linear degradation trend. As discussed in the previous subsection, the degradation during accelerated lifetime tests can be understood as a three stage process. The degradation curve can be fitted using a sigmoidal function [70]. Kaaya et al [33], proposed the following equation to model this three stage process and include equation 4.3.

$$\frac{P_{MPP}(t)}{P_{MPP}(t=0)} = (1 - exp(-(\frac{B}{k_{RH} \cdot t})^u)) \tag{4.4}$$

Where B is the power susceptibility which is assumed to be a material dependent parameter and u is the shape factor [33]. $P_{MPP}(t)/P_{MPP}(t=0)$ is the relative maximum power output at time t. The power output is relative to the maximum power output at time 0. Therefore $P_{MPP}(t)/P_{MPP}(t=0)$ at t = 0 is equal to 1. This expression will reach 0 at longer values for time. This is not observed in accelerated lifetime tests unless complete failure occurs. Therefore, a small modification is proposed to include a maximum amount of degradation by using the parameter L. Other authors have used a similar approach where a limit to degradation is included [70]. Combining equation 4.4 with a limit has not been researched yet. Doing so results in equation 4.5.

$$\frac{P_{MPP}(t)}{P_{MPP}(t=0)} = L \cdot (1 - exp(-(\frac{B}{k_{RH} \cdot t})^u)) + (1 - L) \tag{4.5}$$

Four approaches will be used to try and fit the results of accelerated lifetime tests. Equation4.4 and equation 4.5 will be used in combination with 4.3 will be the equations that will be used to try and validate the degradation model using the COMSOL results as they are the equations used in literature to model degradation during damp heat tests.

1. Results of the FEM model with degradation equation without limit (equation 4.4).
2. Constant ambient RH with degradation equation without limit (equation 4.4)
3. Results of the FEM model with degradation equation with limit (equation 4.5).
4. Constant ambient RH with degradation equation with limit (equation 4.5).

There are alternative equations that can be used instead of equation 4.3 to obtain a value for k_{RH}. Some examples are the other models found in literature that can be used to take into account the effect of relative humidity. For example, the Eyring and the exponential models [29] already presented in 1.4.2. Another option is given by equation 4.6. This expression uses the Brunauer–Emmett–Teller (BET) model to give the dependence of the degradation rate on the RMC [41]. The BET model gives the relation between the surface coverage of water and the RMC. This model has been proposed for scenarios where the degradation reaction is the rate limiting step whereas the Peck model (expression 4.3) is valid when the diffusion of moisture is the rate limiting step [41]. The kinetics of the degradation reactions are outside of the scope of this thesis. Therefore, it is not possible for us to establish which of the two models should be used. For this reason both models will be used to study the degradation of PV modules in different conditions. Equation 4.6 will be used in the modelling of degradation in real life conditions.

$$k_{RH} = k_0 \cdot \frac{RMC}{1 - RMC + \epsilon} \cdot exp(\frac{-E_a}{k_B \cdot T}) \tag{4.6}$$

4.4. Validation with accelerated lifetime tests

In this subsection, the fitting of the degradation model to experimental data will be presented. It was not possible to carry out these measurements in the laboratory. Therefore, data from literature will be used. The data from Zhu et al [69] will be used as they present clear data for the degradation of one module under different conditions (T and RH).

The fitting is carried out using MATLAB's global optimization toolbox. In particular, the function "patternsearch" is used. This is chosen over other alternatives as it gave better results than alternative functions like 'fminsearch', 'fmincon' or 'ga'. The lack of data made the fitting complicated. In particular, a strong dependence on the initial guesses provided for the parameters is observed. Therefore, an iterative fitting process is used to try and avoid local minima which do not reflect a good solution for the parameters. The logic of this process is represented in figure 4.1

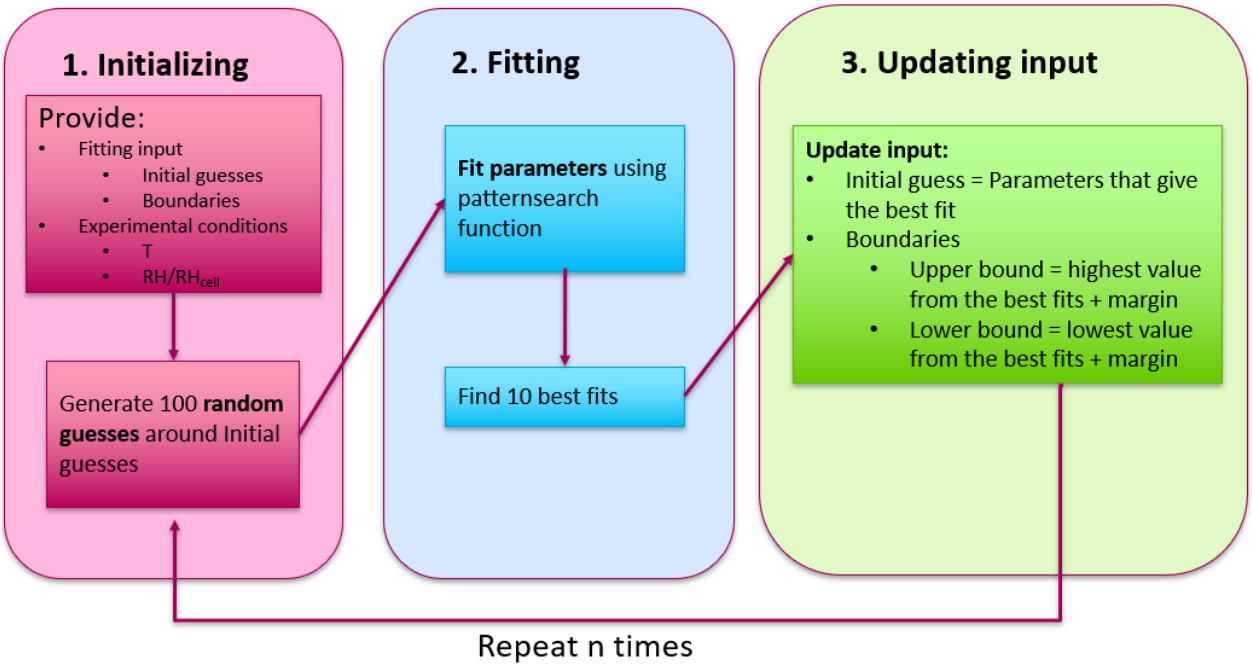

Figure 4.1: Representation of the logic of the fitting process

The fitting process is divided into three steps: Initializing, fitting and updating the input. In the first step the input parameters are specified, these are initial guesses based on values found in literature [33, 69]. This initial guesses are used to generate 100 random guesses around these values. This is done to minimize the effect of the initial guess on the final results. Boundaries are also specified for the parameters. These are chosen based on properties of the parameter to avoid solutions that are unrealistic. For example, the parameter L is bound between 0 and 1. Outside these boundaries the parameter loses its physical significance, resulting in either a performance above 1 (above 100%) or negative performance (below 0%). The allowed deviation for the 100 guesses is between 20 and 200% of the original guess.

	k_0 [1/h]	E_a $[kJ/mol]$	n $[-]$	u $[-]$	L $[-]$
Initial guess	$6.11 \cdot 10^4$	87.8	1.8	1	0.7
boundaries	$[0, +\infty]$	$[0, +\infty]$	$[0.1, 10]$	$[0.1, 10]$	$[0, 1]$

Table 4.1: Input for the fitting script

The other input parameter to the fitting process is the experimental conditions, Temperature and relative humidity. The input for moisture is different depending on whether the results of COMSOL or the fixed conditions are used. In teh first case it is the RMC returned by the model, which changes with time, and in the other is the ambient RH which is constant. The difference can be observed in Figure 4.2. In the second step the fitting is carried out using the 'patternsearch' function and the 10 best results are saved. These 10 results are used to update the input for the next iteration of the fitting. The values that give the best fit for each of the models is taken as the initial guess of the next iteration. The boundaries for the parameters are set as the highest and lowest guess for each parameter with a certain margin. A 10% margin is included above and below the new highest and lowest boundaries at each iteration to prevent that the fitting gets stuck on the boundary condition. The process described above is repeated 5 times, after this amount of iterations good convergence is observed in the fitting.

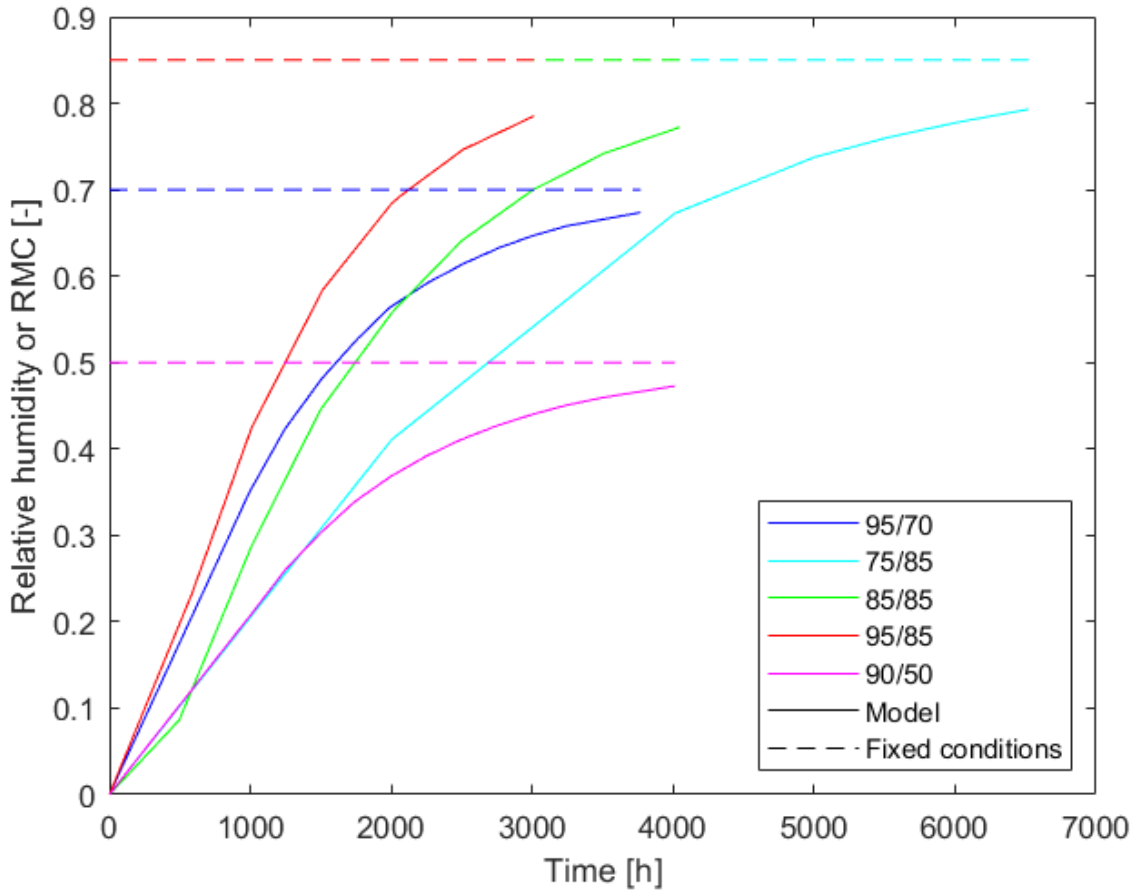

Figure 4.2: Difference in input when using the COMSOL model and the fixed RH. The lines at a constant value are the input when the climatic RH is used. The lines that change value over time are the input from COMSOL. Legend gives the experimental conditions T [K]/RH [-]

The procedure described above explains the fitting procedure to experimental data. However, to check whether the power degradation model is able to predict degradation under different conditions not all the available data will be used for training the model. There are 5 different experimental conditions, they consist of different combinations of RH and temperature. For each set of conditions Zhu et al [69], carried out two sets of measurements. Both sets are included in the calibration, this is done to account for variation of degradation under the same conditions. Three of the five available datasets will be used for training the model. The remaining two datasets will be used to check whether the trained model is able to predict degradation behaviour in different conditions. For clarity, in the next sections 'Fitted' is used for the results obtained from the data used to train the model and 'Predicted' is used for the results obtained for the data that are not used for the training of the model.

4.4.1. Fitting results

In this subsection, the results of the fitting will be presented. These results are used to establish whether using a changing RH profile is possible to predict power degradation behaviour in accelerated lifetime tests. Additionally, these results will show whether using a physical model to reflect the actual behaviour of moisture ingress into PV modules offers any advantage for predicting power degradation behaviour under different conditions. Finally, these results can be used to determine whether the addition of the parameter L to the degradation model improves the fitting and predicting ability of the model.

The parameters that gave the best fit for each of the models are given in table 4.2. In general, the different

parameters are all in the same order of magnitude for all the models and no major disagreement between the models is observed. The best agreement between all models is in the activation energy. This is can be explained by the physical meaning of the activation energy which gives the temperature dependency of the degradation rate. There is no reason for which this should change between models. Additionally, the exponential dependence on this parameters means that the function is likely highly sensitive to a variation in this parameter. Therefore, the correct solution has to be found to get a good fit. The parameter n determines the effect of the concentration on the degradation rate. Therefore, it makes sense that this parameter changes depending on whether the model uses a fixed RH or the results from the moisture ingress model. This is what is observed from the results where the two models using COMSOL results and the two models using a fixed RH have a very similar value for n respectively. The value of u seems to be higher for those models that include a degradation limit by using the parameter L. When L is included, the curve does not tend to 0 at higher times anymore. This makes it possible for the curve to become more ”steep” (higher value of u) without decaying to 0. As already discussed a decrease until 0 gives bad fit at higher times as it does not reflect the real degradation behaviour. Finally, L is pretty similar between the two models that employ it as would be expected.

Model	k_0 $[1/h]$	E_a $[kJ/mol]$	n $[-]$	u $[-]$	L $[-]$
COMSOL	$1.4918 \cdot 10^4$	52.706	0.5182	3.6021	-
Fixed RH	$1.1764 \cdot 10^4$	52.227	0.4522	4.0549	-
COMSOL +limit	$1.605 \cdot 10^4$	52.721	0.5142	5.3638	0.8031
Fixed RH + limit	$8.5664 \cdot 10^3$	51.089	0.4416	6.4309	0.7846

Table 4.2: Parameters that give the best fit for each model

The results of the fitting and prediction are given in figures 4.3 and 4.4. From the figures, it can be seen that all models give an acceptable fit and prediction for the power degradation. The model proposed by Kaaya et al [33] captures the degradation behaviour of modules in Damp-Heat tests. One general observation that is valid for all the models is that a poor fit/prediction is obtained for the beginning of the curve at higher temperatures. The experimental data shows a gradual decrease that starts earlier than the one given by the model.

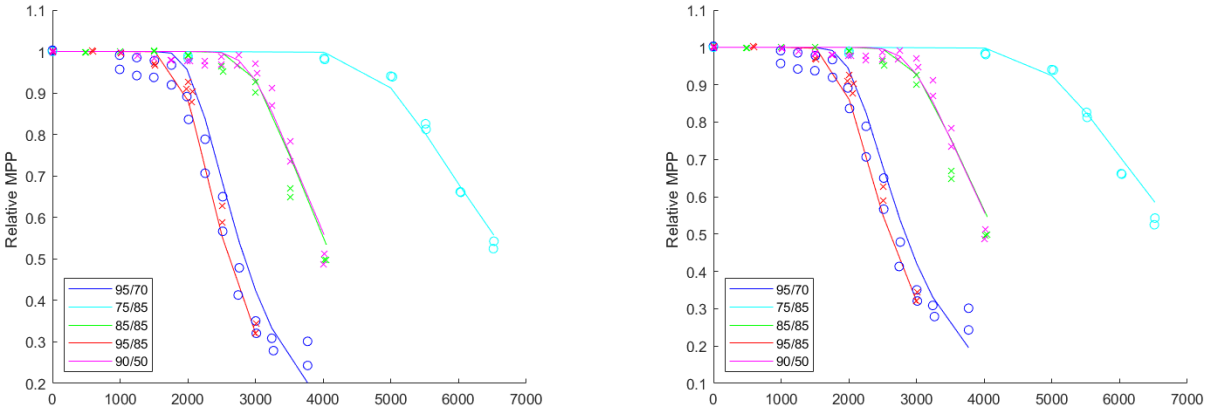

Figure 4.3: Fitting results using equation 4.4. Left: Fitting results using the results of the moisture ingress model. Right: Fitting results using the fixed RH. Lines represent the fitted or predicted trend. Crosses represent the data used to train the model. Circles represent the data that the model will attempt to predict. Legend gives the experimental conditions of each in the form T [K]/RH [-]

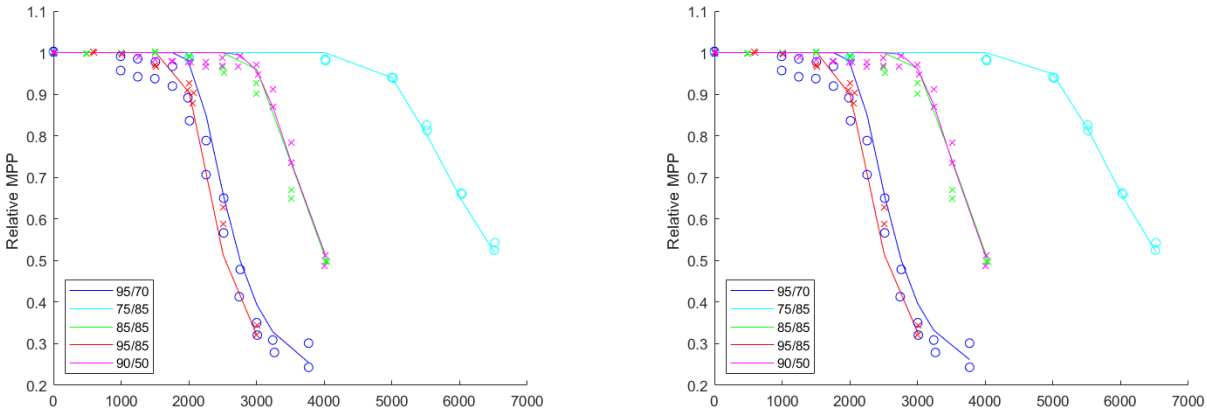

Figure 4.4: Fitting results using equation 4.4 with the addition of parameter L. Left: Fitting results using the results of the moisture ingress model. Right: Fitting results using the fixed RH. Lines represent the fitted or predicted trend. Crosses represent the data used to train the model. Circles represent the data that the model will attempt to predict. Legend gives the experimental conditions of each in the form T [K]/RH [-]

At first glance, the results of all models seem quite similar. The error between the experimental data and the fit/prediction is analyzed. This is done by looking at the mean absolute percentage error (MAPE) and root mean square error (RMS). These results allow us to conclude that the moisture ingress COMSOL model can be used with the model proposed by Kaaya et al [33]. However, it does not improve the results obtained by using a fixed RH. Additionally, it can be seen from these results that including a limit to degradation improves both the fitting and predicting capabilities of the model. This is true when using a fixed RH and a changing RH.

Model	MAPE fit [%]	RMS fit [-]	MAPE predict [%]	RMS predict [-]
COMSOL	3.0540	0.0313	6.8435	0.0435
Fixed RH	3.3641	0.0348	7.0785	0.0458
COMSOL + limit	2.6607	0.03088	5.1288	0.0372
Fixed RH + limit	2.7097	0.0312	5.0260	0.0358

Table 4.3: Statistical analysis of fitting and prediction

Another parameter that could provide variation to the obtained results is which experiments are used to train the model and which experiments are predicted by the model. In all of the results above, the last three experiments are used to train the model. The results when the model is trained with the first three experiments can be found in the appendix.

4.5. Power degradation in real life conditions

In this section the modelling of power degradation during the lifetime of the module in outdoor conditions will be studied. It needs to be underlined that unlike in damp heat tests it is not possible to ignore the effects of other types of degradation. The module will experience temperature cycling, exposure to UV radiation and other causes of degradation. This means that it is not possible to calibrate the moisture induced degradation model independently with outdoor performance data. Additionally, there is a lack of data for degradation through the whole life of a module. This means that it is not possible to accurately calibrate the humidity induced degradation model. Most studies report a yearly degradation rate [6]. However, it is still possible to use the results of a degradation model (without calibration) to compared the degradation that is expected in different conditions.

4.5.1. Input for lifetime degradation model

In order to decide which method is better suited to model the power degradation using the results of the moisture ingress model, the input needs to be analyzed. The input to the model is the relative moisture content inside the module and the module temperature as a function of time. The temperature is given by the Faiman model. For the rest of this section, the term moisture ingress model will be used to refer to the results of module relative humidity and module temperature. The results will be compared to the fixed ambient conditions that were used previously. The results will be shown in comparison to the input used by Kaaya et al [33] for their model for different locations. The chosen locations are Zugspitze (Germany), Negev (Israel) and Gran Canaria (Spain). These locations are meant to represent variability among different climates. Zugspitze represents an alpine climate, Gran Canaria a tropical/maritime climate and Negev an arid climate.

The results from the moisture ingress model can be seen in figure C.3. As can be seen in the figure, the data shows a large variability on the daily scale. As has been shown previously in section 2.5.2 the moisture content at the front of the cell does not show daily fluctuations as the diffusion time is too long. The daily variation in the results of the moisture ingress model are caused by a variation in the saturation concentration in the encapsulant due to temperature changes throughout the day. During the day, when solar irradiance is heating the module up, the saturation concentration of the module increases. This results in a decrease in the relative humidity of the module. The opposite is true for the nighttime when the module reaches lower temperatures. These daily trends can be seen in Figure 4.5.

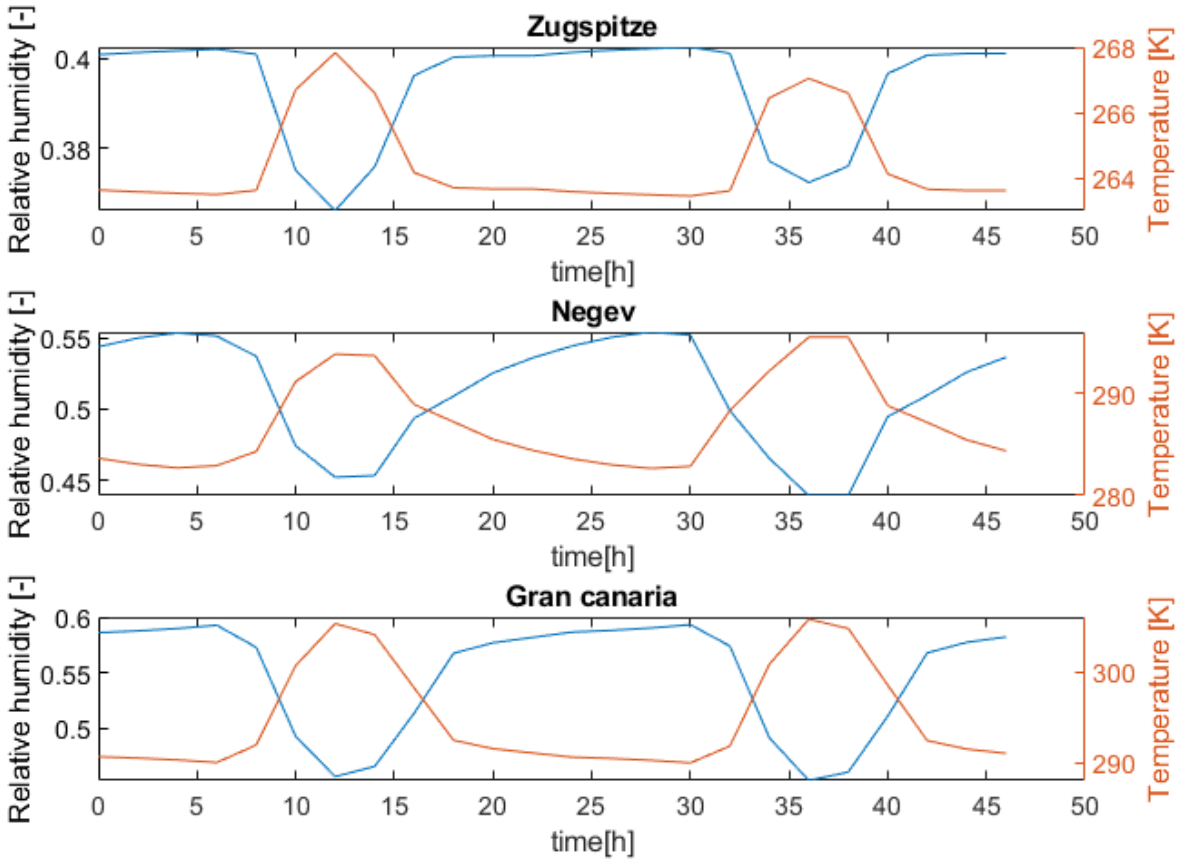

Figure 4.5: Daily trends in module relative humidity and module temperature for the three chosen locations. Results are shown for the first two days of January on the 11^{th} year

The daily trends described in literature seem to agree with the results of our model. Moisture enters at night and the module dries up during the day [22, 41]. However, It is important to underline the trend

observed in the above results is mainly due to the change in solubility of the encapsulation material. Figure C.5 shows the same figure with concentration instead of relative humidity. It can be seen that the same trend is followed. However, this also confirms that the change in saturation concentration is the main driver behind the change in relative humidity as opposed to a true change in concentration. To truly assess whether the model behaves as would expected one has to look at what times water is leaving the module and at what times water is entering the module. This can be observed in figure C.6. Here, the concentration profile under the cell ((air-Backsheet-encapsulant)) is plotted for various times during the day. When there is a negative concentration gradient at the interface between air and the backsheet is when moisture is entering the module. This happens in the colder hours of the day. On the other hand if there is a positive concentration gradient water is leaving the module which happens in the hot hours of the day. This figure allows to confirm that in fact the model follows the expected trend.

In figure 4.6, a moving average over the day is applied. This is done so that the trend followed by the relative humidity inside the module can be observed more clearly. Zugspitze, has the highest ambient RH. However, when looking at the relative moisture in the module it is the lowest throughout most of the module's life (Until 12 years of operation). This is caused by the lower temperatures experienced by the module in Zugspitze compared to the other two locations. The module temperatures can be found in C.4. These results show that temperature plays a key role in determining the rate at which moisture enters the module.

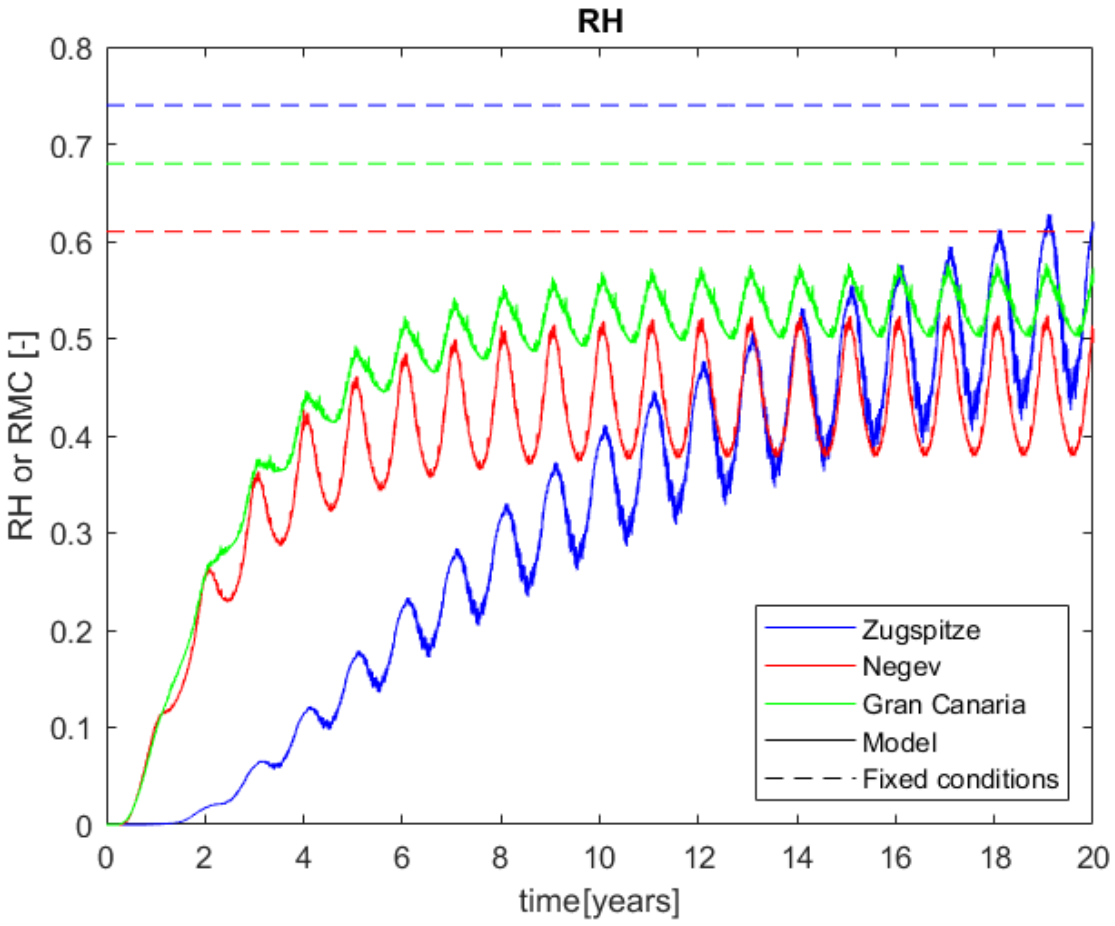

Figure 4.6: Difference in input when using the COMSOL model and the fixed RH. The lines at a constant value are the input when the average climatic RH is used. The lines that change value over time are the input from COMSOL

4.5.2. Modelling lifetime degradation of PV modules

A similar approach to accelerated lifetime tests is possible [33]. In this way, the RH is used in a rate equation (e.g. equation 4.3) which is then placed within a function with a predetermined shape that resembles the expected shape of the degradation of a module in real life conditions. In order to achieve this, the shape factor (u) needs to be changed. This is because in comparison, in accelerated lifetime tests degradation is much faster compared to the timescale that is being observed. This means that the shape factor decreases to make the degradation less steep. The value for the shape factor proposed for real life modelling is 0.19 [33]. This smoother degradation over the lifetime of the module is the reason why it is common to see in literature that a linear degradation is considered to be a good approximation for the behaviour through the lifetime of the module [72]. This makes it possible to model degradation without use of an analytical function with a predetermined shape. Three approaches will be investigated to model the degradation of modules under real life conditions:

- **Power degradation function with model results**: Predetermined power degradation function (equation 4.4) with moisture ingress model results. This approach is similar to the one that gave good results for the accelerated lifetime tests.
- **Power degradation function with averaged model results**: Predetermined power degradation function (equation 4.4) with average moisture ingress model results. This approach is more similar to the approach used in [33]
- **No degradation function**: Using k_{RH} directly as the degradation rate [41]. This eliminates the need for an analytical shape determining function.

As has been shown, in section 4.4.1 the parameter n changes significantly depending on whether a fixed or changing RH is used. This is because the input for the relative humidity is quite different when the results from the moisture ingress model are used. In order to take this into account the value for the parameter n proposed by Kaaya et al [33] is re-calibrated. This is done by solving the equation below. RMC_{model} is the average RMC returned by the model. The equation is solved for the location of Gran Canaria as it is the location used to train the model originally [33]. The new value for n is 0.9315.

$$RH_{fixed}^{n_{fixed}} = RMC_{model}^{n_{model}} \tag{4.7}$$

Power degradation function with model results:Using the same approach that was used for the accelerate lifetime tests presents a challenge. As already mentioned, the input for RH and temperature are meant to be constants. By using time varying values the function can predict an increase in performance if the module has a lower RH or Temperature at a given moment than in previous time steps.

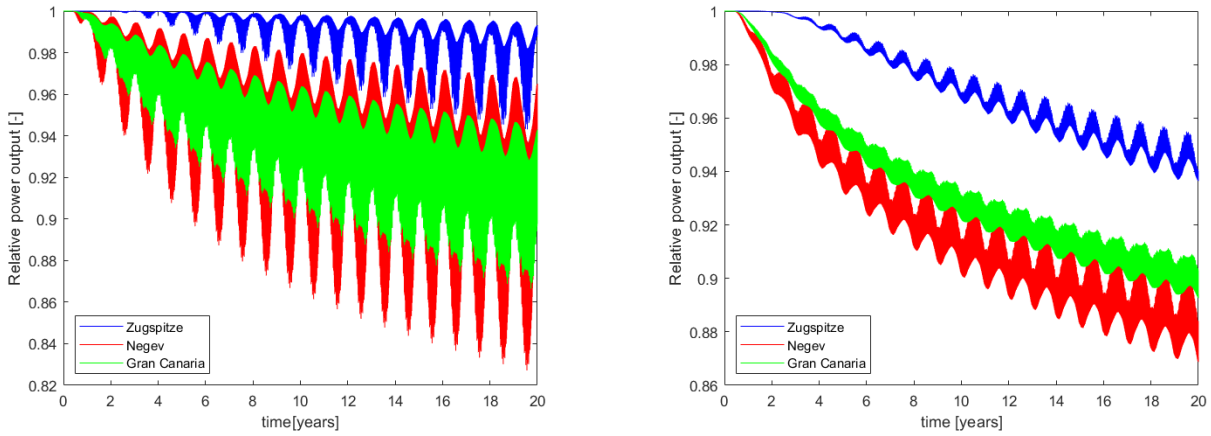

Figure 4.7: Left: Power degradation predicted by equation 4.4 using the results from the moisture ingress model. Right: Power degradation predicted by equation 4.4 with RMC from moisture ingress model and the fixed temperature proposed by [33].

The results shown in figure 4.7 confirm that the power degradation function in combination with the results of the moisture ingress model results in unrealistic behaviour. Figure 4.7 (right) shows the results of modelling using a fixed temperature and the changing relative moisture of the module. This is done to assess whether the fluctuation observed in figure 4.7 (left) is mainly caused by the temperature changes. It can be seen that the cooling/heating is the main cause of fluctuation in the model. However, using a fixed temperature still results in a relative power output that increases at certain moments. Even if it is a much smaller fluctuation than is obtained when using a changing temperature. This does not reflect the expected trend in degradation.

Therefore, this approach is discarded as an option to model the degradation of modules in combination with a moisture ingress model. This was not an issue with the accelerate lifetime tests as the conditions (RH) in the module eventually converge to the values in the environment. Additionally, the module is assumed to be in thermal equilibrium with the environment as there is no external radiation on the module. More importantly, there is no instance in which the module dries up or cools down that could lead to a predicted increase in performance. If the accelerated lifetime test included multiple cycles or instances of drying/cooling then a different approach would have to be considered also for accelerated lifetime tests.

Power degradation function with averaged model results: An alternative to this approach is to use a fixed value for the conditions RH and Temperature that reflect the results of the moisture ingress model. The motive for exploring this approach is that equation 4.4 is used as was intended by the author. The input would become a fixed value for RH and Temperature. The main benefit of this approach is that it takes into account material properties to determine the input to the power degradation function which is not done in when using the average climate conditions. Nevertheless, this approach will not include the seasonal dependence that is given by the moisture ingress model. By computing the average values the information about the dynamics of the system is lost. For example: how much time it would take for moisture to reach the front of the module is ignored.

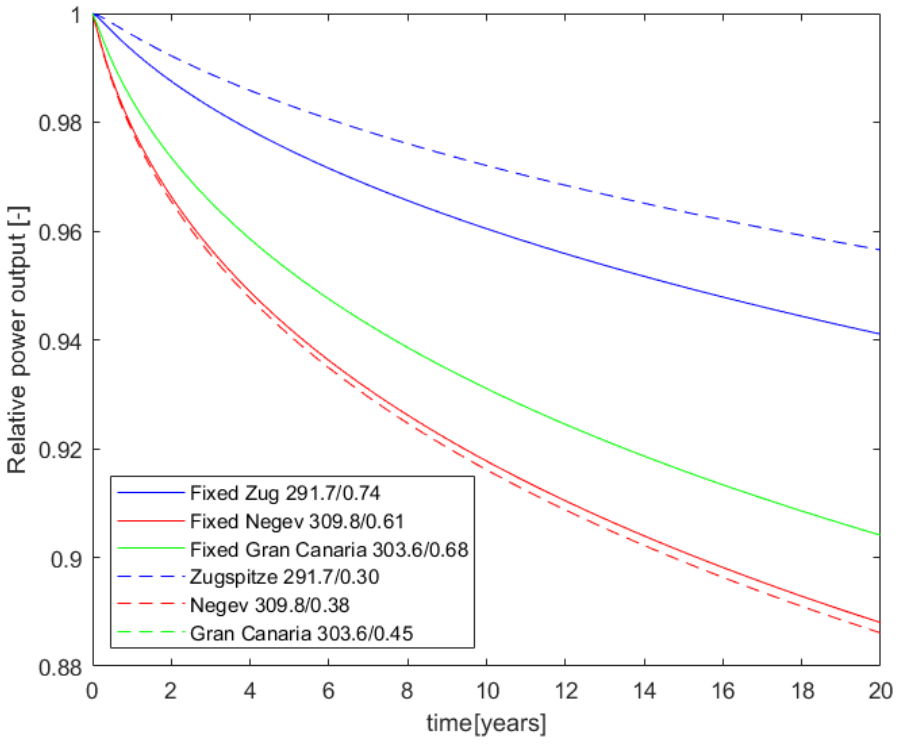

Figure 4.8: Power degradation predicted by equation 4.4 with RMC from averaged moisture ingress model results and the fixed temperature proposed by [33].

As can be seen from the above figures, the behaviour is much closer to what is expected. Figure 4.8 presents the results when the fixed temperature proposed by [33] is used in combination with the averaged RMC results of the moisture ingress model. The results for Gran Canaria are the same, this is due to the way in which the new value for n is determined. The predicted degradation rate is a bit higher for Negev and the degradation is significantly slower for Zugspitze when using the module RH. This difference is due to how much time it takes for RH of the module to reach steady state.

No degradation function: The last approach is to take directly k_{RH} as the degradation rate, eliminating the need for the analytical expression that determines the trend followed by the degradation. This approach has also been used by Coyle et al [49] in combination with module RH moisture. However, they used the simplified model given by equation 2.12 which as has already been discussed in the previous chapter can be used to calculate the concentration of water behind the cell not in front. Moreover, they use a different way to formula to model k_{RH} (equation 4.6). The relative power output is then calculated in the following way:

$$P_{MPP}(t) = P_{MPP}(t-0) - k_h \cdot \Delta t \tag{4.8}$$

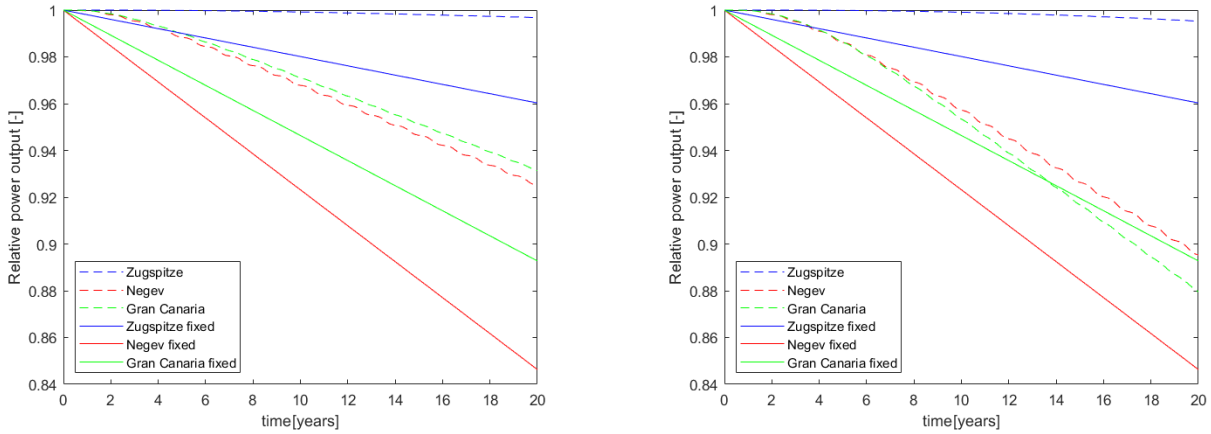

Figure 4.9: Left: Power degradation predicted by equation 4.8 and 4.3 using the results of the moisture ingress model and the fixed conditions for reference. Right: Power degradation predicted by equation 4.8 and 4.6 using the results of the moisture ingress model and the fixed conditions for reference (fixed conditions still using equation 4.3).

It is important to note that this approach differs substantially from the previous two. Therefore, the value of the constant k_0 is adapted to give a similar amount of degradation after 20 years as the previous models. Namely, the value of k_0 is taken to be 5% of what it was originally. Using the results from the moisture ingress model gives results that are closer to what is expected from degradation through the module's life. Firstly, there is a period of time where the degradation is 0 which is the time it takes for moisture to reach the front of the solar cell. Secondly, there is a periodicity to the degradation. It is higher in summer months where the temperatures are more elevated and it decreases in winter when the temperatures drop. The linear degradation that is predicted using the ambient fixed conditions is also shown. The advantages of this approach is that it is taking into account the effect of material parameters by using the results of the moisture ingress model and it does not use an analytical expression to set the shape of the degradation. This approach, is considered to be the most suited approach to combine results from the moisture ingress model which vary heavily through time with a degradation model.

The difference between the two models comes from a difference in the degradation rate that originates from the two different ways of taking into account the relative humidity. In equation 4.3 the degradation rate has an almost linear relationship to the Relative humidity inside the module (n = 0.9315). Whereas in equation 4.6 the degradation rate experiences an exponential increase. Meaning that at higher values of RMC the rate predicted by equation 4.6 will be significantly higher. In figure 4.10 the behaviour of the models as a function

of module temperature and RMC. The figure reflects the exponential dependence of the degradation rate on temperature. The dependence on the RMC is less pronounced. It can be seen that at higher values of RMC the two models behave differently. The Peck model (right) becomes more dependent on this value. This is due to the value in the denominator getting closer to 0. At lower values of RMC the models behave in a similar way.

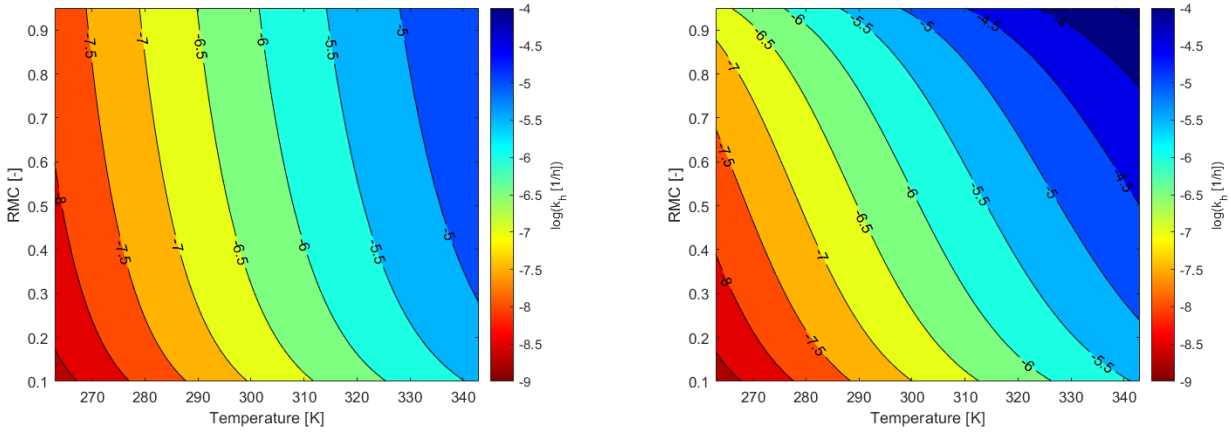

Figure 4.10: Left: Degradation rate given by equation 4.3 as a function of module temperature and RMC. Right: Degradation rate given by equation 4.6 as a function of module temperature and RMC.

4.5.3. Sensitivity analysis of degradation models

As already mentioned, the degradation model has not been calibrated using real life degradation data. The proposed model parameters are derived from the proposed values in literature [33]. The value of these parameters determines the predicted degradation rate. Therefore, a sensitivity analysis will be carried out on the values of these parameters in order to better understand the results given by the model. In this section, the sensitivity analysis will focus on the power degradation rate, k_h, predicted by the different models. When analyzing the power degradation as a function of temperature the RMC is considered constant with a value of 0.5. On the other hand, when the results are presented as a function of RMC the temperature is taken to be constant with a value of 303 K.

The first thing that is analyzed is the value of the parameter n in the Peck model. This value determines the effect of the RMC on the degradation rate. The results can be seen in figure 4.11. On the right, the effect on the degradation as a function of RMC is shown. The chosen values of n are 0.5, 0.9315, 1,4 and 1.9. 1.9 is the value given by the author that develops the model [33]. 0.9315 is the value obtained in the previous section when adapting the model to be utilized with a variable RMC. 0.5 is chosen to show what happens if the value is decrease even further and 1.4 is taken as a value in between the two. As the values of RMC is between 0 and 1, a higher value of n results in a slower degradation. This is shown in both images in figure 4.11. In figure 4.11(right), it can be seen that n determines the shape of the dependency of the degradation rate on the RMC. The value closest to 1 (n = 0.9315) presents an almost linear relationship between the degradation rate and the RMC. Values of n above 1 give a convex relationship and values below 1 a concave relationship. This means that a value above 1 will minimize the degradation rate at low values of RMC with a fast increase of the degradation rate at higher values. This is similar to the behaviour given by the BET model.

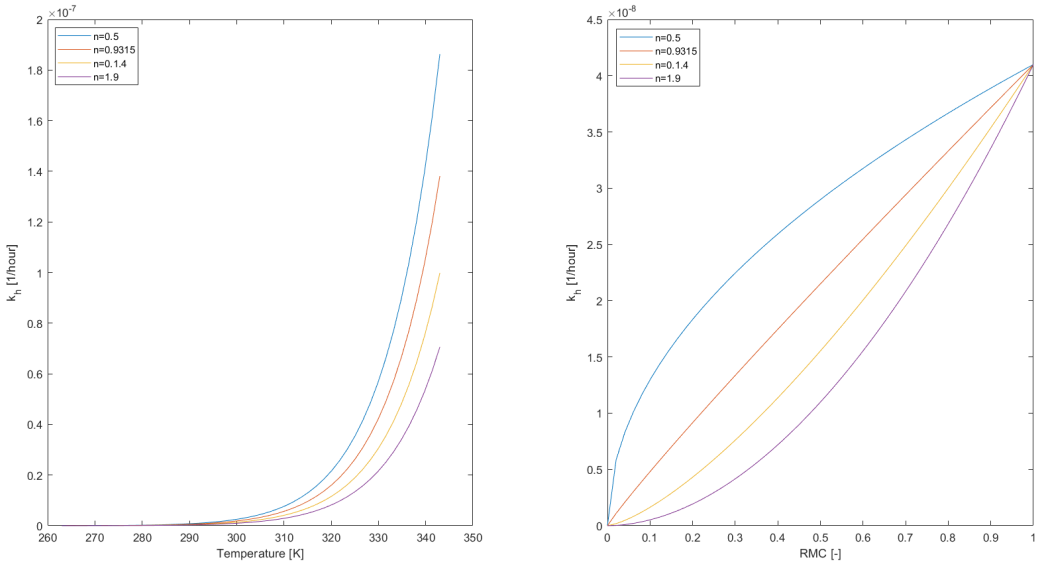

Figure 4.11: Sensitivity analysis for the parameter n in the Peck model. Power degradation after rate k_h n. Left: as a function of temperature. Right: as a function of RMC

One of the goals of the sensitivity analysis is to better understand how the two different models are affected by a change in the parameters. Therefore the results are presented for the sensitivity analysis of both models together. As can be seen in figure 4.12, the effect of changing k_0 on both models is the same. A higher k_0 results in a linear increase in the degradation rate. The results as a function of RMC are given in the appendix in figure C.7. They confirm the linear relationship between k_0 and the degradation rate.

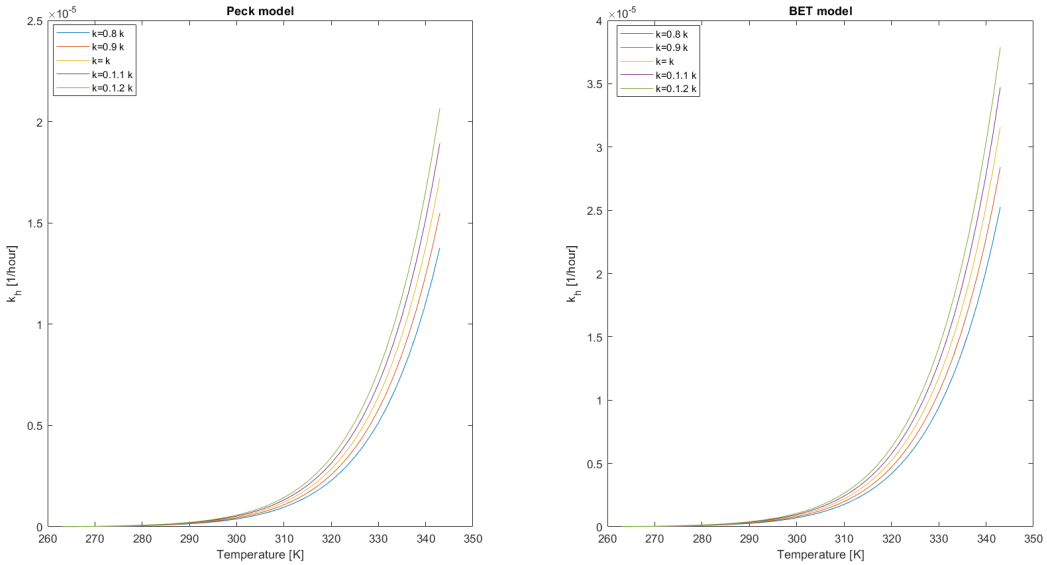

Figure 4.12: Sensitivity analysis of k_0 parameter as a function of temperature. Left: Peck model. Right: BET model

The results of the sensitivity analysis with respect to the parameter E_a as a function of temperature are given in figure 4.13. The results are plotted in the logarithmic scale. This is because the degradation rate has an exponential dependency on the activation energy. A lower activation energy results in an exponentially

higher degradation rate. This is true for both models. The results for the sensitivity analysis as a function of RMC are shown in the appendix in figure C.8. They confirm the exponential dependency of the degradation rate on the activation energy.

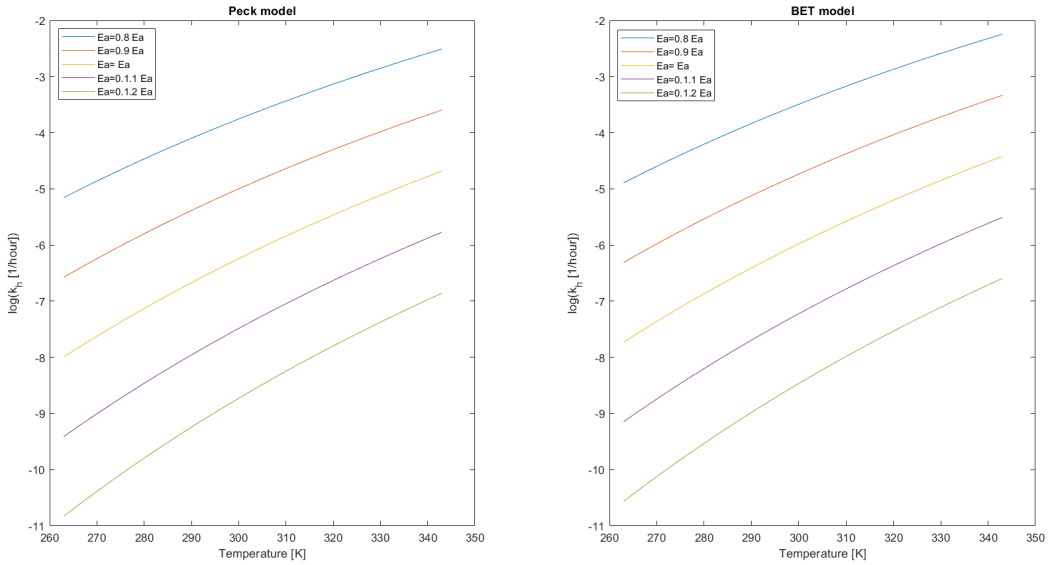

Figure 4.13: Sensitivity analysis of E_a parameter as a function of temperature. Left: Peck model. Right: BET model

4.6. Power degradation under different conditions

This analysis for different encapsulants and glass-glass modules is not possible because the mechanisms behind the degradation will be completely different, therefore it is not possible to compare the results as the values of the constants are would change for each module in those categories. The degradation for different climates will be analyzed. The sensitivity analysis revealed that the difference between the models stems from the way the RMC is taken into account. The degradation for different climates will be analyzed in three different cases:

- Peck model with n= 0.9315
- BET model
- Peck model with n = 1.9

These options are picked to analyze the effect of the different degradation models in different climates. The third option is picked as it is the value for the n parameter given in literature. This should also give results more similar to those delivered by the BET model. The results of the first case (Peck model with n = 0.9315) are shown in figure 4.14. The figure shows the predicted power degradation by the Peck model for the 11 locations which are grouped by climate type.

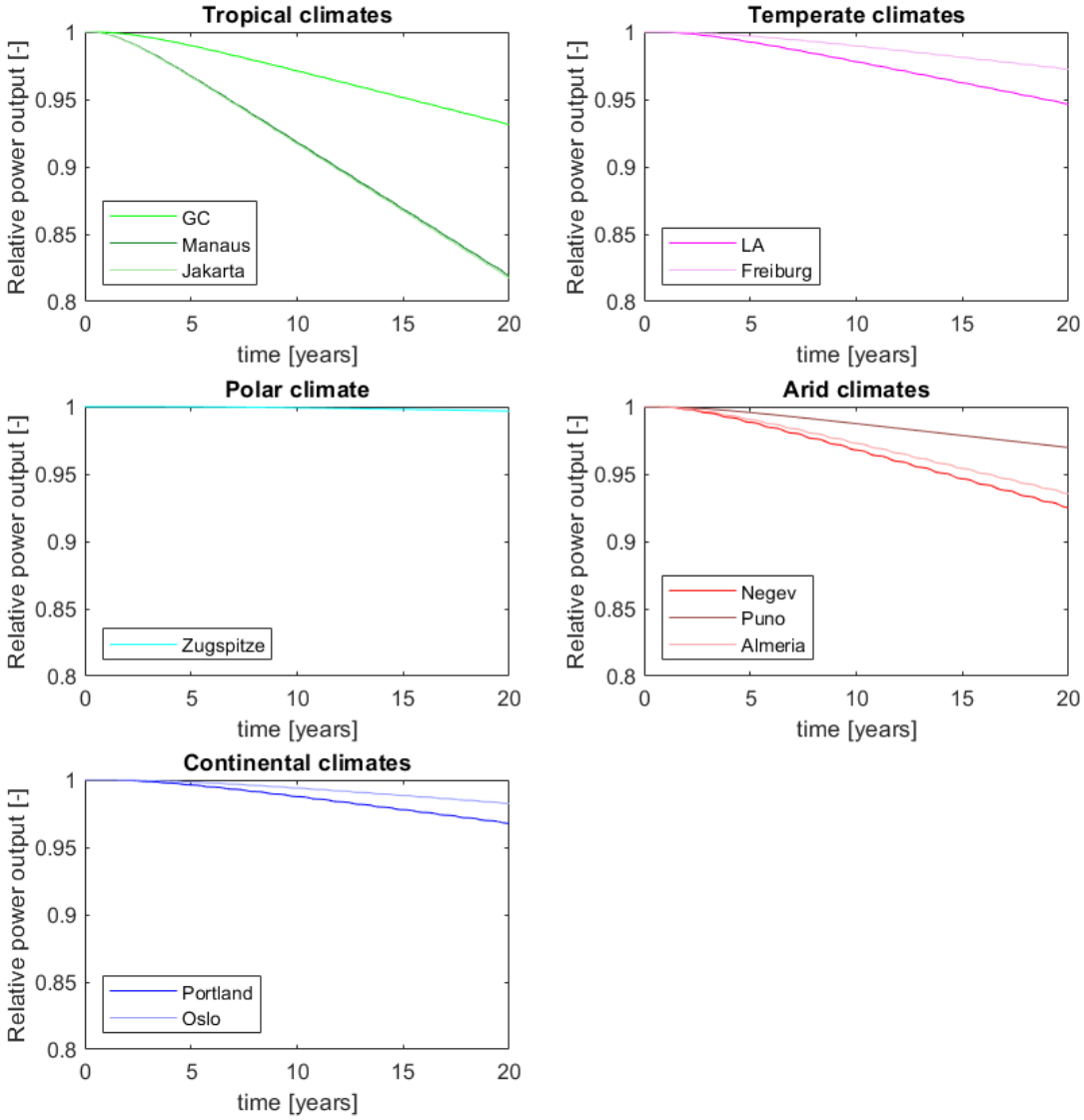

Figure 4.14: Predicted power degradation in different climates using the Peck model

The results for the BET model and the Peck model with n = 1.9 can be found in the appendix in figures C.9 and C.10. As has already been explained, the degradation predicted by these models is completely dependant on the value that is chose for the parameters. These parameters have to be calibrated with real life data which is not available. Therefore, analyzing these results and how the different models compare does not give useful insights. However, what these results can provide is useful insights to compare the different locations. In order to be able to compare the models a new quantity is defined, the relative amount of degradation (RD). RD is calculated by dividing the amount of degradation at the twentieth year ($1 - P(t = 20years)$) by the maximum amount of degradation predicted for any climate for a given model $1 - (P_{min}(t = 20years))$.

$$RD = \frac{1 - P(t = 20years)}{1 - (P_{min}(t = 20years))} \tag{4.9}$$

The results for the three models are shown in figure 4.15. It can be seen that all models predict the highest degradation for the tropical climates of Manaus and Jakarta. The lowest degradation is obtained for the polar

climate of Zugspitze. Differences arise for the rest of the data points but the same general trend is followed. The climates can be organized in the following fashion form the highest degradation to the lowest: Tropical > Arid > Temperate > Continental > Polar.

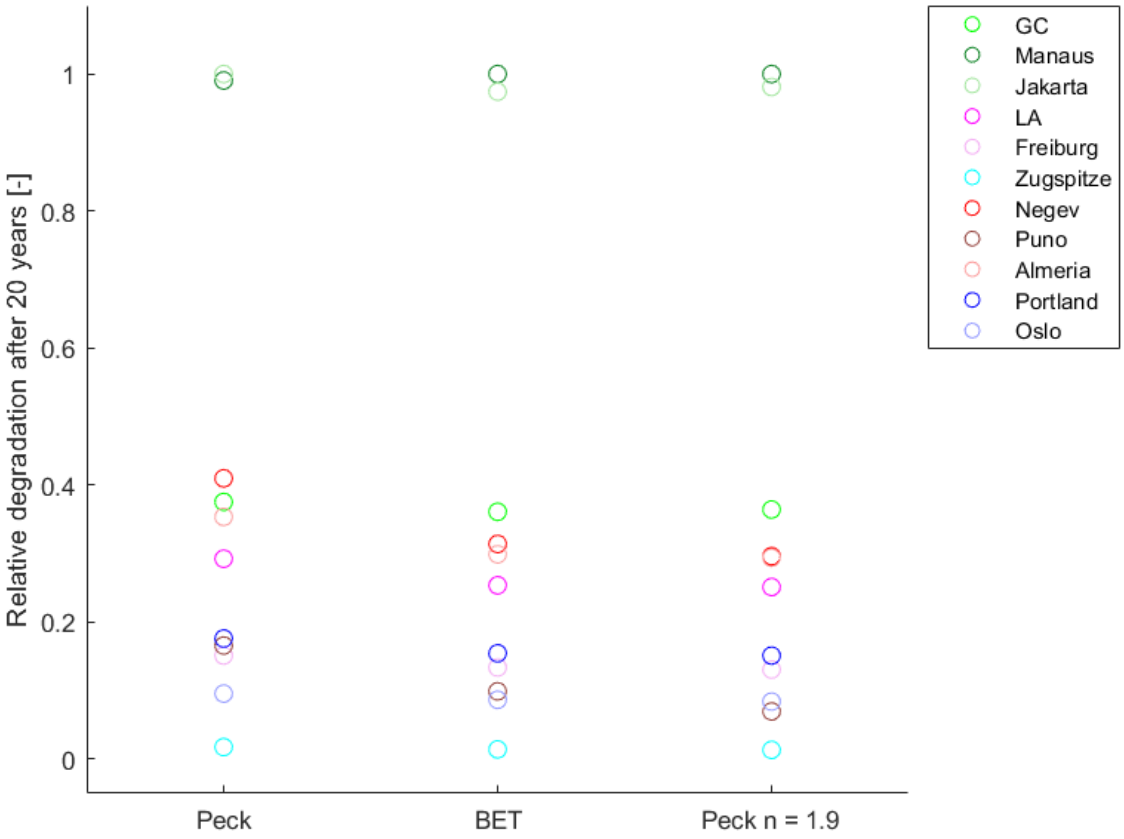

Figure 4.15: RD for all the climates by the three models

4.7. Conclusions

In this chapter, the degradation modelling using the results of the moisture ingress model as input is studied. Firstly, the degradation under accelerated life tests is studied. Damp heat tests are chosen as it is the test that allows to study the degradation caused by relative humidity independently. This is because there is not temperature cycling or UV exposure. The data found in literature allows to calibrate the model and the calibration is validated using data at different temperature or RH values. The results using the RMC obtained from the model and the ambient relative humidity provide similar results. This validates the use of the moisture ingress model to predict degradation in damp heat conditions. However, it does not offer an advantage over using the fixed ambient RH. This is because the accelerating nature of the degradation is captured by the analytical model presented by Kaaya et al [33] (equation 4.4). In this work, an addition to the analytical model proposed by Kaaya is put forward by adding the parameter L. This is a measure of the limit to the degradation caused by water.

The degradation in real life conditions is also studied. Here it is not possible to combine the analytical degradation model with the results of the moisture ingress model. The analytical model was developed to be used with fixed inputs and not time varying parameter. Alternatively, the usage of k_h directly as the degradation is proposed. This eliminates the need for an analytical model. The dynamics of the system are captured by the moisture ingress model. The problem is that there is not enough data to calibrate the parameters of the

model. Without proper calibration the degradation model can still be used to assess the degradation under different conditions. This is done for the simulation results for different climates where the degradation models show that the modules degrade differently in different climates. The degrade faster in hot and humid tropical climates and the slowest in cold polar climates. The general trend is summarized by this sequence: Tropical > Arid > Temperate > Continental > Polar.

In this chapter the first steps in modelling the degradation rate as a function of moisture are taken. If this work is to be continued the following aspects should be considered for future research:

- **Modelling of specific mechanisms**: The modelling of specific degradation mechanisms such as corrosion, delamination or discoloration could eliminate the need for an analytical model such as the Peck or BET model to model degradation.
- **Spatial dependence of degradation**: In this chapter the degradation rate is assumed to be uniform for the whole module. This is not what is observed in reality where the degradation is localized. For example delamination tends to occur closer to the edges [9]. One of the possible explanations is the accumulation of moisture in these locations. The moisture ingress model allows to evaluate the moisture distribution inside the module. It would be interesting if this can be used to predict the localisation of degradation in the PV modules
- **Approximate calibration of degradation model**: The power degradation profile of a module is not available in literature. However, there are studies that provide a yearly degradation rate for a given module in certain conditions. It would be interesting to check whether this data can be used to provide an approximate calibration of the degradation model.
- **Damp Heat tests experiments**: A climate chamber could be used to carry out damp heat tests on different modules to better understand the degradation in different types of modules

5

Conclusions and future work

Degradation is caused by a large variety of factors. The most important of which are temperature, humidity and Ultraviolet light. Modules are installed in different locations worldwide. This means that they are exposed to wide range of climatic conditions. Understanding how the different climatic conditions affect the PV module is important to assess the viability of projects in different locations. The exact physical processes that cause degradation are not fully understood. Degradation processes are generally modeled using analytical functions that reflect the nature of these processes. These models use the environmental conditions as input. However, the environmental conditions are not always a fair representation of the stresses suffered by a PV module. The temperature of the module and its relationship with environmental conditions is well understood. It can be modeled using a detailed approach like the fluid dynamics model or a simplified relation like the Sandia model. UV light exposure throughout its lifetime can be assessed as it is proportional to the irradiance incident on a PV module. On the other hand, the ambient relative humidity is not a good indicator of the amount of moisture inside a module. The ingress of water into the module is affected by the design of the module and the materials it is comprised of. Currently, the ambient relative humidity is used as an indicator of the stress posed by moisture on the solar module.

In chapter 2, A FEM model is developed in order to calculate the amount of moisture inside of a module. The model takes into account all the relevant physical processes. The moisture propagates through the module thanks to diffusion which is modeled using Fick's second law of diffusion. The equilibrium at the interface of the module is modeled using Henry's law. This model takes into account the different material properties that affect moisture ingress. Namely, the diffusion coefficient of materials as well as the solubility. The model therefore can be used to model the moisture ingress into different modules in different climates. The geometry of the model is modified in order to be able to model the moisture ingress into glass-glass modules. The model is validated using experimental and simulated values from literature.

In chapter 3, the developed model is used to simulate the moisture ingress into different modules in different climates. Precisely, the ingress in five different climates is simulated. The effect of material choice is studied by simulating modules with different encapsulants and different backsheets. Finally, glass-glass modules are also analyzed. These results are used to draw a relationship between the model parameters and the results of the model. The most interesting results is that the modules end up reaching an equilibrium with the surrounding environment. This equilibrium is predicted by the effective relative humidity of at the interface of the module. The second interesting result is that the dynamics of moisture ingress can be linked to the diffusion coefficient and length of the path through which the moisture has to propagate. These approximations could provide good estimates of the moisture ingress into a PV module through its lifetime. Although, there are some limitations in the prediction of the results for different backsheets.

One of the goals of this research is to improve our understanding of the link between moisture and degradation, The moisture ingress model calculates the amount of water that enters a module. It provides no insight into how the modules degrade. The best way of combining the results with the analytical degradation model is analyzed in chapter 4. Degradation data for PV modules is available for accelerated lifetime models. The results of accelerated lifetime models is used to validate the compatibility of the moisture ingress model

with analytical models. The results show that it is possible to use the model in combination with analytical degradation models to predict the results of accelerated lifetime tests. On the other hand, the analytical models can't be combined with the model to predict the degradation through the lifetime of the module. This is because the analytical models are built to use a constant value for the ambient relative humidity. Swapping this with the time changing value of moisture inside the module which is a time varying value that fluctuates does not give good results. Therefore, a different approach has to be followed for modelling the degradation in real life conditions. The Peck and BET model are studied as alternatives for real life degradation. These models differ in how they relate the amount of moisture to the degradation rate. Due to the lack of data it is not possible to calibrate these models correctly and use them to predict an amount of degradation. It is still possible to use them to compare the degradation under different conditions. The degradation in different climates follows the general trend (higher degradation to lowest degradation):Tropical > Arid > Temperate > Continental > Polar.

5.1. Future work

There are three areas in which the work presented in this thesis can be continued: Improving the moisture ingress modelling, Experimental data collection and improving the degradation modelling. The possible improvements for the moisture ingress modelling and the power degradation modelling are already discussed in the corresponding section in Chapter 2 and in Chapter 4. Here, they are just outlined for the sake of completeness

- **Moisture ingress modelling**
  - Improving the efficiency of the COMSOL model
  - Non-Fickian diffusion
  - Material ageing
- **Experimental data collection**
  - Damp heat experiments on different modules
  - Approximate calibration of degradation model with literature data.
- **Power degradation modelling**
  - Modelling of specific mechanisms
  - Spatial dependence of degradation

References

[1] Iea - International Energy Agency. *Renewables 2022*. Tech. rep. 2022. URL: www.iea.org.

[2] Anik Goswami et al. “Degradation analysis and the impacts on feasibility study of floating solar photovoltaic systems”. In: *Sustainable Energy, Grids and Networks* 26 (June 2021), p. 100425. DOI: 10.1016/J.SEGAN.2020.100425.

[3] Ali O M Maka et al. “Solar energy technology and its roles in sustainable development”. In: 6 (2022), pp. 476–483. DOI: 10.1093/ce/zkac023. URL: https://doi.org/10.1093/ce/zkac023.

[4] M. Aghaei et al. *Review of degradation and failure phenomena in photovoltaic modules*. May 2022. DOI: 10.1016/j.rser.2022.112160.

[5] Namsu Kim et al. “Experimental characterization and simulation of water vapor diffusion through various encapsulants used in PV modules”. In: *Solar Energy Materials and Solar Cells* 116 (Sept. 2013), pp. 68–75. DOI: 10.1016/J.SOLMAT.2013.04.007.

[6] Dirk C. Jordan et al. “Compendium of photovoltaic degradation rates”. In: *Progress in Photovoltaics: Research and Applications* 24.7 (July 2016), pp. 978–989. DOI: 10.1002/pip.2744.

[7] Oscar Kwame Segbefia et al. *Moisture ingress in photovoltaic modules: A review*. Aug. 2021. DOI: 10.1016/j.solener.2021.06.055.

[8] Vikrant Sharma et al. *Performance and degradation analysis for long term reliability of solar photovoltaic systems: A review*. 2013. DOI: 10.1016/j.rser.2013.07.046.

[9] Michele Cândida Carvalho de Oliveira et al. *The causes and effects of degradation of encapsulant ethylene vinyl acetate copolymer (EVA) in crystalline silicon photovoltaic modules: A review*. Jan. 2018. DOI: 10.1016/j.rser.2017.06.039.

[10] Neha Bansal et al. *Comparative investigation of performance evaluation, degradation causes, impact and corrective measures for ground mount and rooftop solar PV plants – A review*. Oct. 2021. DOI: 10.1016/j.seta.2021.101526.

[11] Manish Kumar et al. *Performance assessment and degradation analysis of solar photovoltaic technologies: A review*. 2017. DOI: 10.1016/j.rser.2017.04.083.

[12] Bhushan Sopori et al. “Understanding light-induced degradation of c-Si solar cells”. In: *Conference Record of the IEEE Photovoltaic Specialists Conference*. 2012, pp. 1115–1120. DOI: 10.1109/PVSC.2012.6317798.

[13] Osarumen O. Ogbomo et al. “Effect of operating temperature on degradation of solder joints in crystalline silicon photovoltaic modules for improved reliability in hot climates”. In: *Solar Energy* 170 (Aug. 2018), pp. 682–693. DOI: 10.1016/j.solener.2018.06.007.

[14] Manju Santhakumari et al. *A review of the environmental factors degrading the performance of silicon wafer-based photovoltaic modules: Failure detection methods and essential mitigation techniques*. Aug. 2019. DOI: 10.1016/j.rser.2019.04.024.

[15] Swapnil Dubey et al. “Temperature dependent photovoltaic (PV) efficiency and its effect on PV production in the world - A review”. In: *Energy Procedia*. Vol. 33. Elsevier Ltd, 2013, pp. 311–321. DOI: 10.1016/j.egypro.2013.05.072.

[16] Ababacar Ndiaye et al. “Degradations of silicon photovoltaic modules: A literature review”. In: *Solar Energy* 96 (2013), pp. 140–151. DOI: 10.1016/j.solener.2013.07.005.

[17] Philip Hülsmann et al. *Simulation of water ingress into PV-modules: IEC-testing versus outdoor exposure*. May 2015. DOI: 10.1016/j.solener.2015.03.007.

[18] Wei Luo et al. *Potential-induced degradation in photovoltaic modules: A critical review*. Jan. 2017. DOI: 10.1039/c6ee02271e.

[19] Ernest Hasselbrink et al. “Validation of the PVLife model using 3 million module-years of live site data”. In: *Conference Record of the IEEE Photovoltaic Specialists Conference*. Institute of Electrical and Electronics Engineers Inc., 2013, pp. 7–12. DOI: 10.1109/PVSC.2013.6744087.

[20] Stefan Mitterhofer et al. *WORLDWIDE MOISTURE INGRESS EVALUATION IN PHOTOVOLTAIC MODULES USING FINITE ELEMENT SIMULATIONS AND MACHINE LEARNING*. Tech. rep.

[21] Michael Koehl et al. “Modelling of conditions for accelerated lifetime testing of Humidity impact on PV-modules based on monitoring of climatic data”. In: *Solar Energy Materials and Solar Cells* 99 (Apr. 2012), pp. 282–291. DOI: 10.1016/j.solmat.2011.12.011.

[22] M KEMPE. “Modeling of rates of moisture ingress into photovoltaic modules”. In: *Solar Energy Materials and Solar Cells* 90.16 (Oct. 2006), pp. 2720–2738. DOI: 10.1016/j.solmat.2006.04.002.

[23] A. Omazic et al. “Relation between degradation of polymeric components in crystalline silicon PV module and climatic conditions: A literature review”. In: *Solar Energy Materials and Solar Cells* 192 (Apr. 2019), pp. 123–133. DOI: 10.1016/j.solmat.2018.12.027.

[24] M. Gagliardi et al. “A reaction-diffusion formulation to simulate EVA polymer degradation in environmental and accelerated ageing conditions”. In: *Solar Energy Materials and Solar Cells* 164 (May 2017), pp. 93–106. DOI: 10.1016/j.solmat.2017.02.014.

[25] Bechara Fadi Nehme et al. “Real-Time Thermoelectrical Model of PV Panels for Degradation Assessment”. In: *IEEE Journal of Photovoltaics* 7.5 (Sept. 2017), pp. 1362–1375. DOI: 10.1109/JPHOTOV.2017.2711430.

[26] Dirk C. Jordan et al. “Photovoltaic failure and degradation modes”. In: *Progress in Photovoltaics: Research and Applications* 25.4 (Apr. 2017), pp. 318–326. DOI: 10.1002/pip.2866.

[27] Jaeun Kim et al. *A review of the degradation of photovoltaic modules for life expectancy*. July 2021. DOI: 10.3390/en14144278.

[28] S. Pingel et al. “Potential induced degradation of solar cells and panels”. In: *Conference Record of the IEEE Photovoltaic Specialists Conference*. 2010, pp. 2817–2822. DOI: 10.1109/PVSC.2010.5616823.

[29] Sascha Lindig et al. *Review of statistical and analytical degradation models for photovoltaic modules and systems as well as related improvements*. Nov. 2018. DOI: 10.1109/JPHOTOV.2018.2870532.

[30] Erick Martinez-Loran et al. “Finite Element Simulation of Potential-Induced Degradation Kinetics in p-Type Silicon Solar Modules”. In: *IEEE Journal of Photovoltaics* 12.1 (Jan. 2022), pp. 45–52. DOI: 10.1109/JPHOTOV.2021.3123870.

[31] Michael Gostein et al. “Light soaking effects on photovoltaic modules: Overview and literature review”. In: *Conference Record of the IEEE Photovoltaic Specialists Conference*. 2011, pp. 003126–003131. DOI: 10.1109/PVSC.2011.6186605.

[32] Philip Ingenhoven et al. “Comparison of statistical and deterministic smoothing methods to reduce the uncertainty of performance loss rate estimates”. In: *IEEE Journal of Photovoltaics* 8.1 (Jan. 2018), pp. 224–232. DOI: 10.1109/JPHOTOV.2017.2762523.

[33] Ismail Kaaya et al. “Modeling Outdoor Service Lifetime Prediction of PV Modules: Effects of Combined Climatic Stressors on PV Module Power Degradation”. In: *IEEE Journal of Photovoltaics* 9.4 (July 2019), pp. 1105–1112. DOI: 10.1109/JPHOTOV.2019.2916197.

[34] Arun Bala Subramaniyan et al. “Quantification of Environmental Effects on PV Module Degradation: A Physics-Based Data-Driven Modeling Method”. In: *IEEE Journal of Photovoltaics* 8.5 (Sept. 2018), pp. 1289–1296. DOI: 10.1109/JPHOTOV.2018.2850527.

[35] Archana Sinha et al. “Prediction of Climate-Specific Degradation Rate for Photovoltaic Encapsulant Discoloration”. In: *IEEE Journal of Photovoltaics* 10.4 (July 2020), pp. 1093–1101. DOI: 10.1109/JPHOTOV.2020.2989182.

[36] Michael D Kempe et al. “Evaluation of moisture ingress from the perimeter of photovoltaic modules”. In: (2013). DOI: 10.1002/pip.2374. URL: https://onlinelibrary.wiley.com/doi/10.1002/pip.2374.

[37] Eleonora Annigoni et al. *Modelling Potential-Induced Degradation in crystalline silicon solar cells: from accelerated-aging laboratory testing to outdoor prediction*. Tech. rep. EPFL, 2016.

[38] Nora Jullok et al. “Sorption and diffusivity study of acetic acid and water in polymeric membranes”. In: *Chemical Engineering Science* 78 (Aug. 2012), pp. 14–20. DOI: 10.1016/J.CES.2012.04.022.

[39] Philip Hülsmann et al. “Temperature-dependent water vapour and oxygen permeation through different polymeric materials used in photovoltaic-modules”. In: (2012). DOI: 10.1002/pip.2273. URL: https://onlinelibrary.wiley.com/doi/10.1002/pip.2273.

[40] Stefan Mitterhofer. “Modelling and monitoring of moisture transport phenomena in polymeric materials and photovoltaic modules”. PhD thesis. University of Ljubjana, 2021.

[41] Dennis J Coyle. “Life prediction for CIGS solar modules part 1: modeling moisture ingress and degradation”. In: (2011). DOI: 10.1002/pip.1172. URL: https://onlinelibrary.wiley.com/doi/10.1002/pip.1172.

[42] Stefan Mitterhofer et al. “A Dual-Transport Model of Moisture Diffusion in PV Encapsulants for Finite-Element Simulations”. In: *IEEE Journal of Photovoltaics* 10.1 (Jan. 2020), pp. 94–102. DOI: 10.1109/JPHOTOV.2019.2955182.

[43] Soney C. George et al. “Transport phenomena through polymeric systems”. In: *Progress in Polymer Science* 26.6 (Aug. 2001), pp. 985–1017. DOI: 10.1016/S0079-6700(00)00036-8.

[44] Akhilesh Dadaniya et al. “Multilayer Backsheet Characterization Using Diffusion Experiments and Optimization Method for Water Diffusion Simulation Inside the Photovoltaic Module”. In: *IEEE Journal of Photovoltaics* 10.1 (Jan. 2020), pp. 306–314. DOI: 10.1109/JPHOTOV.2019.2953400.

[45] Akhilesh Dadaniya et al. “Water diffusion simulation in photovoltaic module based on the characterization of encapsulant material using in-situ gravimetric technique”. In: *Solar Energy Materials and Solar Cells* 201 (Oct. 2019). DOI: 10.1016/J.SOLMAT.2019.110063.

[46] Michael D. Kempe et al. “Acetic acid production and glass transition concerns with ethylene-vinyl acetate used in photovoltaic devices”. In: *Solar Energy Materials and Solar Cells* 91.4 (Feb. 2007), pp. 315–329. DOI: 10.1016/J.SOLMAT.2006.10.009.

[47] P. Hülsmann et al. “Permeation of water vapour through polyethylene terephthalate (PET) films for back-sheets of photovoltaic modules”. In: *Polymer Testing* 58 (Apr. 2017), pp. 153–158. DOI: 10.1016/J.POLYMERTESTING.2016.11.028.

[48] Nivedita S. Sangaj et al. “Permeability of polymers in protective organic coatings”. In: *Progress in Organic Coatings* 50.1 (June 2004), pp. 28–39. DOI: 10.1016/J.PORGCOAT.2003.09.015.

[49] Dennis J Coyle et al. “Life prediction for CIGS solar modules part 2: degradation kinetics, accelerated testing, and encapsulant effects”. In: (2011). DOI: 10.1002/pip.1171. URL: https://onlinelibrary.wiley.com/doi/10.1002/pip.1171.

[50] Volker Naumann et al. “Influence of soiling and moisture ingress on long term PID susceptibility of photovoltaic modules”. In: *AIP Conference Proceedings*. Vol. 2147. American Institute of Physics Inc., Aug. 2019. DOI: 10.1063/1.5123873.

[51] David Wisniewski et al. “Measurement and modelling of water ingress into double-glass photovoltaic modules”. In: *Progress in Photovoltaics: Research and Applications* 27.2 (Feb. 2019), pp. 144–151. DOI: 10.1002/PIP.3069.

[52] Sagarika Kumar et al. “Imaging and micro-structural characterization of moisture induced degradation in crystalline silicon photovoltaic modules”. In: *Solar Energy* 194 (Dec. 2019), pp. 903–912. DOI: 10.1016/J.SOLENER.2019.11.037.

[53] Marko Jankovec et al. “In-Situ Monitoring of Moisture Ingress in PV Modules Using Digital Humidity Sensors”. In: *IEEE Journal of Photovoltaics* 6.5 (Sept. 2016), pp. 1152–1159. DOI: 10.1109/JPHOTOV.2016.2583779.

[54] Nikoleta Kyranaki. “Corrosion in crystalline silicon photovoltaic modules and the influence on performance”. PhD thesis. Loughborough University, 2020.

[55] Shikha Marwaha et al. “Analytical Modeling of Diffusion of Moisture in Silicon Photovoltaic Module under Damp Heat Testing Condition”. In: (2021). DOI: 10.1007/s12633-021-01156-7/Published. URL: https://doi.org/10.1007/s12633-021-01156-7.

[56] Rishi E. Kumar et al. “Quantitative Determination of Moisture Content in Solar Modules by Short-Wave Infrared Reflectometry”. In: *IEEE Journal of Photovoltaics* 9.6 (Nov. 2019), pp. 1748–1753. DOI: 10.1109/JPHOTOV.2019.2938108.

[57] E. R. Anagha et al. “Moisture Ingress Modeling in c-Si PV Modules using Finite Element Simulations Based on Dual Transport Diffusion”. In: *Conference Record of the IEEE Photovoltaic Specialists Conference* (June 2021), pp. 2470–2474. DOI: 10.1109/PVSC43889.2021.9518770.

[58] M C Peel et al. “Hydrology and Earth System Sciences Updated world map of the Köppen-Geiger climate classification”. In: *Hydrol. Earth Syst. Sci* 11 (2007), pp. 1633–1644. URL: www.hydrol-earth-syst-sci.net/11/1633/2007/.

[59] Nadka Tz. Dintcheva et al. “Encapsulant Materials and Their Adoption in Photovoltaic Modules: A Brief Review”. In: *Sustainability* 15.12 (June 2023), p. 9453. DOI: 10.3390/su15129453.

[60] Salman Amin et al. *THERMOPLASTIC ELASTOMERIC (TPE) MATERIALS AND THEIR USE IN OUTDOOR ELECTRICAL INSULATION*. Tech. rep. 2011, pp. 15–30.

[61] Cornelia Wiesmeier Peike et al. *Overview of PV module encapsulation materials CTM of BIPV modules View project PV-Mate View project*. Tech. rep. 2015. URL: https://www.researchgate.net/publication/256374925.

[62] Michael D. Kempe et al. “Modeling moisture ingress through polyisobutylene-based edge-seals”. In: *Progress in Photovoltaics: Research and Applications* 23.5 (May 2015), pp. 570–581. DOI: 10.1002/PIP.2465.

[63] Rico Meitzner et al. “Method for determination of parameters for moisture simulations in photovoltaic modules and laminated glass”. In: (2015). DOI: 10.1016/j.solmat.2015.08.014. URL: http://dx.doi.org/10.1016/j.solmat.2015.08.014.

[64] C. Peike et al. “Origin of damp-heat induced cell degradation”. In: *Solar Energy Materials and Solar Cells* 116 (Sept. 2013), pp. 49–54. DOI: 10.1016/J.SOLMAT.2013.03.022.

[65] Nicholas R Wheeler et al. “Degradation Pathway Models for Photovoltaics Module Lifetime Performance”. In: ().

[66] Huaping Xiong et al. “Corrosion behavior of crystalline silicon solar cells”. In: *Microelectronics Reliability* 70 (Mar. 2017), pp. 49–58. DOI: 10.1016/J.MICROREL.2017.01.006.

[67] Gernot Oreski et al. “Properties and degradation behaviour of polyolefin encapsulants for photovoltaic modules”. In: *Progress in Photovoltaics: Research and Applications* 28.12 (Dec. 2020), pp. 1277–1288. DOI: 10.1002/PIP.3323.

[68] Joseph Karas et al. “Degradation of copper-plated silicon solar cells with damp heat stress”. In: (2020). DOI: 10.1002/pip.3331. URL: https://onlinelibrary.wiley.com/doi/10.1002/pip.3331.

[69] Jiang Zhu et al. “Changes of solar cell parameters during damp-heat exposure”. In: *Progress in Photovoltaics: Research and Applications* 24.10 (Oct. 2016), pp. 1346–1358. DOI: 10.1002/PIP.2793. URL: https://onlinelibrary.wiley.com/doi/full/10.1002/pip.2793%20https://onlinelibrary.wiley.com/doi/abs/10.1002/pip.2793%20https://onlinelibrary.wiley.com/doi/10.1002/pip.2793.

[70] Michael Koehl et al. “Evaluation of damp-heat testing of photovoltaic modules”. In: *Progress in Photovoltaics: Research and Applications* 25.2 (Feb. 2017), pp. 175–183. DOI: 10.1002/PIP.2842.

[71] Wonwook Oh et al. “The degradation of multi-crystalline silicon solar cells after damp heat tests”. In: (2014). DOI: 10.1016/j.microrel.2014.07.071. URL: http://dx.doi.org/10.1016/j.microrel.2014.07.071.

[72] Manuel Vázquez et al. “Photovoltaic module reliability model based on field degradation studies”. In: *Progress in Photovoltaics: Research and Applications* 16.5 (2008), pp. 419–433. DOI: 10.1002/PIP.825.

A

Moisture ingress model development

A.1. Diffusion coefficient from different sources

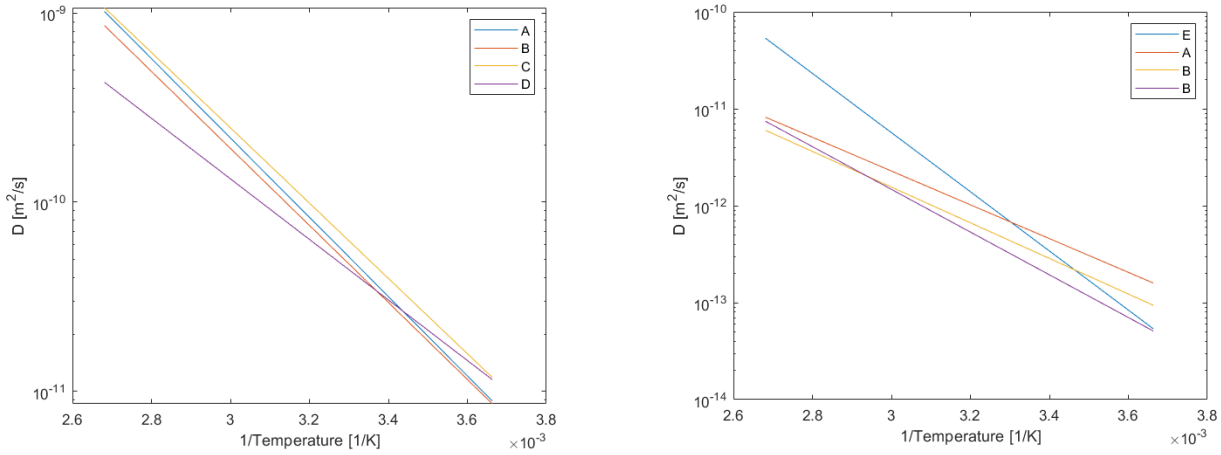

Figure A.1: Left: Diffusion coefficient from different sources for EVA ; Right: Diffusion coefficient from different sources for PET Backsheets. Sources: A = [17], B = [40], C =[36], D = [45], E =[44]

The diffusion coefficients found for EVA show good correlation for the range of temperatures that are relevant for the model. At higher temperatures the values for the values reported in [45] deviate from the other values reported. This should be taken into account but these high temperatures are reached less frequently. Similarly, for backsheets the diffusion coefficients from different sources have similar values. However, the values reported in [44] deviate significantly at higher temperatures. The higher deviation for backsheets can be explained due to the different layouts and components that can compose the backsheet. All the data shown in figure A.1 (right) corresponds to PET based backsheets. However, they have more layers which can be different and have different properties.

	$D_0\ [m^2/s]$	$E_a\ [kJ/mol]$	Source
Encapsulant (EVA)	$4.22 \cdot 10^{-4}$	40.12	[17]
	$2.46 \cdot 10^{-4}$	38.97	[40]
	$2.31 \cdot 10^{-4}$	38.1	[36]
	$8.41 \cdot 10^{-6}$	30.64	[45]
Backsheet (PET)	$3.84 \cdot 10^{-7}$	33.35	[17]
	$5.1 \cdot 10^{-7}$	35.2	[40]
	$6 \cdot 10^{-6}$	42.18	[40] (White PET)
	$8.13 \cdot 10^{-3}$	58.43	[44]

Table A.1: Arrhenius expression parameters from different sources for Diffusion coefficient of EVA and PET based backsheets

A.2. Solubilities from different sources

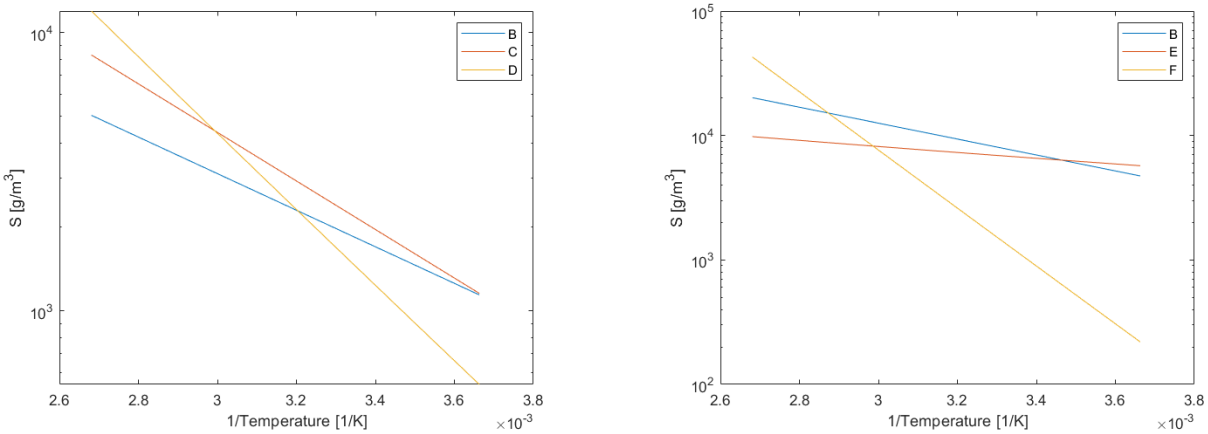

Figure A.2: Left: Solubility coefficients for EVA encapsulants from different sources. Right: Solubility coefficient for PET based backsheets from different sources. B = [40], C =[36], D = [45], E =[44], F = [39]

The values from the paper of Hulsmann et al [39] are not given because they do not provide solubility measurements. The curve is obtained by using the Diffusion coefficient and the Permeation coefficient. The values reported for the EVA encapsulant show a relatively good agreement. However, the values for the solubility in the backsheet differ more. This could be caused by a greater variability in the chemistry of the backsheets used as they are comprised of multiple layers. The backsheets are called by the composition of the core layer (PET) but the other layers can have a different composition and still be referred to as PET backsheets.

	$S_0\ [g/m^3]$	$E_a\ [kJ/mol]$	Source
Encapsulant (EVA)	$2.91 \cdot 10^5$	12.58	[40]
	$1.81 \cdot 10^6$	16.7	[36]
	$8.41 \cdot 10^{-6}$	30.64	[45]
Backsheet (PET)	$1.048 \cdot 10^6$	12.26	[40]
	$S_0\ [g/(m^3 \cdot Pa)]$	$E_a\ [kJ/mol]$	Source
Encapsulant (EVA)	$4.92 \cdot 10^{-4}$	-16.836	[45]
Backsheet (PET)	$3.81 \cdot 10^{-7}$	-38.44	[44]

Table A.2: Arrhenius expression parameters from different sources for Solubility coefficient of EVA and PET based backsheets

A.3. Model validation

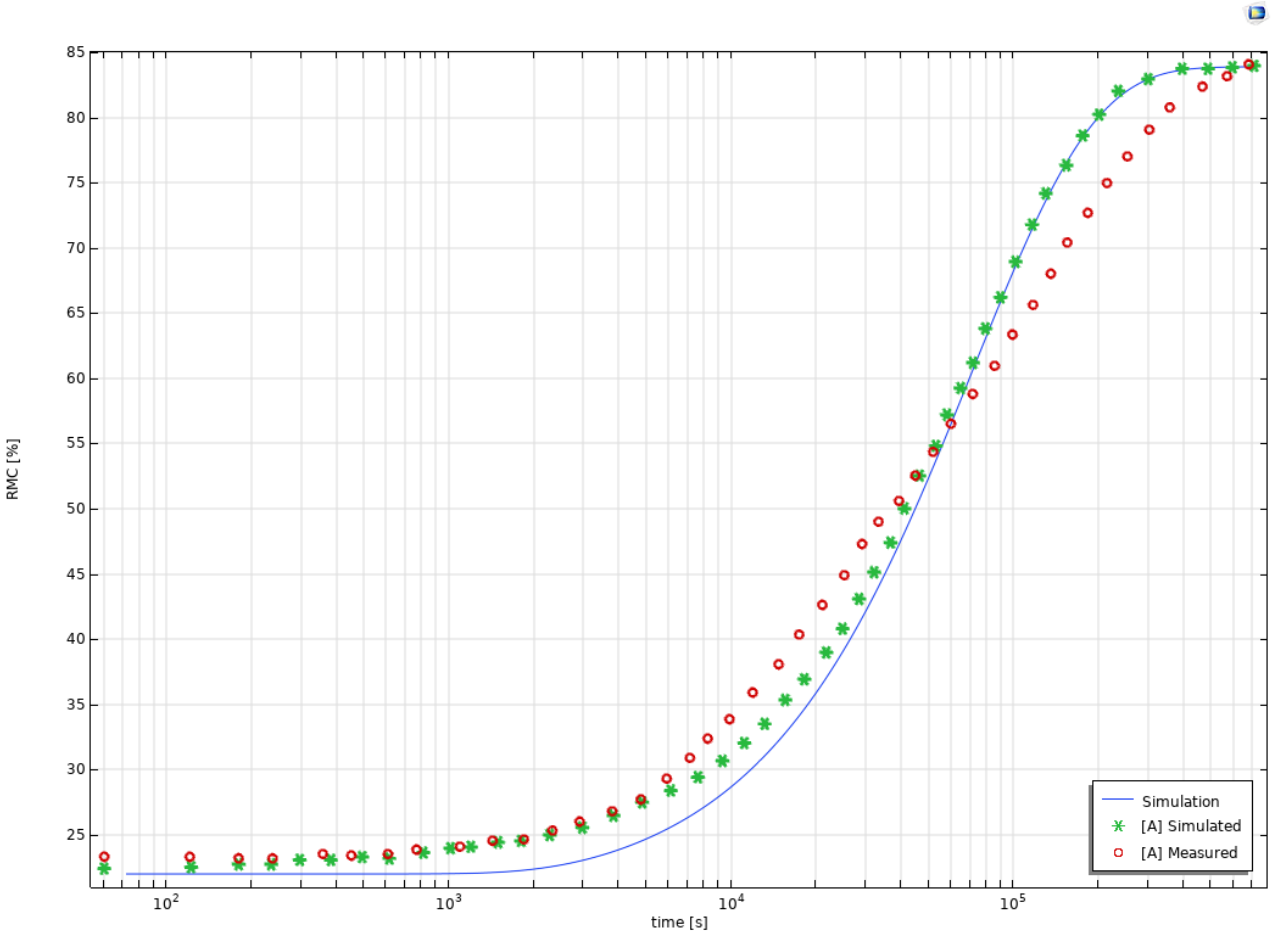

Figure A.3: Comparison of experimental and simulated results from literature and results of the model presented in this thesis. [A] = [54]

B

Moisture ingress model results

B.1. Moisture ingress for different climates

In the figure below the ambient conditions for the different locations are given together with the values for the hottest/coldest and most/least humid months. This gives an idea not only about the average conditions but how varied they are through the year.

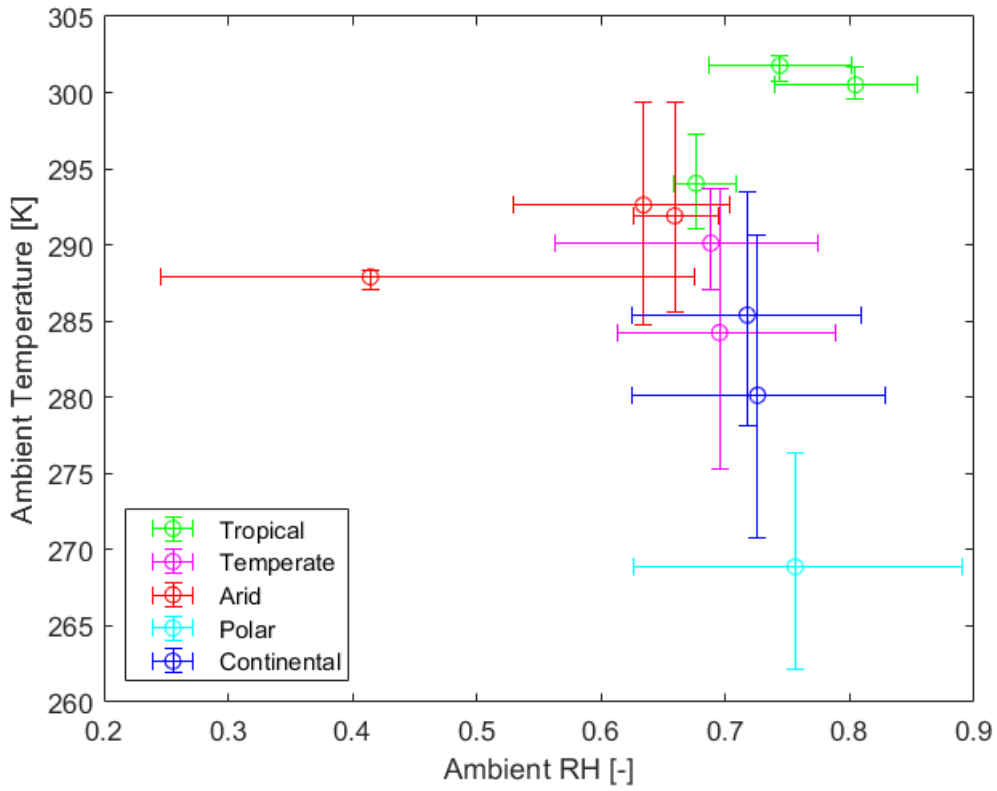

Figure B.1: Average RH and ambient temperature for each location with error bars representing the hottest/coldest and highest/lowest RH months for each location

In figure B.2 the results for the RMC inside the modules without applying an averaging over the day are shown. These results are included as they are the actual results delivered by the moisture ingress model. however, these graphs are ot easily readable that is why they are included in teh appendix and not in the main body of the report.

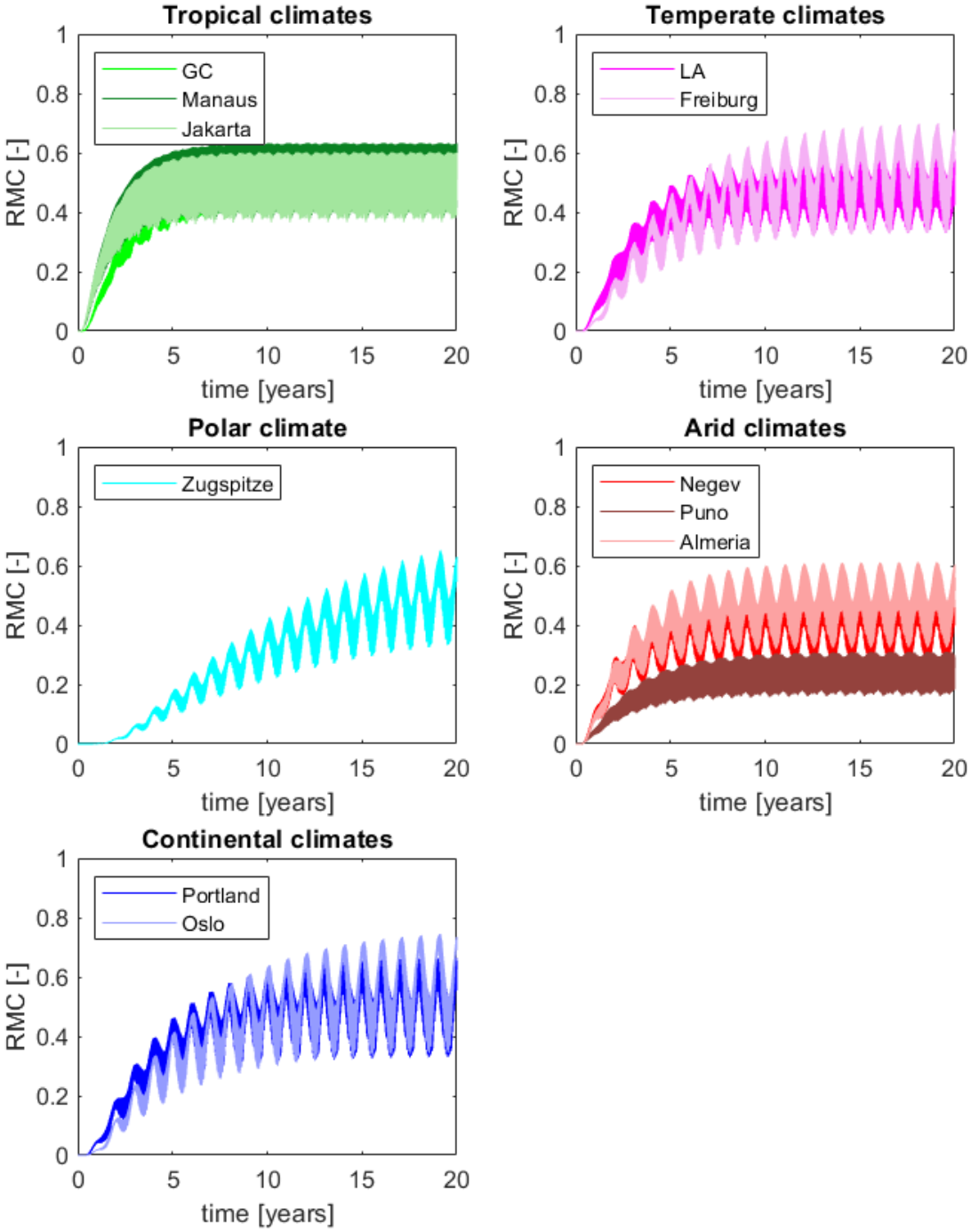

Figure B.2: RMC for the different climates

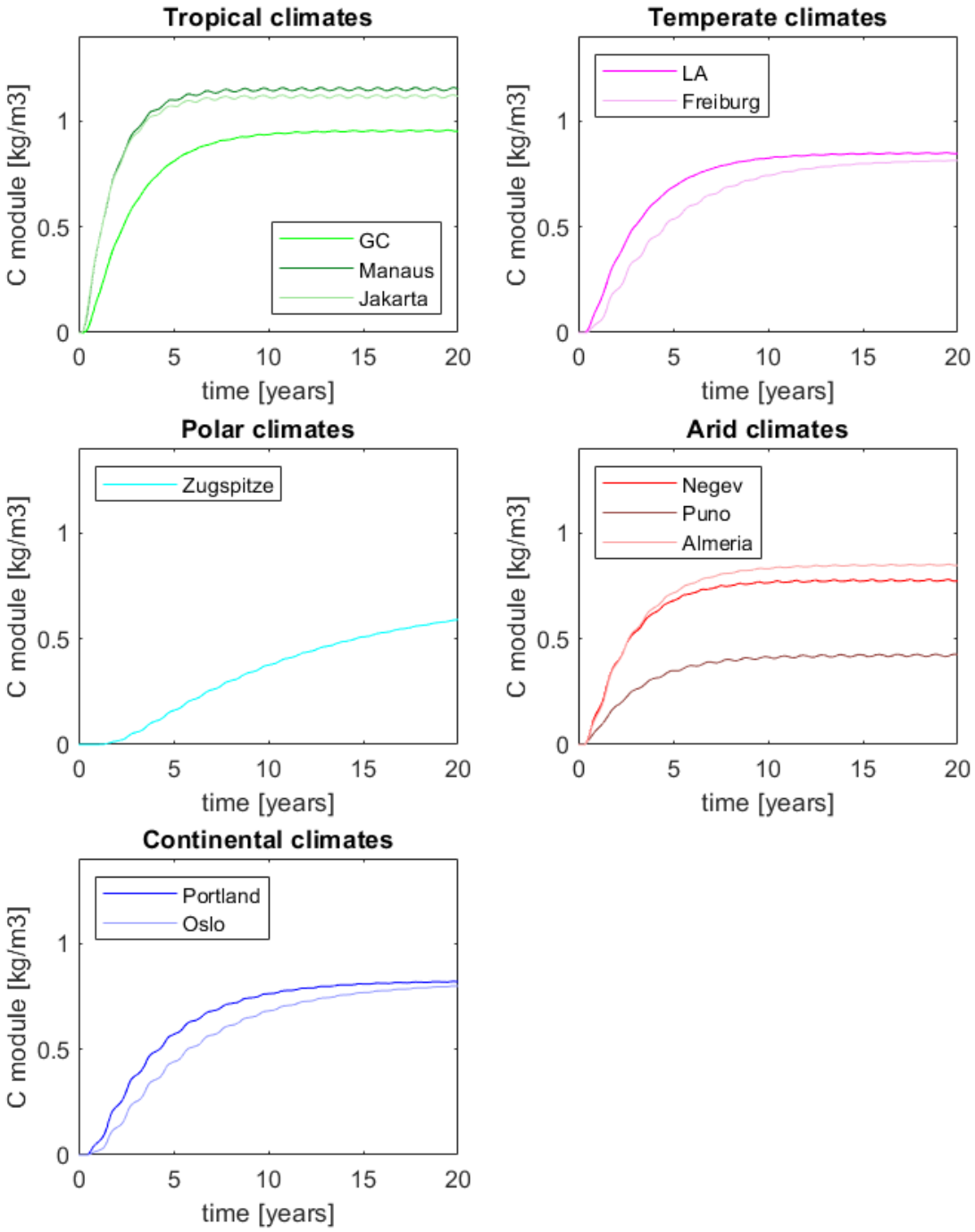

Figure B.3: Concentration of water in module for the different climates

The trend when looking at concentration instead of RMC is less clear with respect to the dependence on ambient RH. This can be seen in figures B.4 and B.5 In general, a higher RH results in a higher concentration. However, the same can be said for the dependence on temperature. A higher temperature results in a higher concentration of water in the module for most samples. This can be explained by the dependence of the solubility on temperature, which follows the same behaviour.

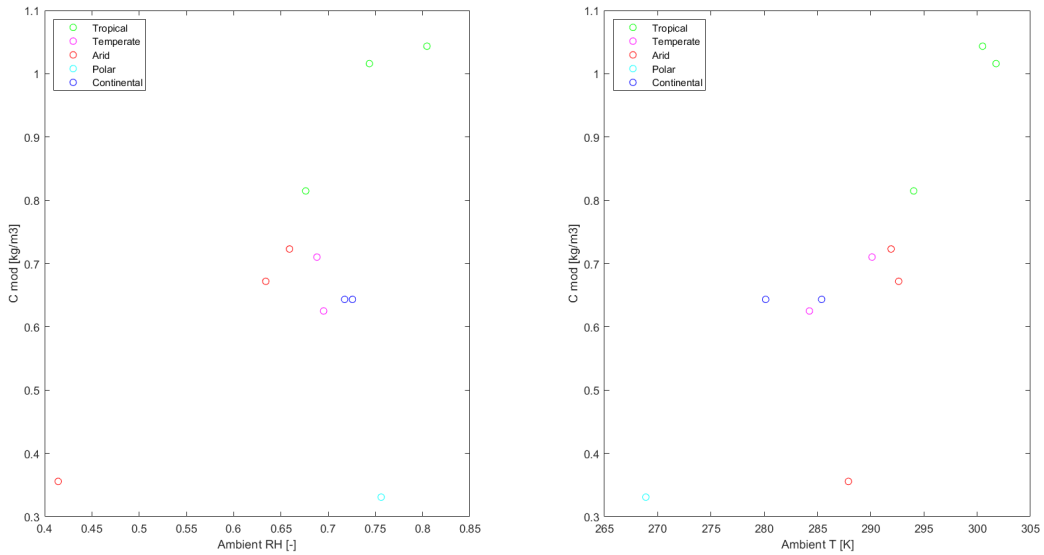

Figure B.4: Average module concentration through the lifetime of the module as a function of the average ambient conditions.

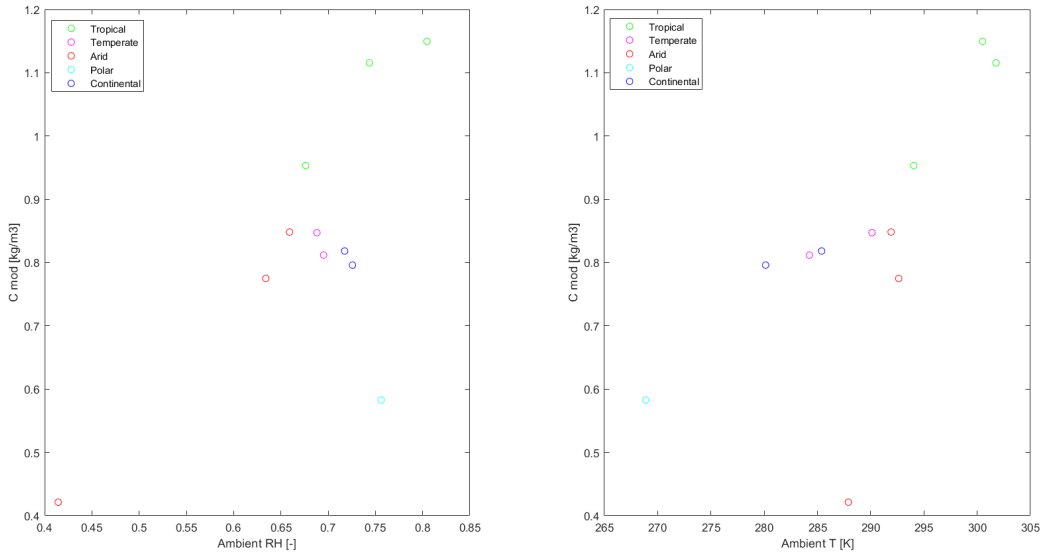

Figure B.5: Average module water concentration in the module during the last year simulated as a function of the average ambient conditions.

Figures B.6,B.8, B.7 are included to show that the conclusions for the penetration time are valid for different values of concentration or RMC which confirm the insights discussed in the main body.

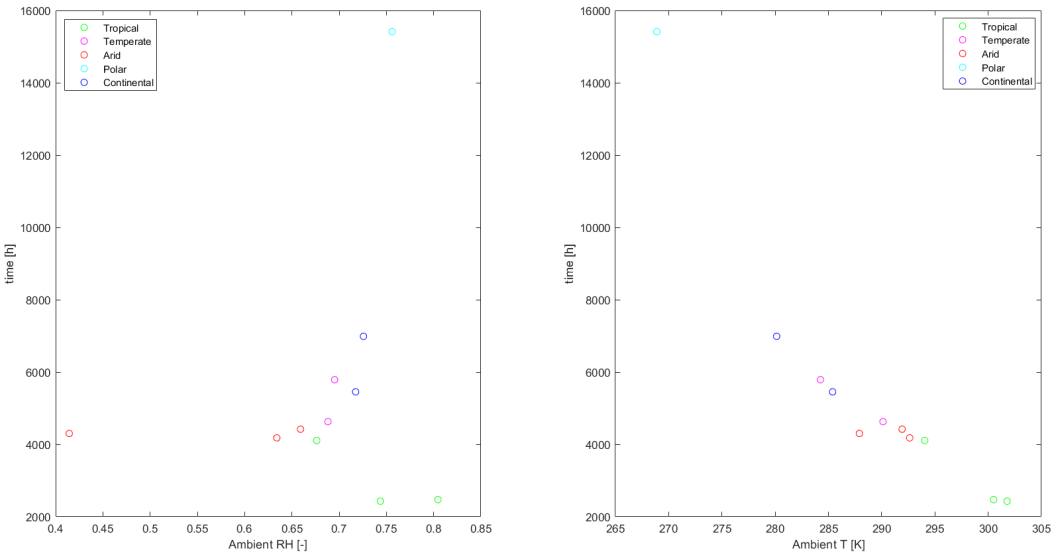

Figure B.6: Time elapsed before a RMC of 0.01 is reached inside the module as a function of average ambient RH and temperature.

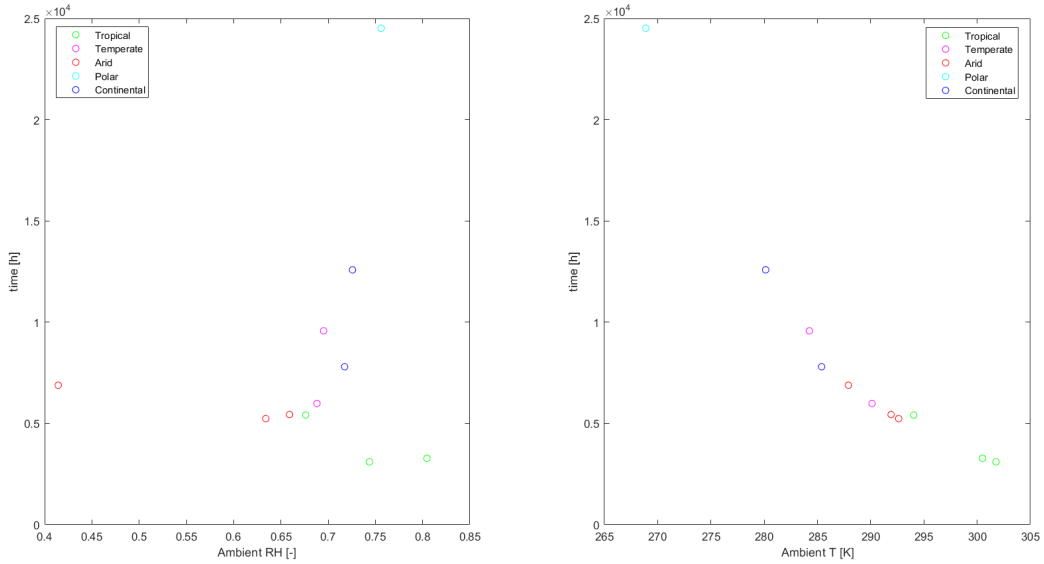

Figure B.7: Time elapsed before a moisture concentration of 0.05 kg/m^3 is reached inside the module as a function of average ambient RH and temperature.

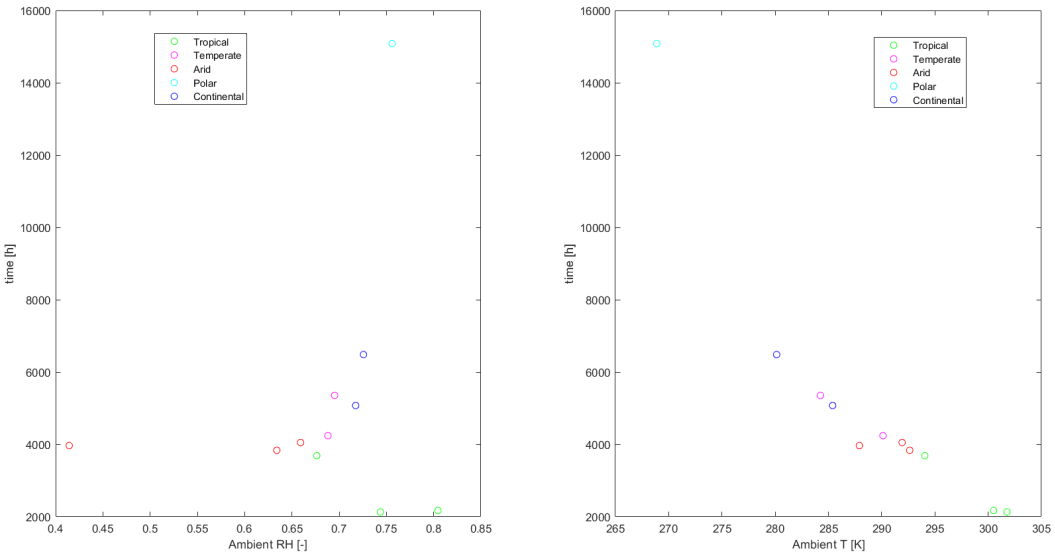

Figure B.8: Time elapsed before a moisture concentration of 0.01 kg/m^3 is reached inside the module as a function of average ambient RH and temperature.

B.2. Moisture ingress for different encapsulants

In the next two figures the difference between the diffusion coefficient and solubility for the same materials coming from different sources are shown. This is done to show that there is intrinsic uncertainty with using values from literature for the moisture ingress parameter as there can be a large discrepancy from different sources as the materials can vary and different measurements techniques can be employed.

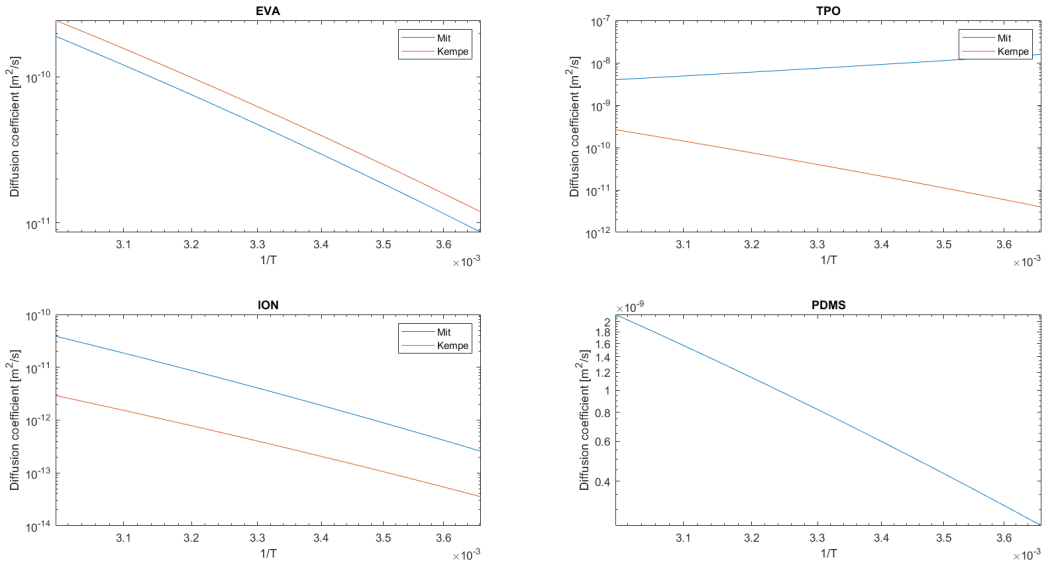

Figure B.9: Diffusion coefficients for different encapsulants from different sources as a function of the inverse of temperature (0-60 $°C$). Mit = [40], Kempe = [36]

In the figure below the results in terms of water concentration for the different encapsulants are included.

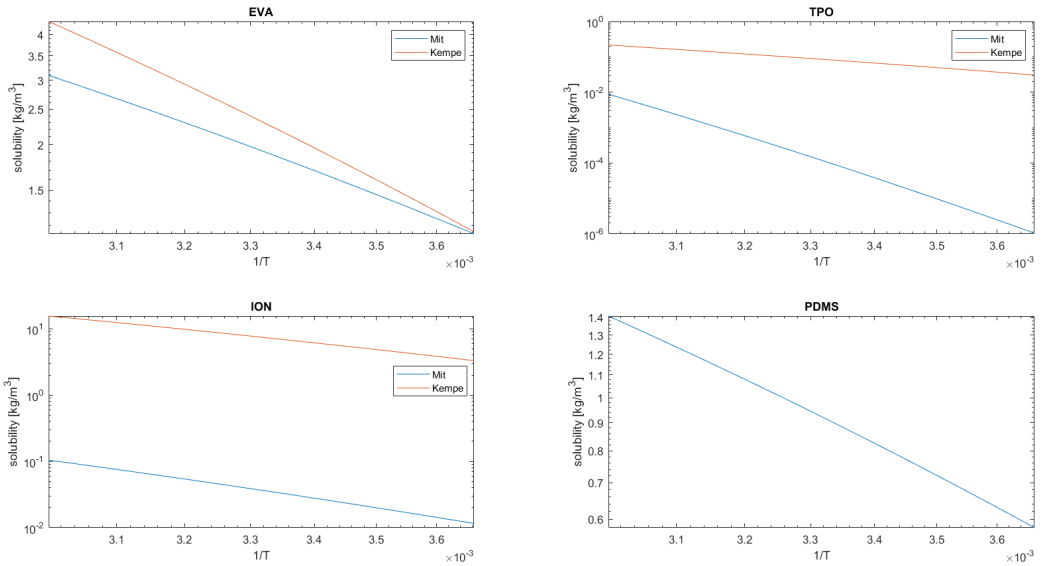

Figure B.10: Solubility for different encapsulants from different sources as a function of the inverse of temperature (0-60 $^{\circ}C$). Mit = [40], Kempe = [36]

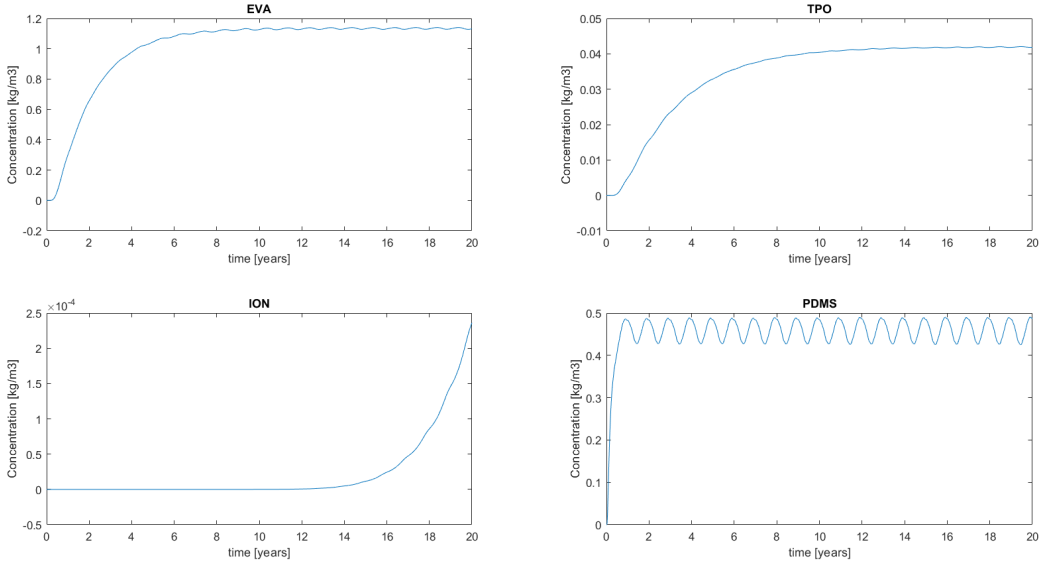

Figure B.11: Moisture concentration using different encapsulants

B.3. Moisture ingress for different backsheets

In this section appendix results in terms of RMC (without averaging) and water concentration are shown for completeness.

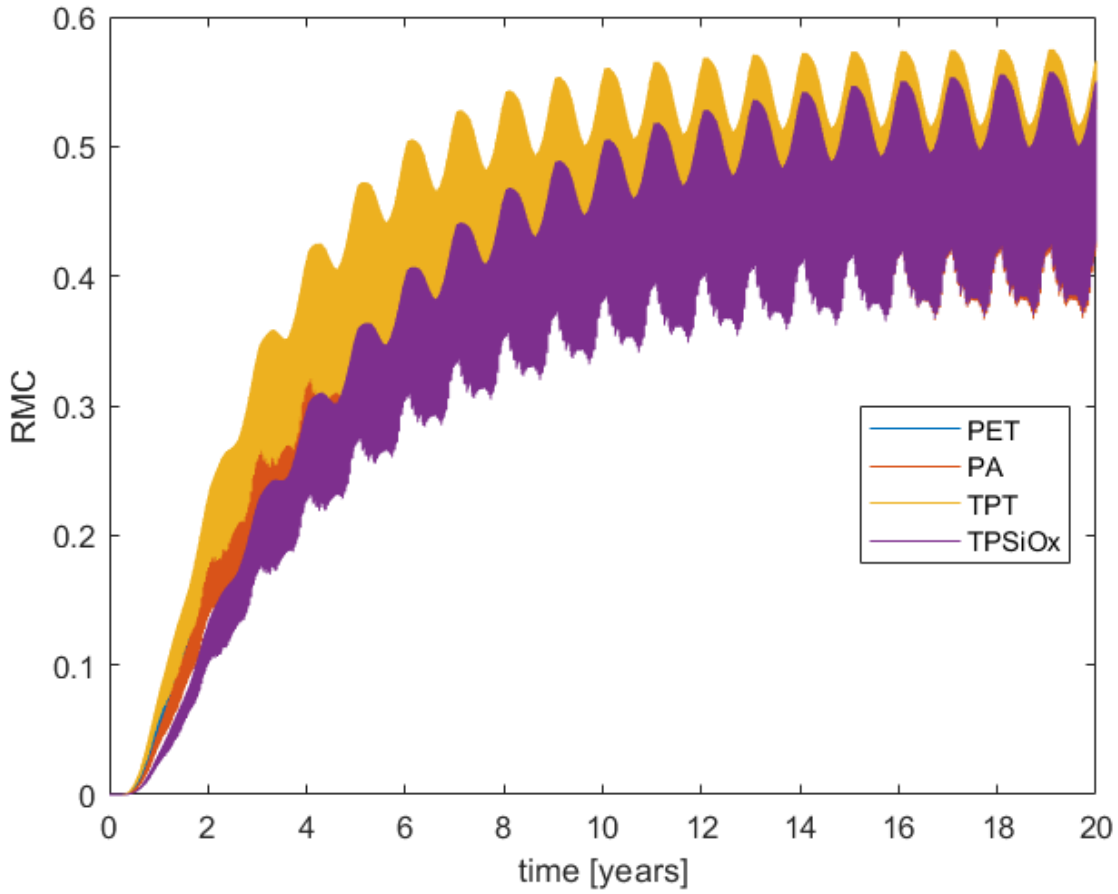

Figure B.12: Averaged RMC for modules with EVA encapsulant and different BS

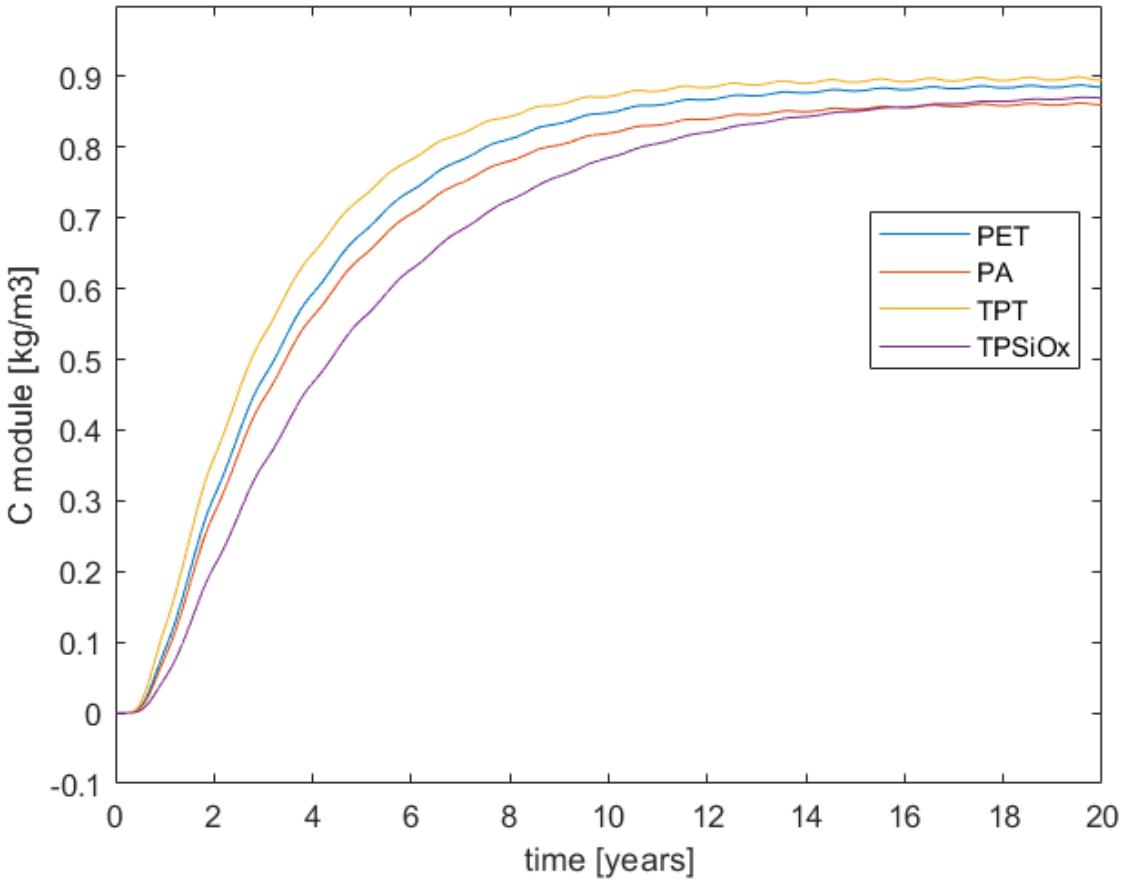

Figure B.13: Water concentration for modules with EVA encapsulant and different BS

B.4. Moisture ingress for glass-glass modules

The next two figures give the temperature dependence of the moisture ingress parameters for the glass-glass modules simulations.

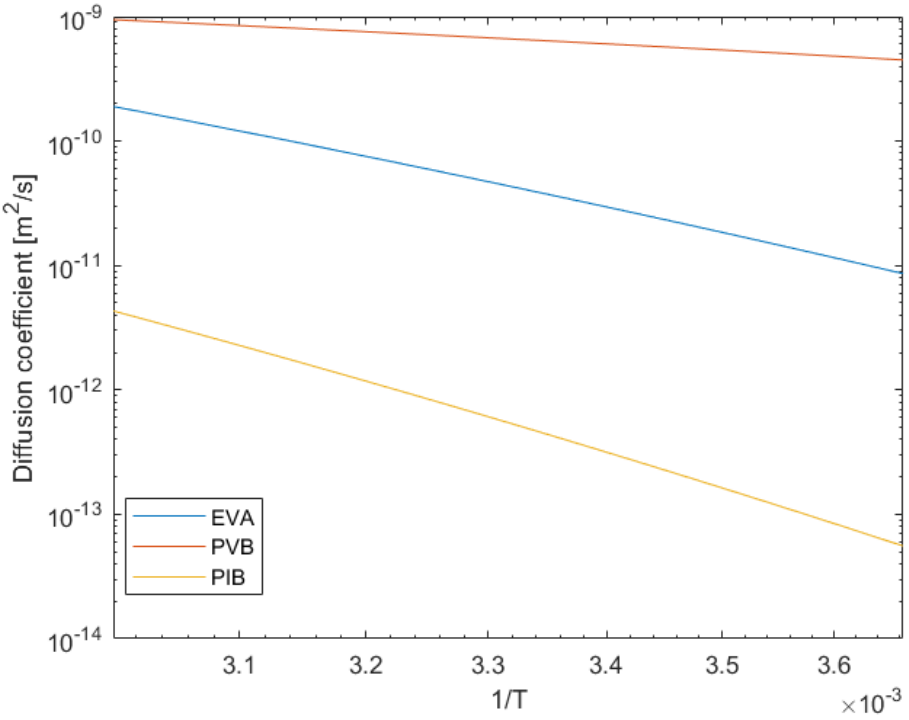

Figure B.14: Diffusion coefficients for the materials used in the glass-glass simulations as a function of the inverse of temperature (0-60 $^{\circ}C$)

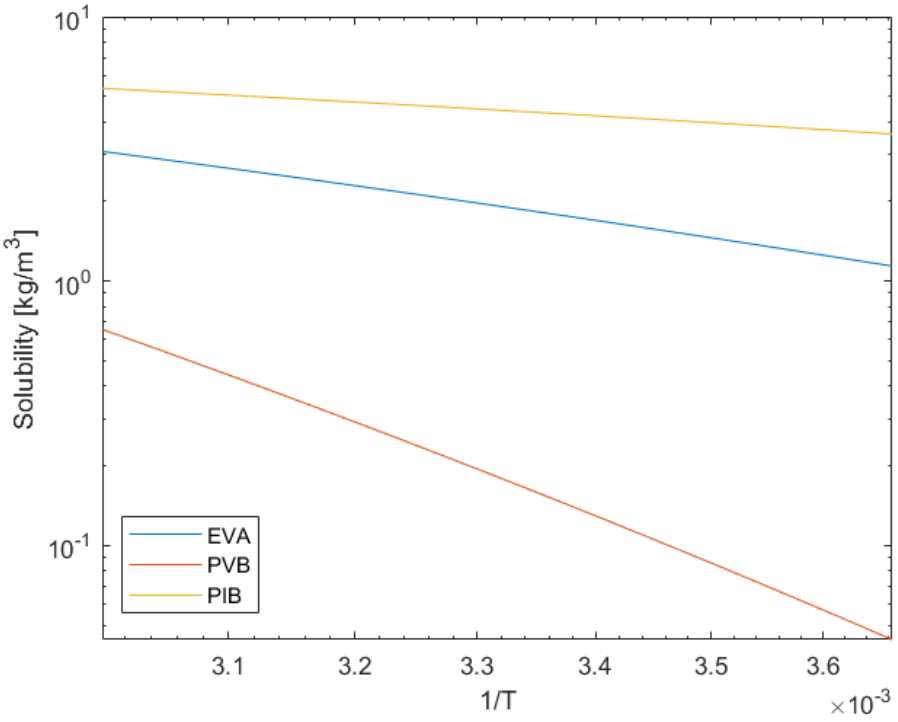

Figure B.15: Solubility for for the materials used in the glass-glass simulations as a function of the inverse of temperature (0-60 $^{\circ}C$)

The next four figures give the results for the moisture ingress simulations for the glass-glass modules expressed in concentration and RMC (without averaging).

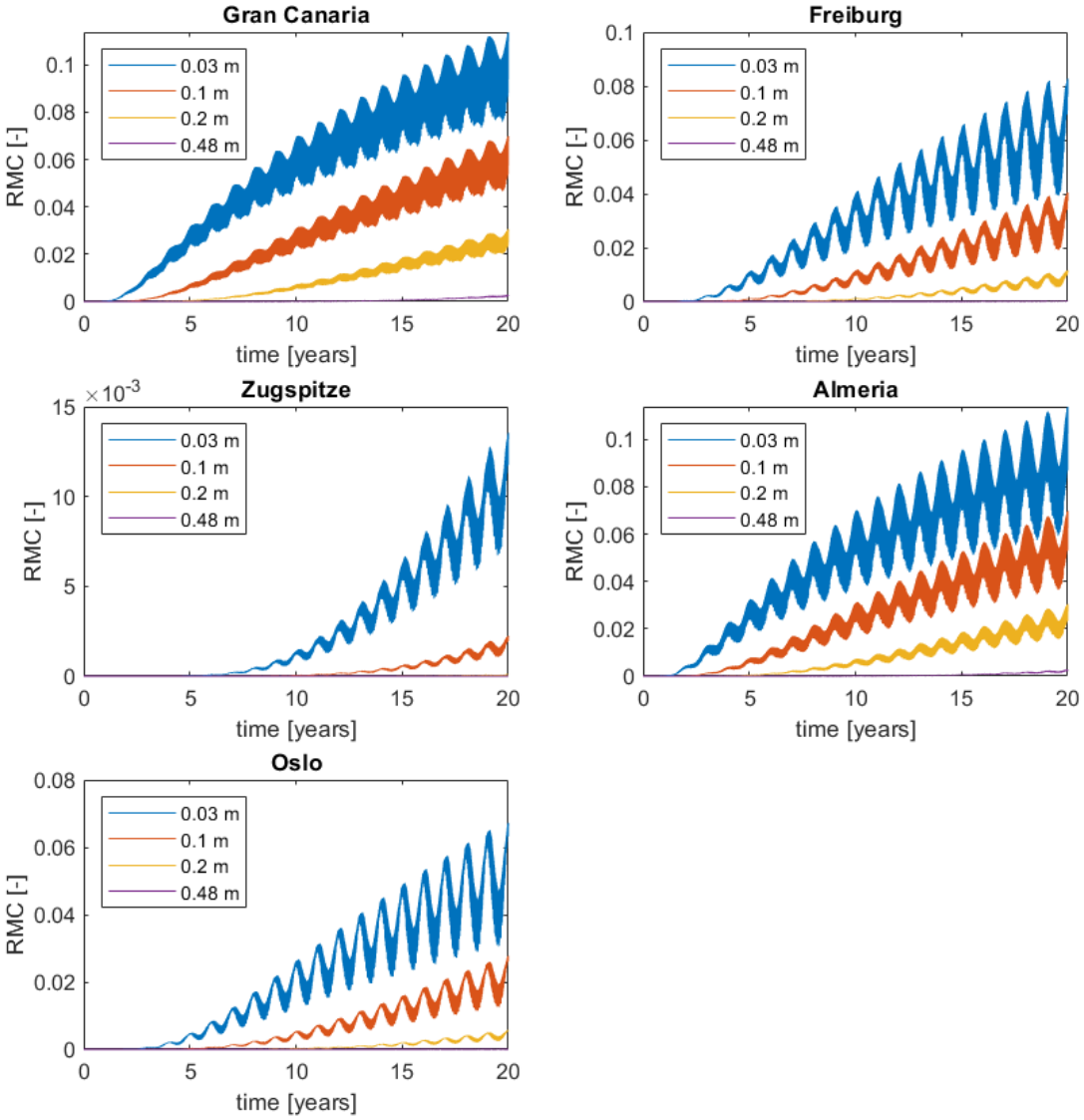

Figure B.16: RMC for glass-glass modules with EVA encapsulant and PIB edge seals in the five different locations

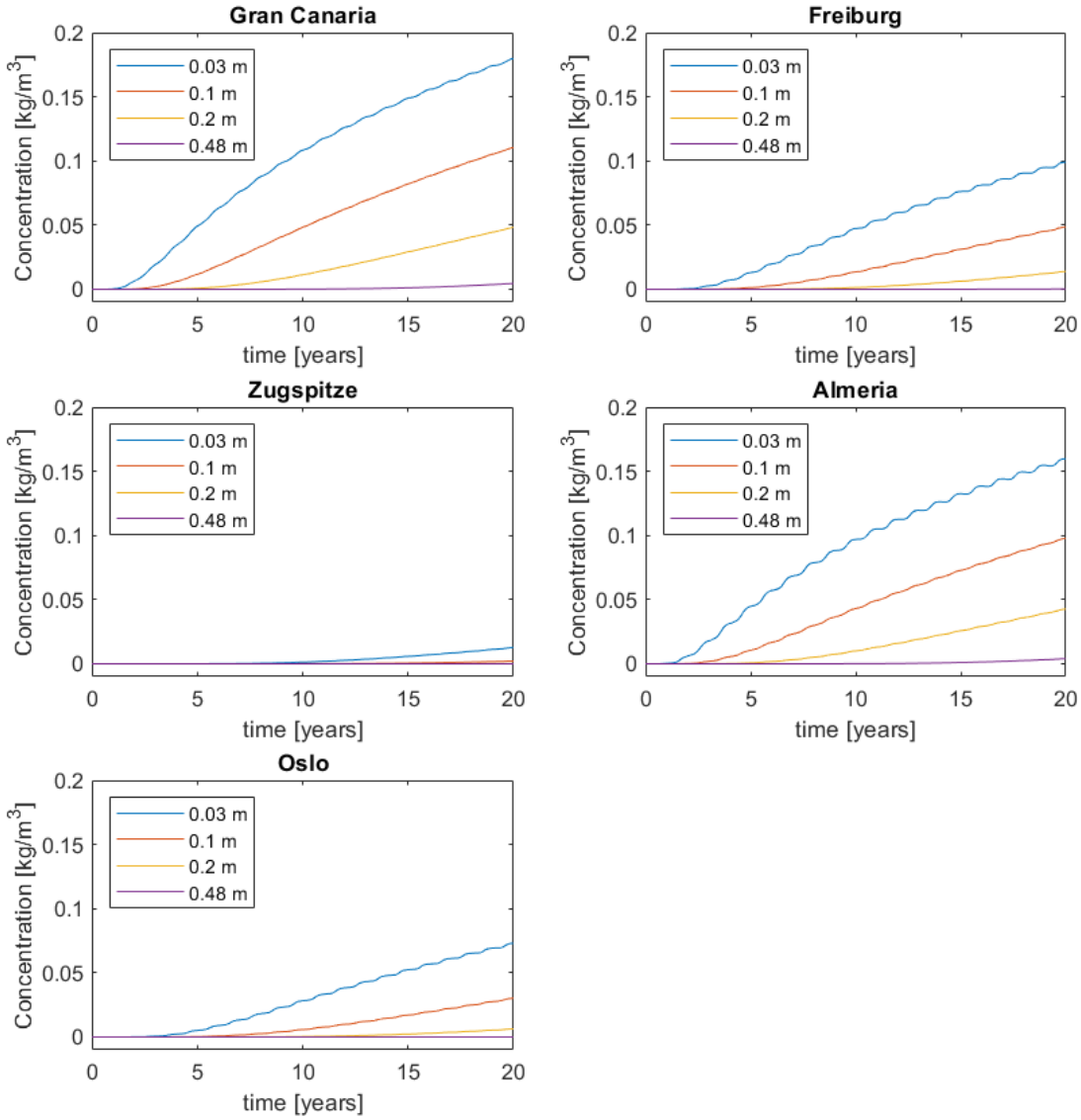

Figure B.17: Water concentration for glass-glass modules with EVA encapsulant and PIB edge seals in the five different locations

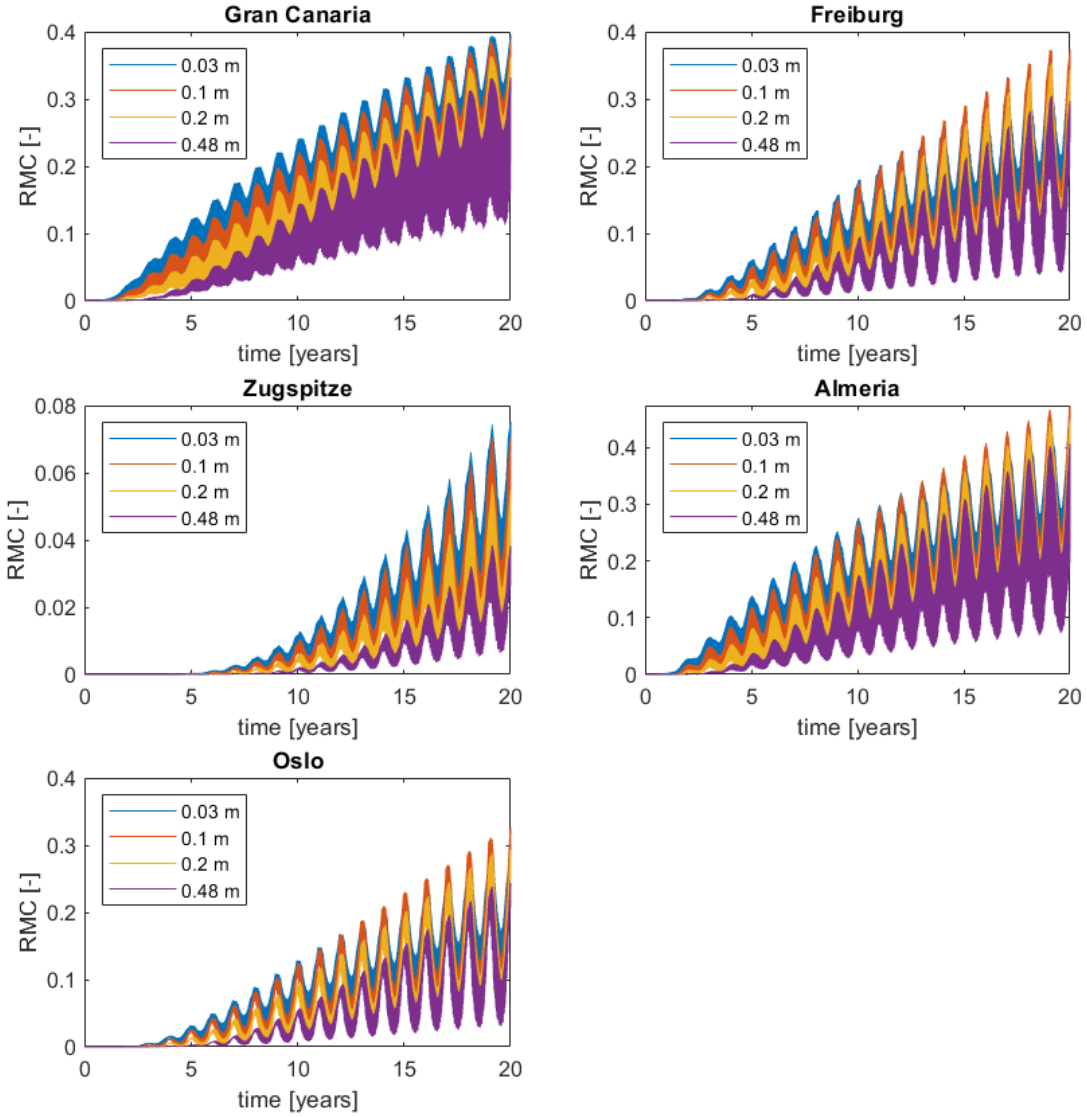

Figure B.18: RMC for glass-glass modules with PVB encapsulant and PIB edge seals in the five different locations

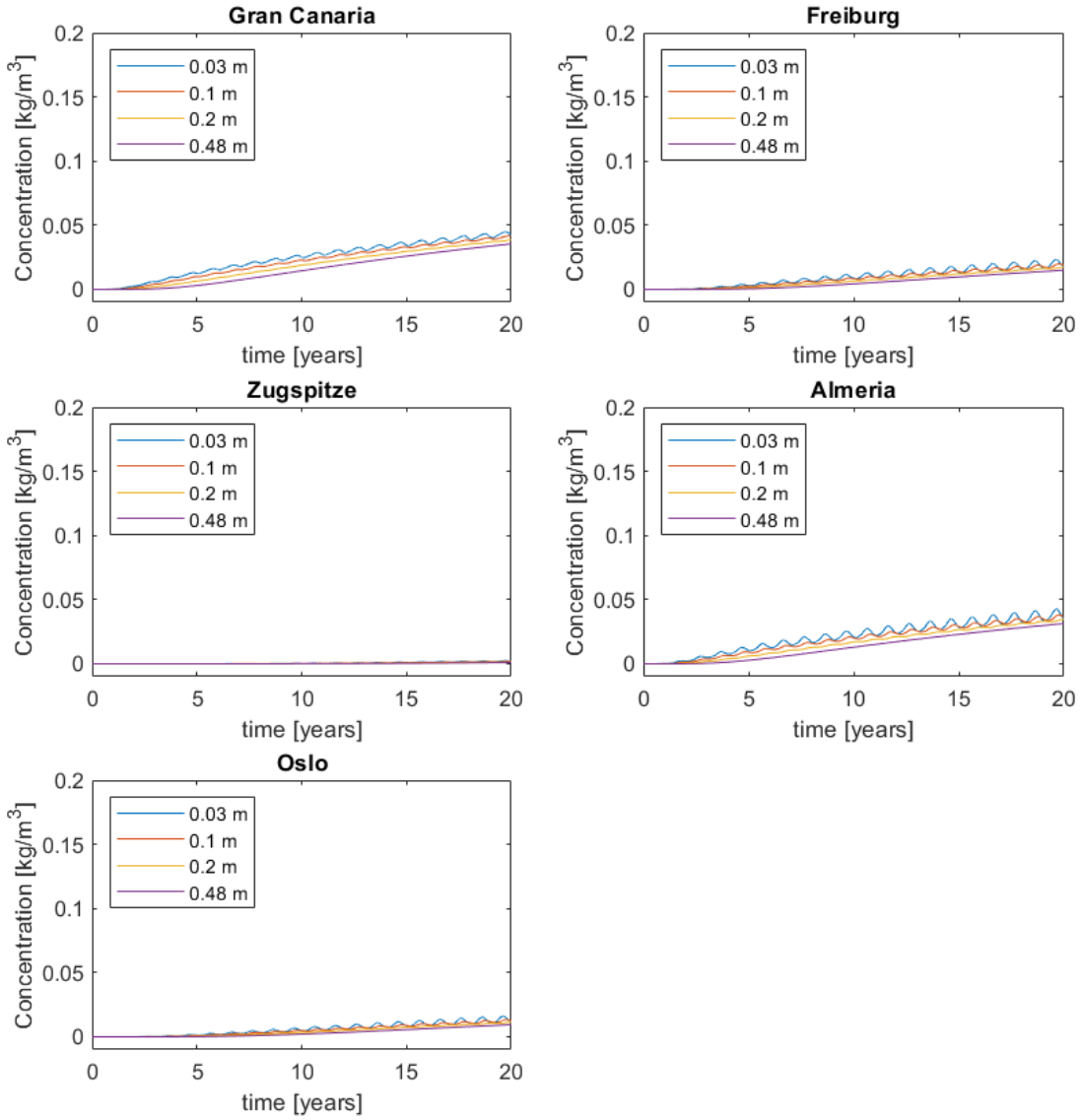

Figure B.19: Water concentration for glass-glass modules with PVB encapsulant and PIB edge seals in the five different locations

C

Fitting power degradation

C.1. Fitting accelerated lifetime tests: Training with other three experiments

Model	k[1/h]	$E_a[kJ/mol]$	n	u	L
COMSOL	$7.1957 \cdot 10^4$	57.228	0.5388	3.2193	-
Fixed RH	$2.4487 \cdot 10^4$	54.265	0.4673	3.7848	-
COMSOL +limit	$6.9165 \cdot 10^4$	57.029	0.4370	4.7892	0.8083
Fixed RH + limit	$3.7653 \cdot 10^4$	55.384	0.4421	5.4519	0.8028

Table C.1: Parameters that give the best fit for each model when trained with the first three experiments

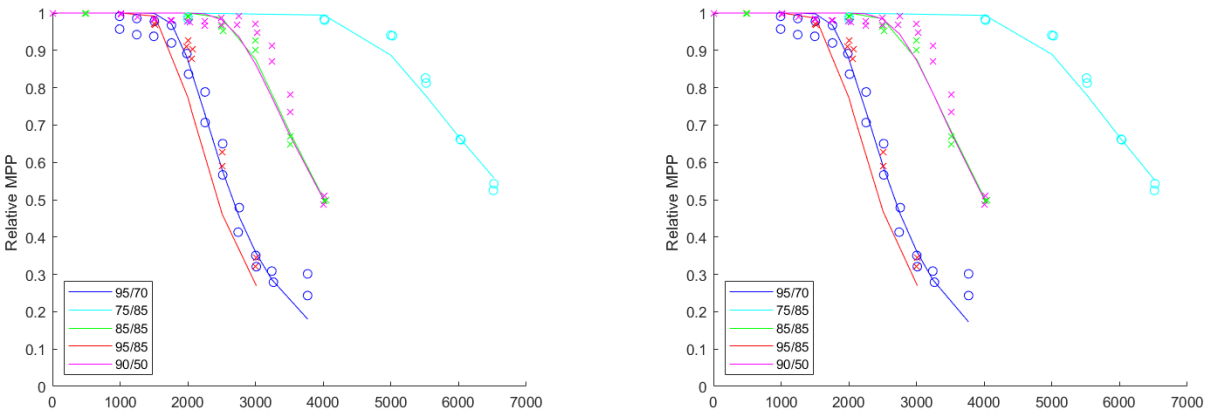

Figure C.1: Fitting results using equation 4.4. Left: Fitting results using the results of the moisture ingress model. Right: Fitting results using the fixed RH. Lines represent the fitted or predicted trend. Crosses represent the data used to train the model. Circles represent the data that the model will attempt to predict. Legend gives the experimental conditions of each in the form T/RH

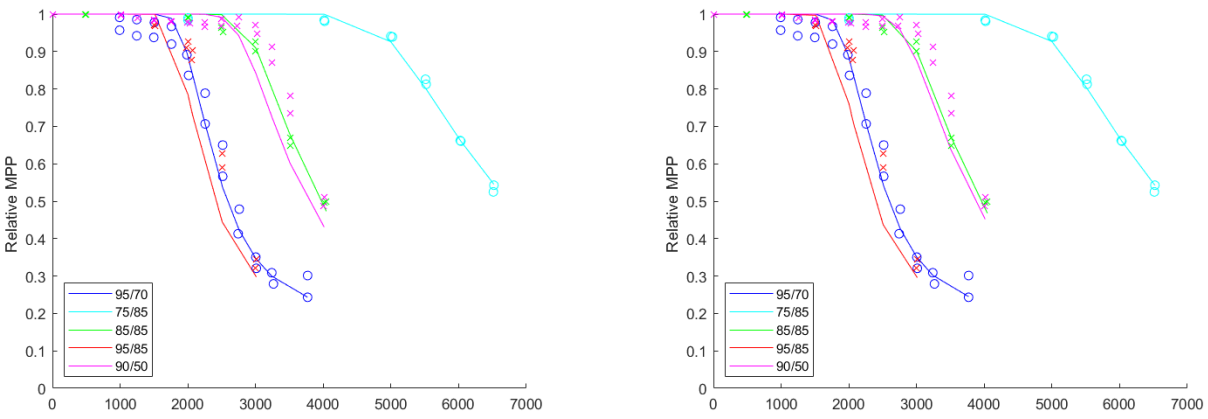

Figure C.2: Fitting results using equation 4.4 with the addition of parameter L. Left: Fitting results using the results of the moisture ingress model. Right: Fitting results using the fixed RH. Lines represent the fitted or predicted trend. Crosses represent the data used to train the model. Circles represent the data that the model will attempt to predict. Legend gives the experimental conditions of each in the form T/RH

Model	MAPE fit [%]	RMS fit [-]	MAPE predict [%]	RMS predict [-]
COMSOL	3.5695	0.0304	6.9104	0.0728
Fixed RH	3.5901	0.0301	6.6203	0.0694
COMSOL + limit	2.6923	0.0249	7.5563	0.0842
Fixed RH + limit	2.6092	0.0243	7.2833	0.0806

Table C.2: Statistical analysis of fitting and prediction when training with the first three experiments

C.2. Results for the moisture ingress model used as input for the lifetime degradation modelling

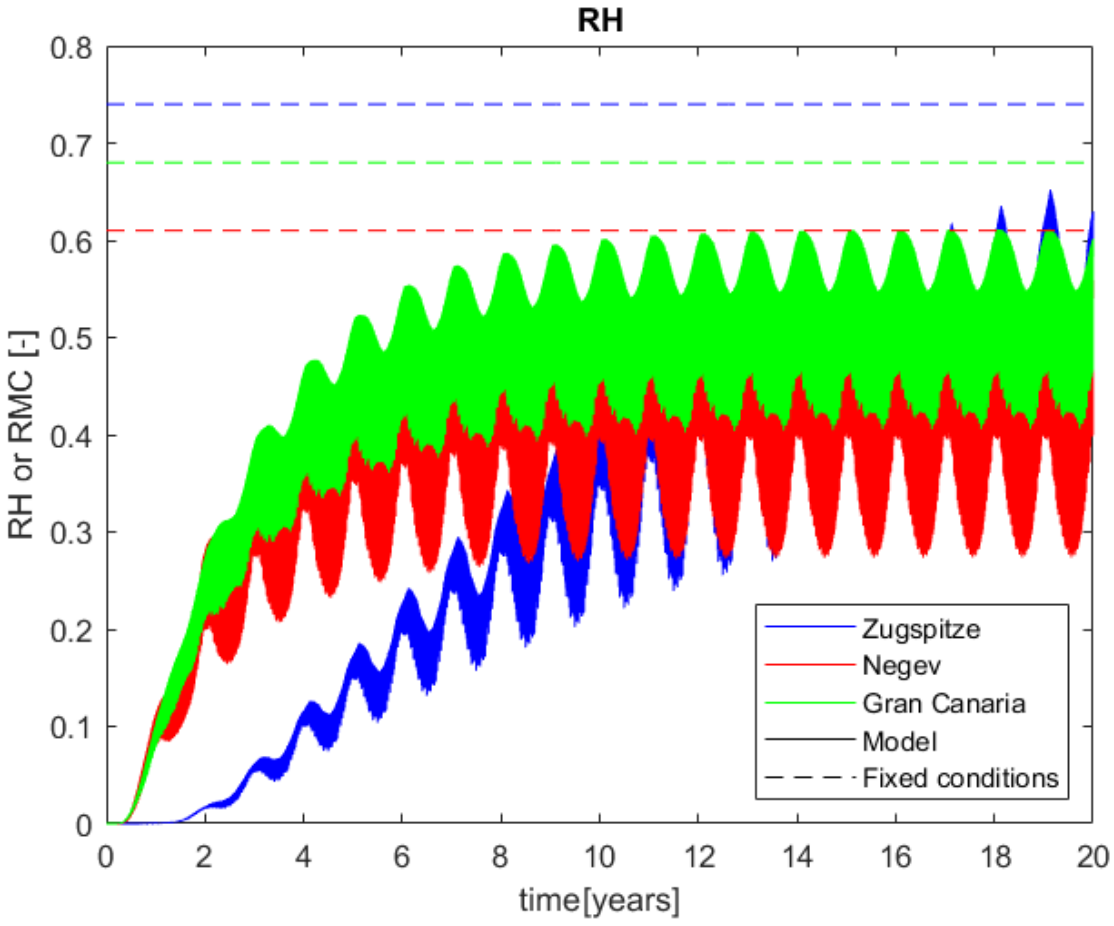

Figure C.3: Difference in input when using the COMSOL model and the fixed RH for different locations. The lines at a constant value are the input when the climatic RH is used. The lines that change value over time are the input from COMSOL

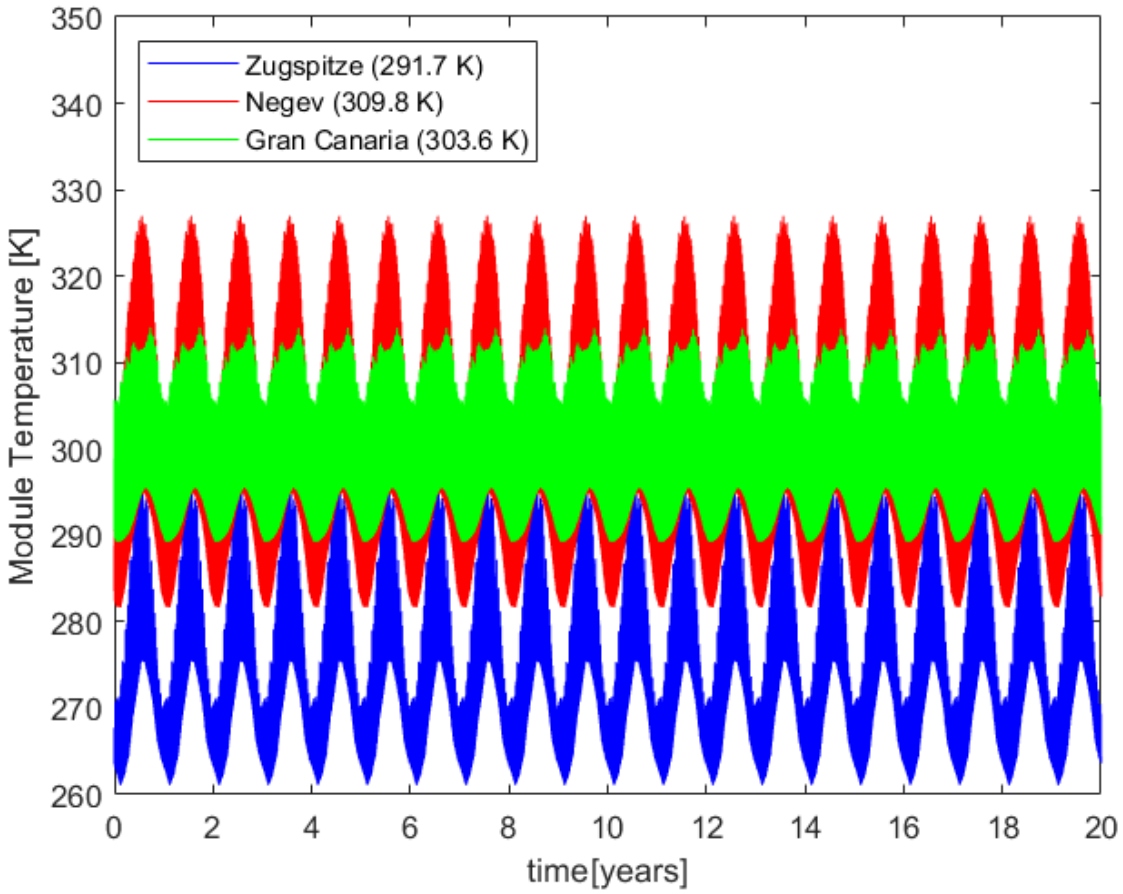

Figure C.4: Module temperature at different locations. In brackets is the input for the fixed conditions model

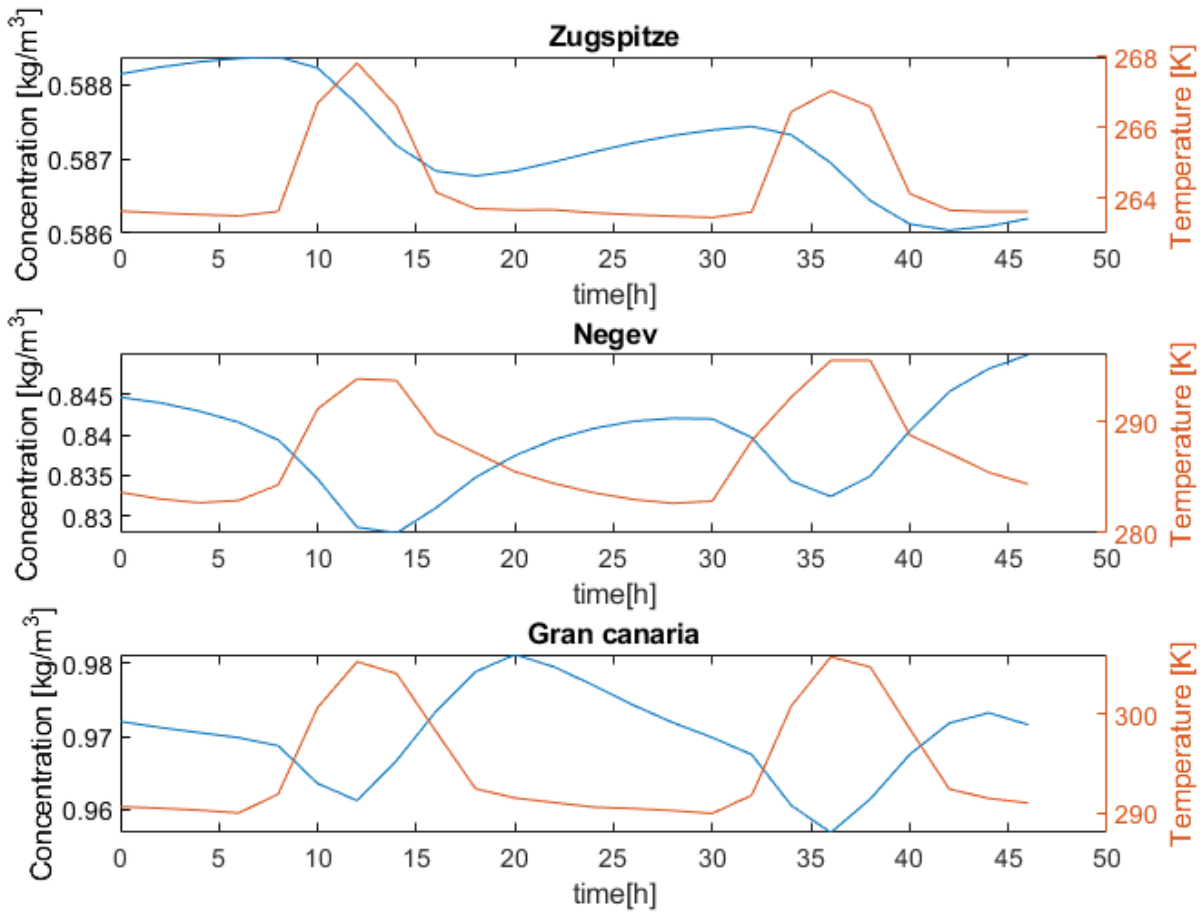

Figure C.5: Daily trends in water concentration in the encapsulant below the solar cell and module temperature for the three chosen locations. Results for two first days of January of the 11^{th} year

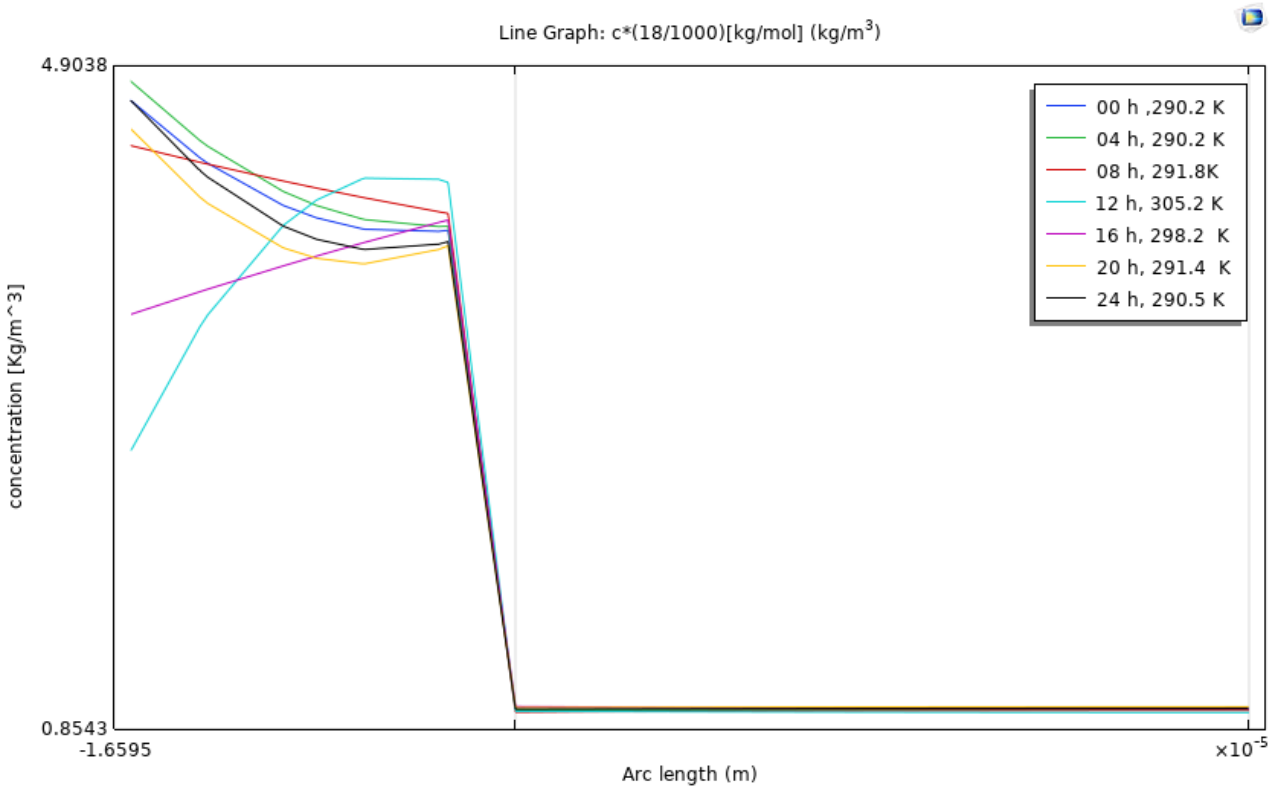

Figure C.6: Concentration profile in backsheet and encapsulant under solar cell. Results for Gran Canaria, the 01/01 of the 10th year of simulation

C.3. Sensitivity analysis of degradation models

The next two figures represent where the data points in figure 4.15 come from. They show the degradation through the lifetime of the module in the different climates using the BET and Peck (n = 1.9) models.

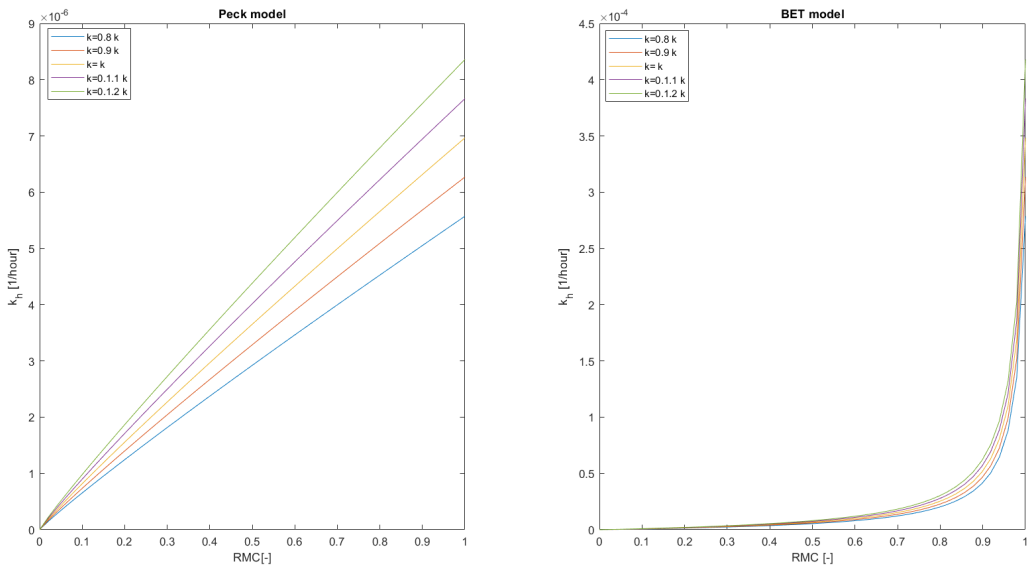

Figure C.7: Sensitivity analysis of k parameter as a function of RMC. Left: Peck model. Right: BET model

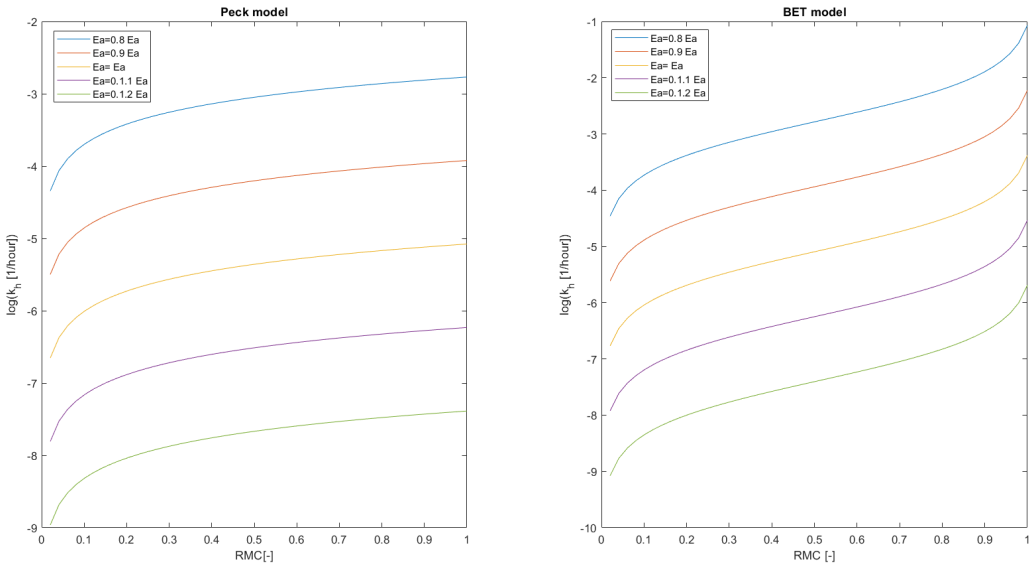

Figure C.8: Sensitivity analysis of E_a parameter as a function of temperature. Left: Peck model. Right: BET model

C.4. Degradation modelling for different climates

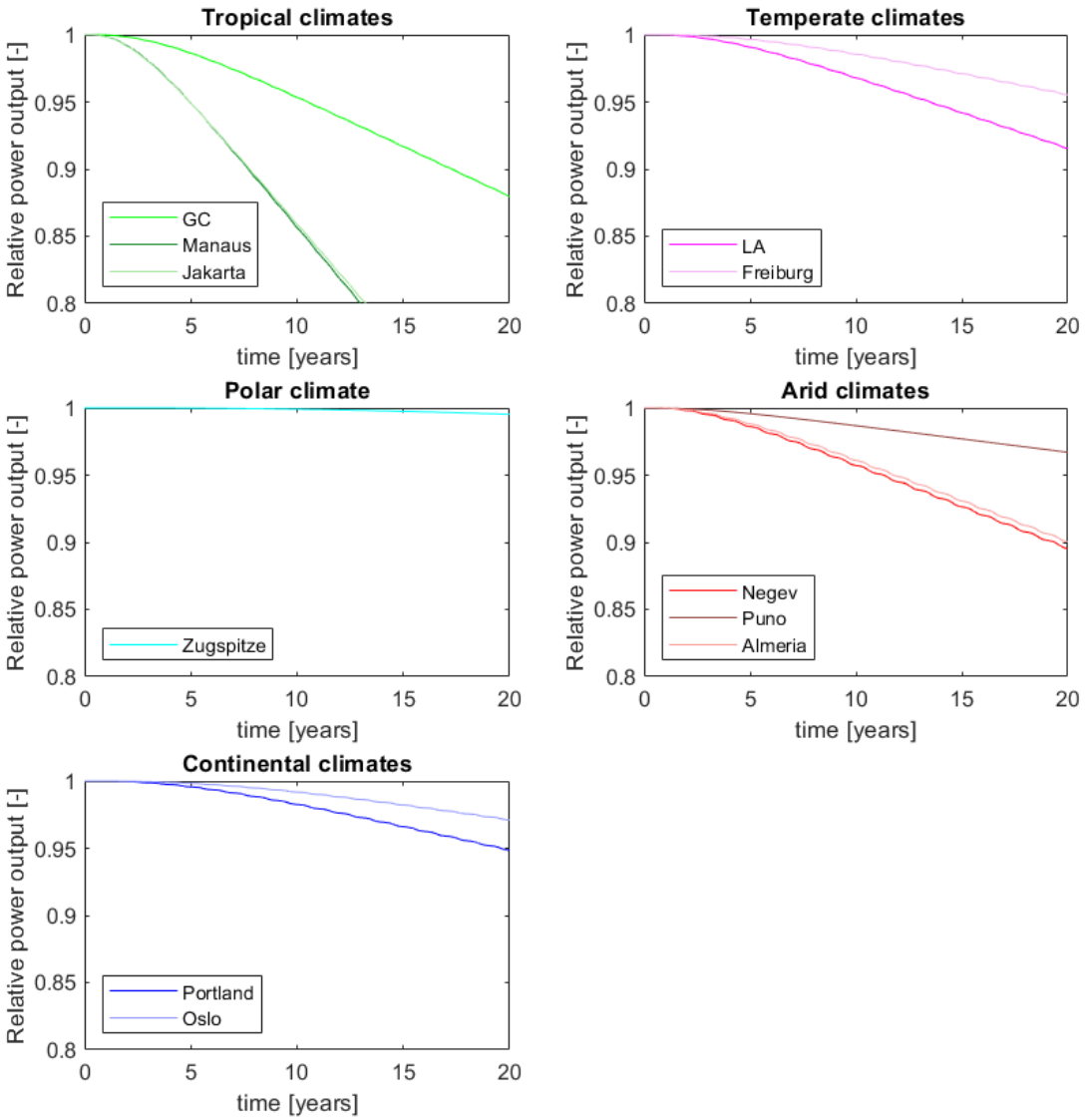

Figure C.9: Predicted power degradation in different climates using the BET model

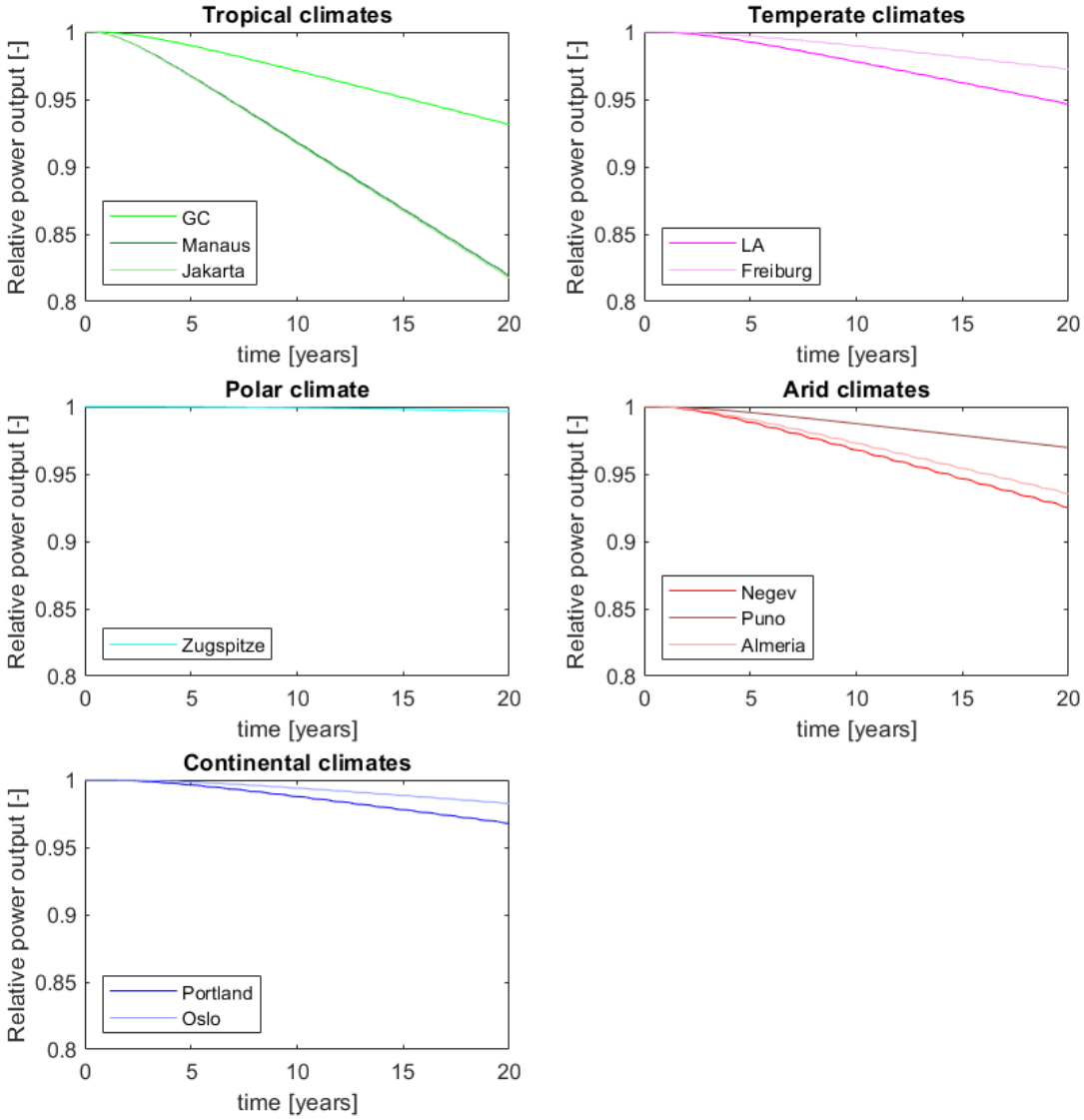

Figure C.10: Predicted power degradation in different climates using the Peck model with constant n = 1.9